National Library of Canada
Bibliothèque nationale du Canada

Canadian Theses Service
Service des thèses canadiennes

Ottawa, Canada
K1A 0N4

NOTICE

The quality of this microform is heavily dependent upon the quality of the original thesis submitted for microfilming. Every effort has been made to ensure the highest quality of reproduction possible.

If pages are missing, contact the university which granted the degree.

Some pages may have indistinct print especially if the original pages were typed with a poor typewriter ribbon or if the university sent us an inferior photocopy.

Previously copyrighted materials (journal articles, published tests, etc.) are not filmed.

Reproduction in full or in part of this microform is governed by the Canadian Copyright Act, R.S.C. 1970, c. C-30.

AVIS

La qualité de cette microforme dépend grandement de la qualité de la thèse soumise au microfilmage. Nous avons tout fait pour assurer une qualité supérieure de reproduction.

S'il manque des pages, veuillez communiquer avec l'université qui a conféré le grade.

La qualité d'impression de certaines pages peut laisser à désirer, surtout si les pages originales ont été dactylographiées à l'aide d'un ruban usé ou si l'université nous a fait parvenir une photocopie de qualité inférieure.

Les documents qui font déjà l'objet d'un droit d'auteur (articles de revue, tests publiés, etc.) ne sont pas microfilmés.

La reproduction, même partielle, de cette microforme est soumise à la Loi canadienne sur le droit d'auteur, SRC 1970, c. C-30.

NL-339 (r. 88/04)

Canada

THE UNIVERSITY OF ALBERTA

LASER-BASED REFRACTIVE INDEX, ABSORBANCE, AND FLUORESCENCE MEASUREMENTS WITH THE SHEATH-FLOW CUVETTE.

by

© YUNG-FONG CHENG

A THESIS

SUBMITTED TO THE FACULTY OF GRADUATE STUDIES AND RESEARCH IN PARTIAL FULFILMENT OF THE REQUIREMENTS FOR THE DEGREE OF DOCTOR OF PHILOSOPHY

DEPARTMENT OF CHEMISTRY

EDMONTON, ALBERTA

FALL, 1988

Permission has been granted to the National Library of Canada to microfilm this thesis and to lend or sell copies of the film.

The author (copyright owner) has reserved other publication rights, and neither the thesis nor extensive extracts from it may be printed or otherwise reproduced without his/her written permission.

L'autorisation a été accordée à la Bibliothèque nationale du Canada de microfilmer cette thèse et de prêter ou de vendre des exemplaires du film.

L'auteur (titulaire du droit d'auteur) se réserve les autres droits de publication; ni la thèse ni de longs extraits de celle-ci ne doivent être imprimés ou autrement reproduits sans son autorisation écrite.

ISBN 0-315-45690-6

University of Alberta
Edmonton

Department of Chemistry
Faculty of Science

Canada T6G 2G2

E3-43 Chemistry Building East, Telephone (403) 432-3254

July 12, 1988

Mr. Yung-Fong Cheng
Department of Chemistry
University of Alberta
Edmonton, Alberta

Dear Yung-Fong:

I grant you permission to utilize in your Doctoral Thesis any material co-authored by you and me.

Sincerely,

Norman J. Dovichi
Associate Professor

THE UNIVERSITY OF ALBERTA

RELEASE FORM

NAME OF AUTHOR : YUNG-FONG CHENG

TITLE OF THESIS : LASER-BASED REFRACTIVE INDEX, ABSORBANCE, AND FLUORESCENCE MEASUREMENTS WITH THE SHEATH-FLOW CUVETTE.

DEGREE : DOCTOR OF PHILOSOPHY

YEAR THIS DEGREE GRANTED : 1988

Permission is hereby granted to THE UNIVERSITY OF ALBERTA LIBRARY to reproduce single copies of this thesis and to lend or sell such copies for private, scholarly or scientific research purposes only.

The author reserves other publication rights, and neither the thesis nor extensive extracts from it may be printed or otherwise reproduced without the auther's written permission.

(Signed) .....

Permanent Address :
No 50, Aly 7, Ln 104, Jen-Ai Rd,
Yung-Ho, Taipei, Taiwan, R.O.C

DATED July 4 1988

THE UNIVERSITY OF ALBERTA

FACULTY OF GRADUATE STUDIES AND RESEARCH

The undersigned certify that they have read, and recommend to the Faculty of Graduate Studies and Research for acceptance, a thesis entitled LASER-BASED REFRACTIVE INDEX, ABSORBANCE, AND FLUORESCENCE MEASUREMENTS WITH THE SHEATH-FLOW CUVETTE.

submitted by YUNG-FONG CHENG

in partial fulfilment of the requirements for the degree of DOCTOR OF PHILOSOPHY.

N. J. Dovichi, supervisor

Byron Kratochvil

B. G. Kratochvil

Frederick F. Cantwell

F. F. Cantwell

Loren Hepler

L. G. Hepler

H. J. J. Seguin

Richard A. Keller

R. A. Keller, External Examiner

Date July 11 1988

ABSTRACT

A sheath-flow cuvette is used as a detector cell for three analytical applications incorporating lasers as the light source.

First, the sheath-flow cuvette is used to determine the refractive index of neat solutions by a flow-modulation technique. In this technique, diffraction of the laser beam within the cuvette produces a change in the far-field beam-center intensity which is proportional to the difference in refractive index between the sample and sheath streams. If the flow is switched rapidly between sample and sheath, synchronous demodulation of the laser beam intensity leads to improved refractive index precision. Detection limits of $7 * 10^{-8}$ ΔRI were obtained across a 40 μm diameter sample stream.

Second, the cuvette is used to determine absorbance of neat solutions by a thermo-optical technique. In this technique, the sample is heated by a 2 mW modulated pump beam. A second coplanar probe beam is used to detect the change of the refractive index induced by the pump beam. A lock-in amplifier is used to demodulate the periodic change of refractive index. Absorbance detection limits of $1.1 * 10^{-5}$ were obtained in a 100 to 140 μm diameter sample stream.

Third, the cuvette is used to determine fluorescence of neat solutions and is also combined with capillary zone electrophoresis (CZE) as a laser-induced fluorescence detector. In this technique, a one watt argon ion laser operating at 488 nm is used as the excitation

source and a microscope set at a right angle to the laser beam is used to collect the fluorescent signal. Detection limits of $1.25 * 10^{-12}$ M for fluorescein solution were obtained across a 40 μm diameter sample stream. When combined with CZE, detection limits in the order of 10^{-20} mole for separation and determination of eighteen fluorescein isothiocyanate derivatized amino acids injected onto the capillary were obtained.

ACKNOWLEDGMENTS

I would like to express my most sincere appreciation to my advisor, Professor Norman Dovichi, for his never ending encouragement and invaluable guidance throughout my program. In the four years I have known him, he has also been a model of patience which has helped me to handle this course work and shown me how to deal with anything encountered in my path.

Special thanks are due to Professors B. G. Kratochvil, F. F. Cantwell, L. G. Hepler, H. J. J. Seguin, and R. A. Keller for their willingness to serve as members of the advisory committee.

Thanks also go to Dovichi's former graduate students, Drs. T. G. Nolan, D. Borhop, and D. Burgi for their helps in the beginning of my graduate study, and to Miss Launna Townsley for her support during the writing process.

I wish to acknowledge the staffs of the machine shop, photocopying department, and electronic shop for their cooperation.

Finally, my deep gratitude is expressed to my parents, Mr. and Mrs. Cheng ( ); and my sisters and brother who constantly provided psychological support and news from home.

TABLE OF CONTENTS

CHAPTER PAGE

I. INTRODUCTION 1

1.1. The sheath-flow cuvette 1

1.2. The laser 8

1.3. The thesis 9

REFERENCES 12

II. REFRACTIVE INDEX MEASUREMENT (Refractive Index Measurement Within The Sheath-Flow Cuvette) 14

1. INTRODUCTION 14

2. EXPERIMENTAL 19

2.1. Refractive index detection using the sheath-flow cuvette 19

2.2. Flow-modulation within a sheath-flow cuvette for refractive index measurement 23

3. RESULTS AND DISCUSSION 27

3.1. Without flow-modulation 27

3.2. With flow-modulation 28

REFERENCES 32

III. ABSORBANCE MEASUREMENT (Thermo-Optical Determination Within The Sheath-Flow Cuvette) 33

1. INTRODUCTION 33

2. EXPERIMENTAL 42

3. RESULTS AND DISCUSSION 45
REFERENCES 54

IV. FLUORESCENCE MEASUREMENT (I)
(Laser-Induced Fluorescence Detection Using The
Sheath-Flow Cuvette) 55
1. INTRODUCTION 55
1.1. Introduction to fluorescence 55
1.2. Fluorescence quantum yield 58
1.3. Fluorescence intensity and concentration 58
1.4. Excitation spectrum and emission spectrum 60
1.5. Structure effects 61
1.6. Environmental effects 64
1.7. Background signal in laser induced fluorescence..... 67
2. EXPERIMENTAL 70
2.1. Instrumental 70
2.2. Chemicals 72
3. RESULTS AND DISCUSSION 72
REFERENCES 80

V. FLUORESCENCE MEASUREMENT (II)
(Laser-Induced Fluorescence Detection Using The
Sheath-Flow Cuvette For Capillary Zone Electrophoresis)..... 82
1. INTRODUCTION 82
1.1. Capillary Zone Electrophoresis (CZE) 82
1.1.1 Transport mechanism 85

1.1.1.1 Zeta potential (ζ) and electric double layer 85
1.1.1.2 Electrophoretic mobility (μ_{ep})..... 85
1.1.1.3 Electro-osmotic flow (μ_{eo})..... 87
1.1.2 Effect of pH on transport machanism 88
1.1.3 Causes of zone broadening in electrophoresis 89
1.1.4 Migration velocity and time, separation efficiency, and resolution 90
1.1.4.1 Migration velocity (v) and migration time (t) 90
1.1.4.2 Separation efficiency (N) 91
1.1.4.3 Resolution (Rs) 93
1.1.5 Practical Limitation --- heat generation..... 94
1.1.6 Advantages of small diameter tubes 95
1.1.7 Detectors for CZE 96
1.1.8 Estimation of injection volume, concentration at peak maximum, and detection limits 96
1.1.8.1 Injection volume 96
1.1.8.2 Concentration at peak maximum..... 98
1.1.8.3 Detection limit 98
1.2. Fluorescein-isothiocyanate (FITC) derivatives of amino acids 99
2. THEORY 102
3. EXPERIMENTAL 109
3.1. Instrumental 109

3.2. Chemicals 111
3.3. Preparation of FTC-AA 112
3.4. Electrophoresis procedures 113
4. RESULTS AND DISCUSSION 113
4.1. Preliminary study for capillary zone electrophoresis 113
4.2. Diffusion study 121
4.3. Effect of sheath flow rate on theoretical plate and resolution 126
4.4. Separation of fluorescein-isothiocyanate derivatives of 18 amino acids 132
REFERENCES 148

VI. CONCLUSION AND FUTURE WORK 152
REFERENCES 157

APPENDIX 158
1. Electropherograms for chapter five, section 4.3: Effect of sheath flow rate on theoretical plate and resolution 159
2. Electropherograms for chapter five, section 4.4: Separation of fluorescein-isothiocyanate derivatives of 18 amino acids 162
3. Electropherogram of eighteen amino acids treated with FITC solution all at once 168

LIST OF TABLES

NUMBER	DESCRIPTION	PAGE
3-1	Detection limits for the system consisting of methanol sheath/methanol sample solution at three different sample radii.	51
5-1	Values of K_{LOD} for calculating C_{LOD}.	100
5-2	The concentration of FITC-I (limiting reagent), C_{rea}, for the reaction of 18 AAs; and the concentration of each FTC-AA, C_{inj}, being diluted with 5 mM pH 9.0 carbonate buffer for the injection, assuming that the FITC-I is completely bound to each AA.	133
5-3	Based upon figure 5-14, pH 9.0 for the electrophoresis. Retention time, tr, of each FTC-AA relative to the third blank peak; estimated sample being injected in volume, V_{inj}; in moles, $mole_{inj}$; and the theoretical plates, N; under the assumption that the FITC-I is completely bound to AA.	138
5-4	Based upon figure 5-15. The retention time, tr, of each FTC-AA relative to the third blank peak, the estimated sample being injected in volume, V_{inj}; in moles, $mole_{inj}$; and the theoretical plate, N; buffer pH	141

10 used for the electrophoresis, under the assumption that the FITC-I is completely bound to AA.

5-5 Detection limits, at three times background noise, in terms of concentration, C_{LOD}; of moles, Moles; and of molecules, Molecules injected onto the column. All these data are generated based upon figure 5-14, using pH 9.0 buffer for the electrophoresis and sheath streams under the assumption that the FITC-I is one hundred percent pure and is completely bound to AA. 144

5-6 Detection limits, at three times background noise, in terms of concentration, C_{LOD}; of moles, Moles; and of molecules, Molecules injected onto the column. All these data are generated based upon figure 5-15, using pH 10 buffer for the electrophoresis and sheath streams under the assumption that the FITC-I is one hundred percent pure and is completely bound to AA. 145

LIST OF FIGURES

NUMBER	DESCRIPTION	PAGE
1-1	The sheath-flow cuvette. The sample stream enters the top of the cuvette through a narrow diameter tube. The sheath stream enters the cuvette from the side and surrounds the sample stream. Both streams normally exit the cuvette through the waste tube at the bottom of cuvette. A drain port is provided for removal of bubbles from the flow chamber.	2
1-2	Sample stream radius at different ratios of sample flow rate, Q_{sample}, to sheath flow rate, Q_{sheath}. The right hand axis of this figure also shows that the probe volume which is produced by the intersection of the sample stream and a 10 μm spot size laser beam is within the picoliter range.	4
2-1	Refraction of light in passing from a less dense medium, n_1, into a more dense medium, n_2.	15
2-2	Schematic diagram for a laser passing through a sheath-flow cuvette. A diffraction pattern is formed at far-field detector plane.	18

2-3 Beam profile in the laser-based refractive index detection using the sheath-flow cuvette. (a) shows that when the laser beam interacts with the flow chamber walls and no sample is present, a diffraction pattern is formed in the far-field detector. (b) shcws that the far-field diffraction pattern is distorted when the sample stream and sheath are both present. 20

2-4 Experimental diagram for the laser-based refractive detection using the sheath-flow cuvette. The beam of light produced by the laser is focused with a microscope objective, passes through the cuvette, is reflected by a mirror, and propagates to a small area photodiode. 21

2-5 Beam profile for the high precision laser-based refractive index determination within picoliter volumes using flow-modulation of the sheath-flow cuvette. (a) When the valve is open, the sample does not interact with the laser beam and an unperturbed beam profile is observed. (b) When the valve is closed, the profile is established, the sample interacts with the laser, and the perturbed profile is observed. 24

2-6	Experimental diagram for the refractive index determination using flow-modulation of the sheath-flow cuvette.	26
2-7	Sensitivity vs sample flow rate for flow-modulation system, at a constant sheath flow rate of 64 ml/hr.	30
3-1	Attenuation of a quantum of light by absorbing matter.	35
3-2	Schematic energy-level diagram associated with thermo-optical detection.	36
3-3	Cross-beam thermal-optical technique.	40
3-4	Experimental diagram. The pump laser is a 2 mW helium-cadmium laser operating at 442 nm. The probe laser is a 2 mW helium-neon laser operating at 632.8 nm. The laser beams are focused with microscope objectives: a 7X lens is used to focus the probe beam and a 18X lens is used to focus the pump beam. M are mirrors, and CHOP is a mechanical chopper.	43
3-5	Plot of signal versus chopping frequency. Solid symbols indicate the pump and probe beam alignment is optimized at a low chopping frequency. Open symbols indicate the pump and probe beam alignment at a high chopping frequency.	47

4-1	Schematic energy-level diagram for a photoluminescent process.	56
4-2	Fluorescence spectra of fluorescein shown as a dotted line at λ_{ex} = 488 nm. Rayleigh scatter (not shown) occurs at the same wavelength as the excitation wavelength, 488 nm. Raman scatter from water is shown as a solid line. The band centered at about 580 nm is due to symmetric and asymmetric stretching modes of water molecules.	62
4-3	Experimental diagram for laser-induced fluorescence detection using the sheath-flow cuvette for neat sample solutions. HV is a high voltage supply, PMT is a photomultiplier tube, and DMM is a digital multimeter.	71
4-4	Diagram of the microscope for the figure 4-3.	73
4-5	Fluorescent signal vs argon ion laser power.	75
4-6	Fluorescent signal vs sample radius.	76
4-7	Detection limits vs sample radius.	78
5-1	Schematic diagram for capillary zone electrophoresis.	84

5-2	A is the chemical structure for fluorescein; B is the structure for the fluorescein-isothiocyanate (FITC)-I. Both of them have similar excitation and emission spectra.	101
5-3	Experimental diagram for laser-induced fluorescence detection using the sheath-flow cuvette for CZE.	110
5-4	Sample stream linear velocity vs. high voltage, HV, applied to the electrophoresis.	115
5-5	Sample linear velocity vs. sheath flow rate.	116
5-6	Peak height vs. voltage, HV, applied to the electrophoresis.	118
5-7	Peak height vs. sheath flow rate.	119
5-8	Electropherogram of $2.64 * 10^{-9}$ M of fluorescein injected at 3 KV for 15 s, 4.2 nl; capillary, 50 μm ID and 92 cm long; sheath stream, 5.6 ml/hr; voltage for electrophoresis is 25 KV.	122
5-9	Sample radius vs transit distance. $5.29 * 10^{-8}$ M fluorescein is continuously introduced at 25 KV for electrophoresis as a sample stream; sheath flow rates at 1.6, 6.4, and 12 ml/hr, as indicated in the figure; capillary, 50 μm ID and 99 cm long.	124

5-10 Electropherogram of 4.23 * 10^{-9} M fluorescein injected at 2 KV for 8 s, 2.2 nl; sheath; 5 mM pH 10 carbonate buffer at 0.56 ml/hr; capillary, 50 µm ID and 84 cm; voltage for electrophoresis, 25 KV. 127

5-11 Theoretical plates vs sheath flow rate. Open symbols are theoretical estimates; solid symbols are experimental results. 129

5-12 Resolution vs sheath flow rate. Open symbols are theoretical estimates; solid symbols are experimental results. 131

5-13 Electropherogram of the FITC-I blank reaction. The commercial FITC-I contains some contaminantes as can be seen in this figure. 135

5-14 Separation of between 3 and 11 attomoles of 18 amino acids. The separation is driven by a 25 KV potential and a pH 9 buffer is used for both the separation and also the sheath stream. Injection was 10 seconds at 2 KV. Peak 1 is Arg, 2 is Lys, B are peaks associated with the reagent blank, 3 is Ile, Trp, and Leu, 4 is Val, His, Phe, Tyr, Pro, and Met, 5 is Thr, 6 is Ser, 7 is Ala, 8 is Gly, 9 is Glu, 10 is Asp, and 11 is Cys. 136

5-15 Separation of between 3 and 11 attomoles of 18 amino acids. The separation is driven by a 25 KV potential and a pH 9 buffer is used for both the separation and also the sheath stream. Injection was 10 seconds at 2 KV. Peak 1 is Arg, 2 is Lys, B are peaks associated with the blank, 3 is Leu, 4 is Ile, 5 is Trp, 6 is Met, 7 is Phe, His,Val, and Pro, 8 is Thr, 9 is Ser, 10 is Cys, 11 is Ala, 12 is Gly, 13 is Tyr, 14 is Glu, 15 is Asp. 140

Appendix 1-1 159

Electropherogram of about 1.0 * 10^{-7} M of FITC-I injected at 2 KV for 10 seconds; sheath, 5 mM pH 10 carbonate buffer at 0.56 ml/hr; capillary, 50 μm ID and 97 cm long; voltage for electrophoresis, 25 KV.

Appendix 1-2 160

Electropherogram of about 1.0 * 10^{-7} M of FITC-I injected at 2 KV for 10 seconds; sheath, 5 mM pH 10 carbonate buffer at 5.6 ml/hr; capillary, 50 μm ID and 97 cm long; voltage for electrophoresis, 25 KV.

Appendix 1-3 161

Electropherogram of about 1.0 * 10^{-7} M of FITC-I injected at 2 KV for 10 seconds; sheath, 5 mM pH 10 carbonate buffer at 14 ml/hr; capillary, 50 μm ID and 97 cm long; voltage for electrophoresis, 25 KV.

Appendix 2-1 162

Electropherogram for a mixture of FTC-Gly, FTC-Pro, FTC-Met, and FTC-Tyr. B* is the third blank peak.

Appendix 2-2 162

Electropherogram for FTC-Gly. B* is the third blank peak.

Appendix 2-3 163

Electropherogram for a mixture of FTC-Tyr and FTC-Pro. B* is the third blank peak.

Appendix 2-4 163

Electropherogram for FTC-Met. B* is the third blank peak.

Appendix 2-5 164

Electropherogram for FTC-Tys. B* is the third blank peak.

Appendix 2-6 164

Electropherogram for a mixture of FTC-Trp and FTC-Val. B* is the third blank peak.

Appendix 2-7 165

Electropherogram for a mixture of FTC-Ile, FTC-Thr, and FTC-Ser. B* is the third blank peak.

Appendix 2-8 165

Electropherogram for a mixture of FTC-Leu and FTC-His. B* is the third blank peak.

Appendix 2-9 166

Electropherogram for a mixture of FTC-Ile and FTC-Ser. B* is the third blank peak.

Appendix 2-10 166

Electropherogram for a mixture of FTC-Phe and FTC-Glu. B* is the third blank peak.

Appendix 2-11 167

Electropherogram for a mixture of FTC-Arg, FTC-Ala, and FTC-Asp. B* is the third blank peak.

Appendix 2-12 167

Electropherogram for a mixture of FTC-Ile, FTC-Phe, and FTC-Cys. B* is the third blank peak.

Appendix 3 168

Electropherogram of eighteen amino acids reacted with FITC solution all at once; injection, 2 KV for 8 sec; sheath, 5 mM pH 9.0 buffer; capillary, 50 μm ID and 97 cm; voltage for electrophoresis, 25 KV. Question marks, ?, represent unidentified peaks. B* is the third blank peak.

CHAPTER ONE

INTRODUCTION

1.1. The sheath-flow cuvette

The detection of small amounts of materials in a flowing stream is of importance in a number of fields, including chromatography, flowing injection analysis, and electrophoresis (1-3). As might be expected, the design of the sample cuvette is particularly important when manipulating small volume samples. In this dissertation, the author would like to consider the sheath-flow cuvette as a detector cell which is useful in the analysis of samples ranging from a nanoliter to tens of femtoliters in volume.

In the sheath-flow cuvette, figure 1-1, a sample stream is injected into the center of a flowing sheath stream under laminar flow conditions. The process of hydrodynamic focusing occurs as the cuvette narrows to a small bore flow chamber. The sample stream retains its identity as a small stream flowing through the center of the 250 μm square chamber, surrounded by the flowing sheath stream. Many sheath-flow cuvettes use a square bore flow chamber with flat windows of good optical quality. The square bore and flat windows minimize the scatter of excitation light into the emission optics in fluorescence experiments (4). Furthermore, the

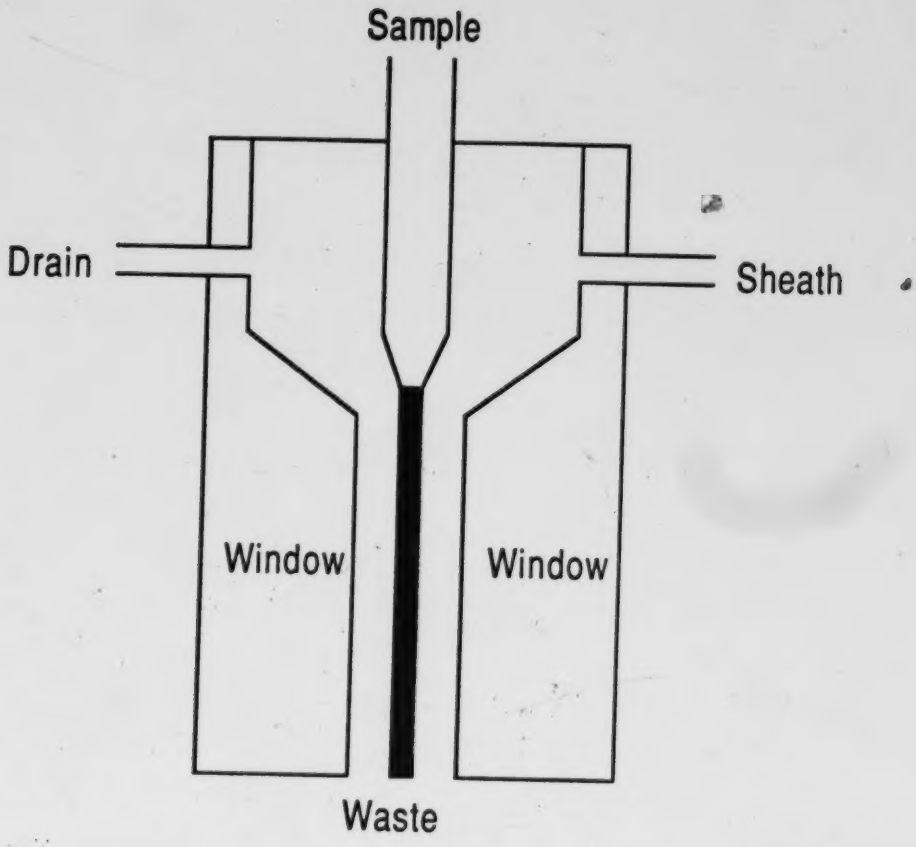

Figure 1-1. The sheath-flow cuvette. The sample stream enters the top of the cuvette through a narrow diameter tube. The sheath stream enters the cuvette from the side and surrounds the sample stream. Both streams normally exit the cuvette through the waste tube at the bottom of cuvette. A drain port is provided for removal of bubbles from the flow chamber.

sheath-flow cuvette locates the sample stream far away from the cuvette windows within a sheath stream of pure solvent. No contamination occurs inside the cuvette window if the sheath stream is flowing. Also, since the solvent and sample stream have virtually the same refractive index, the excitation beam is not scattered at the interface of the sample and sheath streams. The small amount of scatter generated by the cuvette windows is easily reduced by a spatial filter located in the emission optical path in fluorescence experiments.

The sample stream radius is a function of both the flow chamber area and the ratio of the volumetric flow rates of the sample and the sheath streams. The relationship, without considering diffusion of the analyte, is shown in the following equation which was developed by Zarrin and Dovichi (5):

$$R_S = (b/\pi^{1/2})[1 - (\frac{1}{Q_{sample} / Q_{sheath} + 1})^{1/2}]^{1/2} \qquad (1.1)$$

where R_S is the sample radius, b is the flow chamber width, and Q_{sample} and Q_{sheath} are the volumetric flow rates of the sample and sheath streams respectively.

Figure 1-2 presents the sample stream radius at different values of Q_{sample} / Q_{sheath}. The radius of the sample stream ranges from the radius of the cuvette without sheath flow to zero without sample flow. The sample

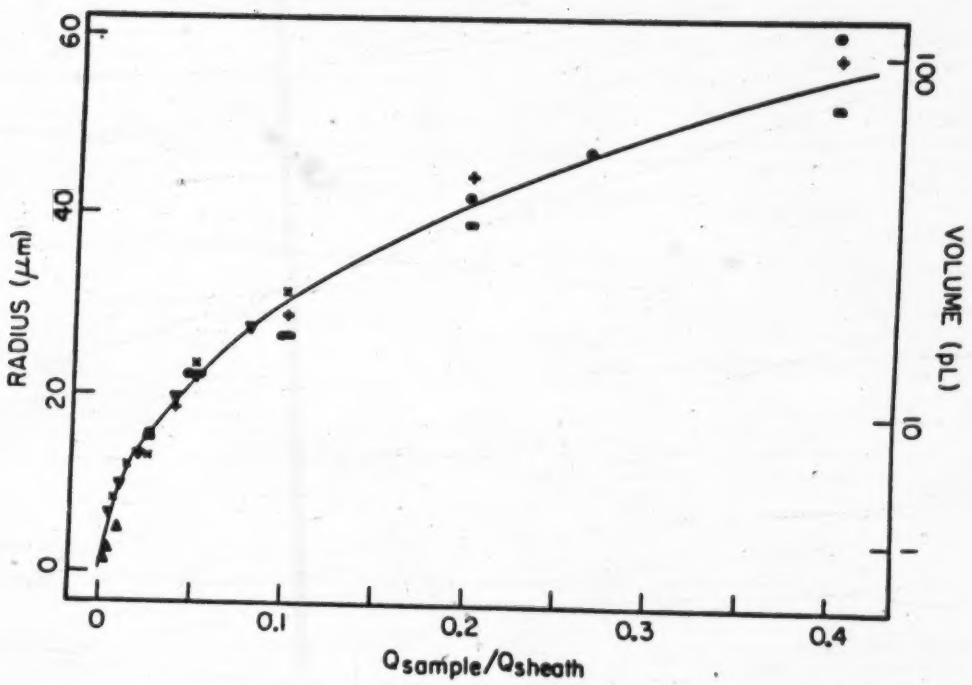

Figure 1-2. Sample stream radius at different ratios of sample flow rate, Q_{sample}, to sheath flow rate, Q_{sheath}. The right hand axis of this figure also shows that the probe volume which is produced by the intersection of the sample stream and a 10 μm spot size laser beam is within the picoliter range. (Modified from Zarrin, F.; Dovichi, N. J. *Anal. Chem*, 1985, 57, 2690)

volume produced by the cuvette and a well focused laser beam is quite small. The right hand axis of figure 1-2 shows that the probe volume which is produced by the intersection of the sample stream and a 10 μm spot size laser beam is on the order of a picoliter.

To summarize, this cuvette has three main advantages as a detector cell:

1. A very small detection volume can be easily obtained. This small volume can eliminate the detector dead volume as a factor in extra column peak spread in chromatography and electrophoresis.
2. Since the sample stream never contacts the cuvette windows, contamination of the windows is eliminated.
3. Light scatter due to the cell window can be easily eliminated because the sample stream is located far away from the windows.

The sheath-flow cuvette appears to have been utilized originally in the study of particulates for the analysis of the quality of gas masks used during World War II. A dioctyl phthalate smoke of about 0.8 μm diameter was chosen for the first experiment. The flow system was designed so that each particle had to pass through the light beam with no chance of recirculation. The stream for the smoke was surrounded by an air stream. Scattered light was detected by a photosensitive cell, producing an electrical impulse for each particle. The quality of gas masks was then determined (6).

Over the past twenty years, the cuvette has become quite popular in the

biomedical technique of flow cytometry (7-9). Here, cells, virus, or chromosomes are labeled with fluorescent dyes and passed in a dilute suspension through the focused laser beam. Light scatter and fluorescence from the particles are detected to provide diagnostic information. Applications of flow cytometry include cell sorting, cancer diagnostics, and chromosome analysis.

Analytical applications of the sheath-flow cuvette have centered upon laser-induced fluorescence detection for chromatography, for flow injection analysis elutants and for neat solutions (3,10-13). Other applications include particle size analysis by means of light scatter and concentration gradient detection by optical deflection (14-18).

Christian et al (10) used this flow cell for fluorescence detection in a chromatographic analysis in 1979. They injected 1 µl of a $4.16 * 10^{-8}$ M solution of mesoporphyrin IX dimethyl ester into a 250 mm X 3.2 mm bore column packed with 10 µm Spherisorb octadecyl silane. The fluorescent signal was collected by a microscope and focused onto a photomultiplier tube (PMT). The PMT current was then converted to voltage by a electrometer and finally recorded by a strip chart recorder. The detection limit for the chromatogram of this eluted peak was calculated to be $8 * 10^{-10}$ M at two times the background noise.

Christian and Kelly (3,11) also applied this cuvette as a detector cell for flow injection analysis in 1981 and 1982. The flow system was constructed from an air pump, loop injector, teflon and glass tubing, and a sheath-flow cell. The sheath line flowed directly into the cuvette and the

same reagent solvent proceeded via the injection loop to the reaction tube and then to the cuvette as the sample stream. Again, the fluorescent signals were collected as in the previous set up. They claimed that an injection of a 25 µl alliquot of 10^{-10} M hydrogen peroxide could be detected.

Dovichi and Zarrin (14-16) applied this cuvette for particle size analysis in 1985. In this application, the cuvette was used as a basis of a light scatter detector for counting individual particles which were eluted from a capillary column hydrodynamic chromatograph. The elution order is based upon the particle size. Concentration detection limits were about 1000 particles/ml. A right angle collection geometry detected particles as small as 45 nm radius.

Laser induced-fluorescence detection for neat sample solutions, using the sheath-flow cuvette, was approaching single molecule limits in liquids in 1984. This work was conducted by Dovichi, Keller, and others (12). Their detection limit was reported to be $8.9 * 10^{-14}$ M at two times background noise for aqueous rhodamine-6G. Three years later, single molecule detection was demonstrated by Keller et al from Los Alamos National Laboratory (13). These two experiments were similar. Dilute, aqueous solutions of highly fluorescent molecules were introduced continuously as the sample into the cuvette and a sheath stream was provided by another pump into the same cuvette to focus the sample as a narrow stream. An argon ion laser was used to excite the molecules and the fluorescent signals were collected at a right angle to the laser beam by a microscope and detected by a PMT. The main difference between these two experiments were the choice of analyte and the detection systems. Rhodamine-6G was

used as the analyte for the first experiment and a large protein molecule, phycoerthrin, containing the equivalent of 25 molecules of rhodamine-6G, was used for the latter one. A lock-in amplifier was used to demodulate the fluorescent signal in the first experiment and a photon counting system was used in the latter.

Pawliszyn (17-18) used the sheath-flow cuvette for a concentration gradient sensor for the detection of flowing sample in 1986. This concentration gradient forms the corresponding refractive index gradient $dn/dx = (dn/dc)(dc/dx)$ due to the nonuniform distribution of the sample concentration in the detector cell, which, in turn, tilts the propagation of the probe beam in the sample flow direction. The concentration detection limit was reported to be $5 * 10^{-6}$ M for a sucrose solution.

1.2. The laser

The laser is a useful light source for the analysis of small volume samples. Laser is an acronym of Light Amplification by Stimulation Emission of Radiation. As a consequence of their light amplifying properties, lasers produce spatially narrow, extremely intense beams of radiation (19-22). The process of stimulated emission produces a beam of highly monochromatic (bandwidth of 0.01 nm or less) and remarkably coherent radiation.

The conditions for coherence are : (1) the sources of radiation must have identical frequency and (2) the phase relationship across the beam must remain constant with time. Because of these properties, all of the

stimulated photons are alike in every way. They carry no information about the location of the excited atoms from which they come. Thus all of the excited atoms or molecules are functionally equivalent and the laser output radiation behaves as if it had originated from a single spot. As a result the laser beam can be focused to a very small spot, as small as half of the wavelength, $\lambda/2$. In conventional light sources, which are incoherent, light is emitted by individual atoms or molecules, and the resulting beam is the summation of countless individual events. The photons carry information about their origin. So, conventional light sources can not be focused to a small spot (23).

It is evident that laser sources can provide higher average and peak powers to a small spot compared to conventional sources. The effect is that lasers can be adapted to illuminate very small volumes, so that their power can be more effectively utilized.

Lasers have many applications in areas such as Raman spectroscopy, absorbance, fluorescence, refractive index, photothermal defraction, and electrophoresis, and have produced excellent detection limits for chemical analysis. The importance of the laser can be seen in the tremendous increase of laser utilization in research since the first paper for laser analysis was published in 1966 (24).

1.3. The thesis

It was the object of this author's research to develop a high

sensitivity, low volume detector by using the sheath-flow cuvette for analytical techniques. In this dissertation, the sheath-flow cuvette is used as the detector cell for three different analytical applications incorporating lasers as the light source.

First, as is described in chapter two, the sheath-flow cuvette is used with and without flow-modulation for refractive index (RI) measurements. Detection limits of $\Delta RI = 7 * 10^{-8}$ are produced across a 40 μm diameter sample stream. The RI detector is universal since it responds to any analyte. The only drawback of this detector is poor sensitivity.

Second, in chapter three, the cuvette is used with thermo-optical determination for absorbance measurements. Detection limits of $A = 1.1 * 10^{-5}$ are produced across a 100 to 140 μm diameter sample stream. The absorption detector is more selective and sensitive than the RI detector since certain analytes only absorb particular wavelengths.

Third, in chapter four, the cuvette is applied to fluorescence detection for neat sample solutions. Detection limits of $1.25 * 10^{-12}$ M are obtained within a 20 μm diameter sample stream. Finally, in chapter five, the cuvette is applied to capillary zone electrophoresis for fluorescence measurements. Detection limits in the order of 10^{-20} mole for separation and determination of eighteen amino acids are produced. The fluorescence detector is even more selective and sensitive because it is influenced by the choice of both the excitation and emission wavelengths

for the requirements of the fluorescent species. Fluorescence is the area that the author is most interested in.

The most important aspect of this dissertation is that it demonstrates state-of-the-art trace analysis (25) by using the sheath-flow cuvette as a detector cell. Especially, when only a minute amount of sample is available, these applications will provide very good quantitative information.

REFERENCES

1. Novotny, M. *Anal. Chem.* 1981, 53, 1294A.
2. Jorgenson, J. W.; Lukas, K.D. *Science.* 1983, 222, 266.
3. Kelly, T. A.; Christian, G.D. *Anal. Chem.* 1982, 54, 1444.
4. Lynos, J. W.; Faulkner, L. R. *Anal. Chem.* 1982, 54, 1960.
5. Zarrin, F.; Dovichi, N. J. *Anal. Chem,* 1985, 57, 2690.
6. Gucker, F. T. O'konski, C.T.; Pickard, H. B.; Pitts, J. N. *J. Am. Chem. Soc.* 1947, 69, 2422.
7. Melamed, M. R.; Mullaney, P. F.; Mendelsohn, M. L. "Flow Cytometry and Sorting", Wiley: New York, 1979.
8. Pinkel, D. *Anal. Chem.* 1982, 54, 503A.
9. Crossland-Taylor, P. J. *Nature,* 1953, 171, 37.
10. Hershberger, L. W.; Callis, J. B.; Christian, G. D. *Anal. Chem.* 1979, 51, 1444.
11. Kelly T. A.; Christian, G. D. *Anal. Chem.* 1981, 53, 2110.
12. Dovichi, N. J.; Martin, J. C.; Jett, J. H.; Trkula, M.; Keller, R. A. *Anal. Chem.* 1984, 56, 348.
13. Nguyen, D. C.; Keller, R. A.; Jett, J. H.; Martin, J. C. *Anal. Chem.* 1987, 59, 2158.
14. Zarrin, F.; Dovichi, N. J. *Anal. Chem.* 1985, 57, 1826.
15. Zarrin, F.; Risfelt, J. A.; Dovichi, N. J. *Anal. Chem,* 1987, 59, 850.
16. Zarrin, F.; Bornhop, D. J. ; Dovichi, N. J. *Anal. Chem,* 1987, 59, 854.
17. Pawliszyn, J. *Anal. Chem,* 1986, 58, 3207.
18. Pawliszyn, J. *Anal. Chem,* 1988, 60, 768.
19. Ammon Yariv, "Introduction to Optical Electronics", 2nd edition. Holt, Rinehart, Winston: New York, 1976.

20. Couillaud, B; Bellani, V. "Lasers and Applications", 1985, 4, No. 2, 91.

21. Welch, M. "Lasers and Applications", 1986 , 5, No. 1, 67.

22. Rockwell, R. J. "Lasers and Applications", 1986, 5, No. 5, 97.

23. "Optics Guide 3", Melles Griot, 1985.

24. Horrocks, D. L.; Studier, M. H. *Anal. Chem,* 1966, 1782.

25. Rogers, L. B. *Microchemical Journal,* 1986, 34, 5.

CHAPTER TWO

REFRACTIVE INDEX MEASUREMENT [1]

(Refractive Index Measurement Within The Sheath-Flow Cuvette)

1. INTRODUCTION

The refractive index, n, of a substance is defined by the ratio of the speed of light in a vacuum, c, to the speed in that particular material, v:

$$n = c/v \tag{2.1}$$

When a ray of light passes obliquely from one medium into another of different density, its direction is bent on passing through the surface. This phenomenon is called refraction and its effects can be seen when a straight stick appears to be bent when put into water. Snell's Law is the basic law of refraction:

$$n_1 \sin \theta_1 = n_2 \sin \theta_2 \tag{2.2}$$

where θ_1 is the angle of incidence and θ_2 is the angle of refraction, n_1 and n_2 are the indices of the materials. In figure 2-1, when the second medium

1. A version of this chapter has been published. Cheng, Y. F.; Dovichi, N. J. *Mikrochimica Acta*, 1986, *III*, 351.

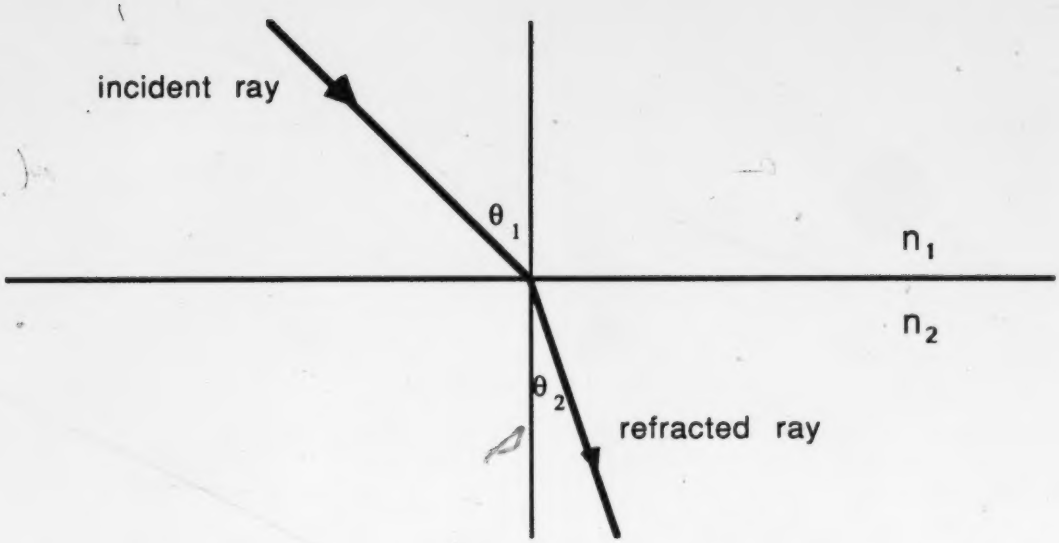

Figure 2-1 Refraction of light in passing from a less dense medium, n_1 , into a more dense medium , n_2 .

is optically denser than the first, the ray becomes more nearly perpendicular to the dividing surfaces indicated by n_1 and n_2 respectively.

The refractive index (RI) of a substance is dependent upon wavelength, pressure, and temperature (1). The variation in refractive index on wavelength is called dispersion. In the dispersion curve, near absorption bands in the ultraviolet (UV) and infrared (IR) regions of this spectrum, the refractive index changes rapidly with wavelength and changes slope. In the visible region, the refractive index gradually decreases with increasing wavelength for most substances. As long as the wavelength remains constant, the detector response will be repeatable. The wavelength dependence of refractive index is negligible if lasers are used as the light source due to their very narrow spectral band.

The refractive index of a substance increases with increasing pressure because of the accompanying rise in density. However, the effect of pressure is much less important than the temperature effect in RI measurements. The pressure coefficient, dn/dp, is in the order of 10^{-10} m^2/N for most liquids. Temperature affects the refractive index of a substance mainly due to the change in density. For many liquids, the temperature coefficient lies in the range of -4 to -6 * 10^{-4} per degree, except water with a coefficient of about -1 * 10^{-4} per degree. Clearly, temperature dependence is a serious problem in refractive index measurements. No wonder all commercial detectors are temperature thermostated (2-6).

The refraction of radiation is important in the RI detector which is a nondestructive, concentration sensitive, and bulk property chromatographic detector. This detector is of interest in the analysis of complex mixtures for all constituents and is a popular universal detector ranking second to the UV absorbance detector for liquid phase analysis. Most substances have different refractive indices so that a change in refractive index of a flowing stream may be associated with the presence of an analyte eluted in the flow system.

It is difficult to miniaturize conventional RI instruments to very small volumes. The primary drawback is the lack of sensitivity when trace analysis is desired. This chapter represents the first description of the sheath-flow cuvette as a refractive index detector of neat solutions. In a refractive index detector using the sheath-flow cuvette, a focused laser beam passes through the cylindrical sample stream at the center of the sheath-flow cuvette. The sample stream acts as a weak scatterer to produce a change in the laser beam propagation properties. Measurement of the far-field beam-center intensity provides a linear measure of the refractive index of the sample stream (7). Figure 2-2 shows the diagram for a laser passing through a sheath-flow cuvette. The beam is diffracted by the sample and cuvette. This diffraction phenomenon is similar to that of light passing through a slit.

Refractive index measurements made with most instrumental designs have high background signals. The presence of an analyte must be measured as a small change in the refractive index of the sample. The background refractive index of the solvent is important as it leads to significant

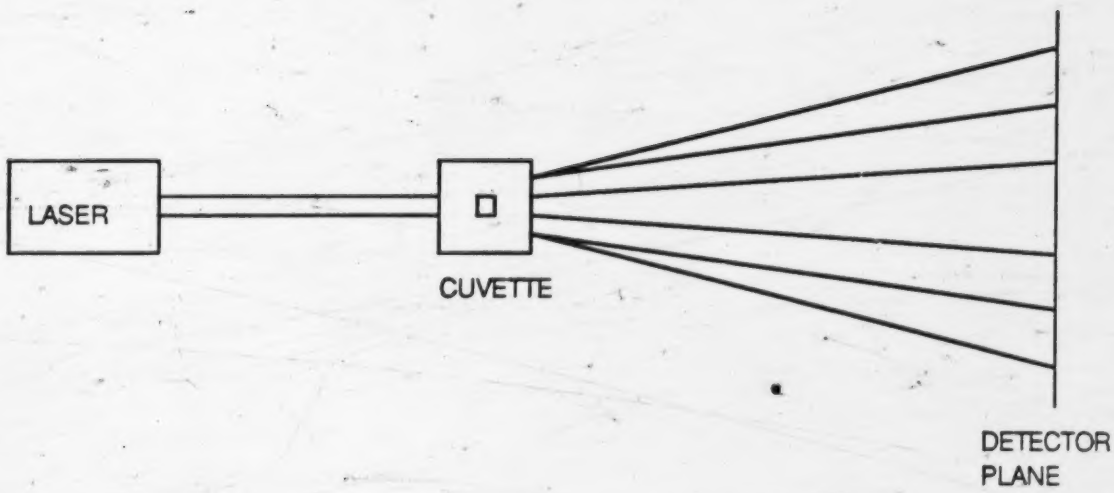

Figure 2-2. Schematic diagram for a laser passing through a sheath-flow cuvette. A diffraction pattern is formed at far-field detector plane.

sensitivity to intensity fluctuations in the light source. Since the measurement is made at low frequency, flicker noise produces a serious interference in the measurement, as shown in this chapter. It is possible to modulate refractive index measurements in the sheath-flow cuvette so that the difference in refractive index between the sample and sheath streams is measured directly (8).

In this application, a loosely focused laser beam passes through the flow chamber. Figure 2-3 (a) shows that, when the laser beam interacts with the flow chamber walls and no sample stream is present, a diffraction pattern is formed at the far-field detector which is similar to that produced by a laser beam passing through a slit. Figure 2-3 (b) shows that the far-field diffraction pattern is distorted when the sample stream and sheath streams are both present. A change in the beam-center intensity is observed and this change in the beam-center intensity is proportional to the difference in refractive index between the sample and sheath streams.

2. EXPERIMENTAL

2.1. Refractive index detection using the sheath-flow cuvette

The optical system, figure 2-4, is constructed on an optical table, NRC Model KST-48. Light from a linearly polarized, 2 mW helium-neon laser, λ = 632.8 nm, is focused with a 25-mm focal length microscope objective into the sheath-flow cuvette. The laser beam waist spot size is estimated to be

(a)

(b)

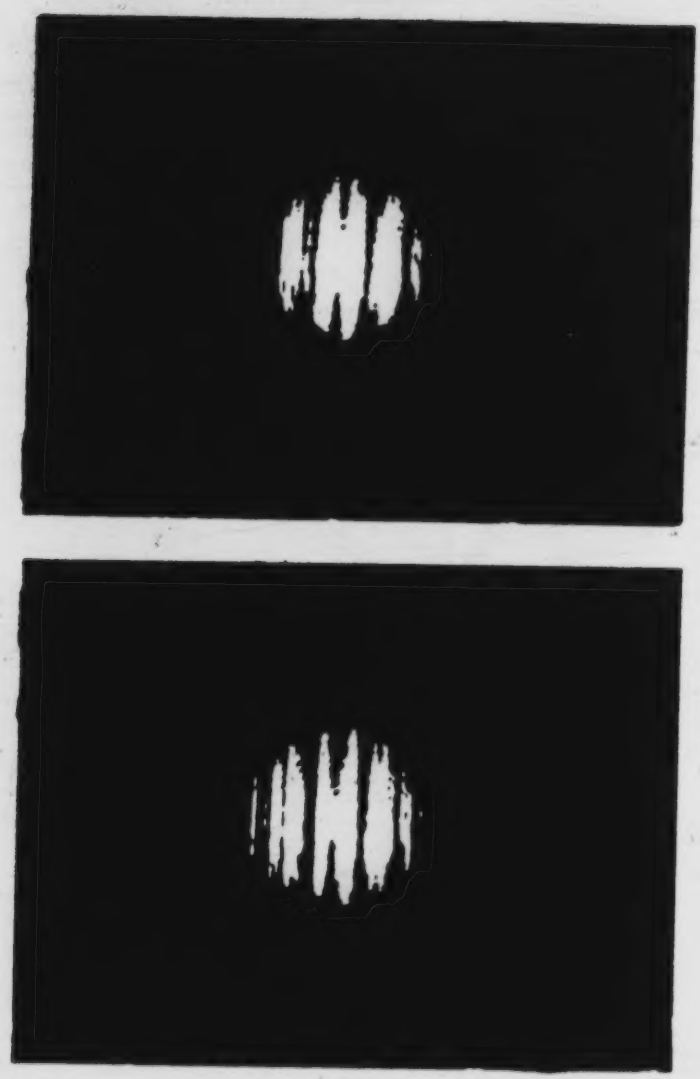

Figure 2-3. Beam profile in the laser-based refractive index detection using the sheath-flow cuvette. (a) shows that when the laser beam interacts with the flow chamber walls and no sample stream is present, a diffraction pattern is formed in the far-field detector. (b) shows that the far-field diffraction pattern is distorted when the sample stream and sheath are both present.

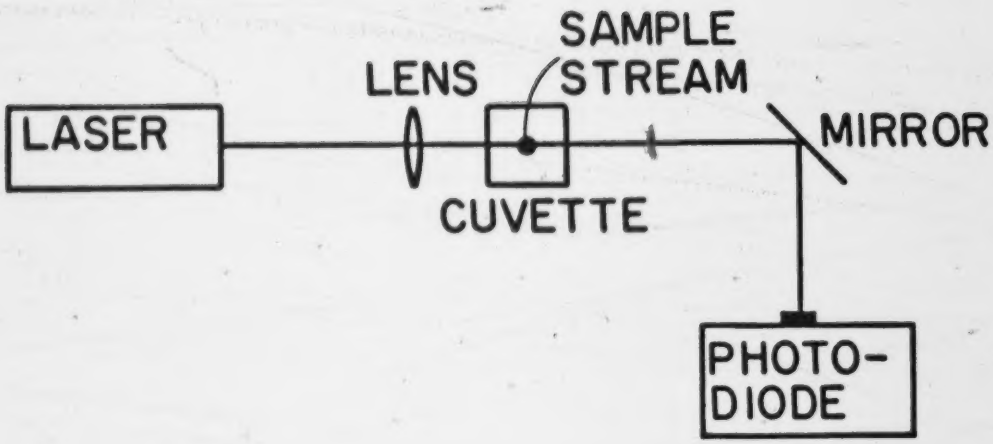

Figure 2-4. Experimental diagram for the laser-based refractive detection using the sheath-flow cuvette. The beam of light produced by the laser is focused with a microscope objective, passes through the cuvette, is reflected by a mirror, and propagates to a small area photodiode.

about 15 μm (9). The sheath-flow cuvette, Ortho Model 300-051100, has a 2 mm thick quartz chamber with a 250 μm square bore flow chamber. The cuvette is mounted on an X-Y translation stage to allow convenient alignment with respect to the laser beam. After propagating through the sample, the laser beam is reflected from a mirror and centered upon a 1 mm^2 silicon photodiode; the total optical path to the photodiode is about 50 cm.

The output of the photodiode is conditioned with a current-to-voltage converter, constructed from a JFET operational amplifier with a 100-kΩ feedback resistor in parallel with a 47-pF capacitor. The output of the current-to-voltage converter is displayed upon a digital multimeter (DMM), Keithly Model 195/1950.

The sheath stream is provided by a high pressure liquid chromatography syringe pump whereas the sample stream is provided by a low pressure syringe pump. Typical flow rates employed are 64 ml/hr for the sheath stream and 2.5 ml/hr for the sample stream. At these flow rates, the sample stream radius is estimated from simple hydrodynamic theory to be about 20 μm (10). A 0.2 μm filter is placed in the flow line to remove particles from both streams. High purity deionized water is used as both the sheath fluid and the sample solvent. Dilute aqueous solutions of methanol are used as samples.

Alignment of the system is important to obtain good results. Since the laser beam and sample stream are both quite small, it is convenient to utilize micrometer driven translation stages to align precisely the beam and stream. The cuvette is located about 15 mm past the beam waist and near the center

of the beam axis. Adjustment of the mirror allows the laser beam profile to be centered on the photodiode. Small changes in the optical configuration are made to maximize the voltage change obtained between a water sample and a low concentration methanol solution.

2.2. Flow-modulation within a sheath-flow cuvette for refractive index measurement

In the sheath-flow cuvette, a drain port is available opposite from the port used to introduce the sheath fluid into the cuvette, figure 1-1. This drain port is often used to remove bubbles which have become trapped in the flow chamber. However, we noticed that the flow profile of the sample stream becomes distorted when the drain port is opened. By connecting a small volume, high speed solenoid valve to the drain port, it is possible to modulate the flow profile of the sheath-flow cuvette. When the valve is open, the sample does not interact with the laser beam and an unperturbed beam profile is observed, figure 2-5 (a). When the valve is closed, the profile is reestablished, the sample interacts with the laser, and the perturbed profile is observed, figure 2-5 (b).

Modulation of the flow profile with the solenoid valve allows rapid switching of sample and solvent in refractive index measurements, reducing 1/f noise. Lock-in detection of the laser intensity referenced to the solenoid driving frequency allows direct measurement of the difference in refractive index of the two streams.

(a)

(b)

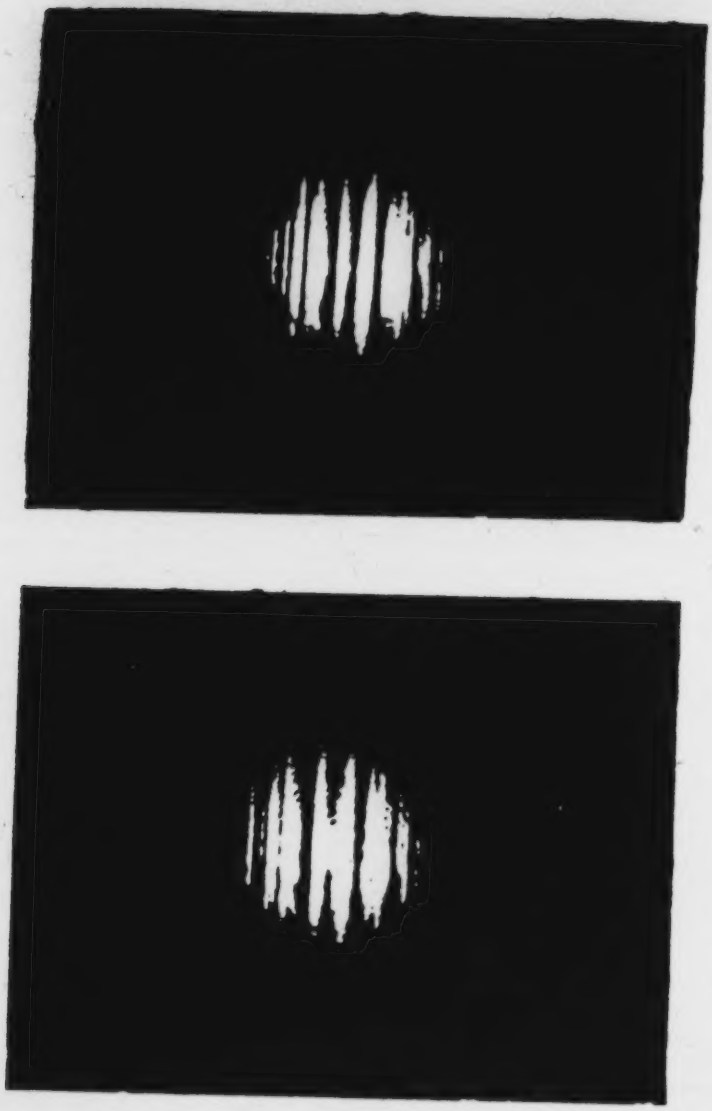

Figure 2-5. Beam profile for the high precision laser-based refractive index determination within picoliter volumes using flow-modulation of the sheath-flow cuvette. (a) When the valve is open, the sample does not interact with the laser beam and an unperturbed beam profile is observed. (b) When the valve is closed, the profile is established, the sample interacts with the laser, and the perturbed profile is observed.

The experimental diagram for the flow-modulation of the sheath-flow cuvette refractive index detector is shown in figure 2-6, which is similar to figure 2-4. The sheath stream is provided by the same high pressure syringe pump at a flow rate of 64 ml/hr whereas the sample stream is provided by a low pressure pump at a flow rate of 2.5 ml/hr. A small volume solenoid valve, the Lee Company Model LFAA1200218H, is connected to the drain of the sheath-flow cuvette. A micrometer controlled metering valve, Whitey Model 22RS2, is connected to the waste line at the bottom of the cuvette. The metering valve, which is not shown in the figure, is adjusted to provide sufficient back pressure so that flow alternates between the waste and drain lines, depending upon the state of the solenoid valve.

A 2 mW linearly polarized helium-neon laser at wavelength 632.8 nm is focused into the sheath-flow cuvette with a 25 mm focal length lens. After propagating through the cuvette, the laser beam again is reflected from a mirror and centered upon the photodiode. A function generator, Hewlett-Packard Model 3311 A, is used to drive the solenoid valve. A lock-in amplifier, Ithaco Model 393, is referenced to the function generator and is used to demodulate the photodiode output. The lock-in amplifier is operated with a 1 second time constant in the amplitude mode.

The cuvette is located about 15 mm past the laser beam focus and near the beam axis. The detector is located about 50 cm past the cuvette. The beam profile is moved across the detector face using the mirror to maximize the lock-in amplifier signal.

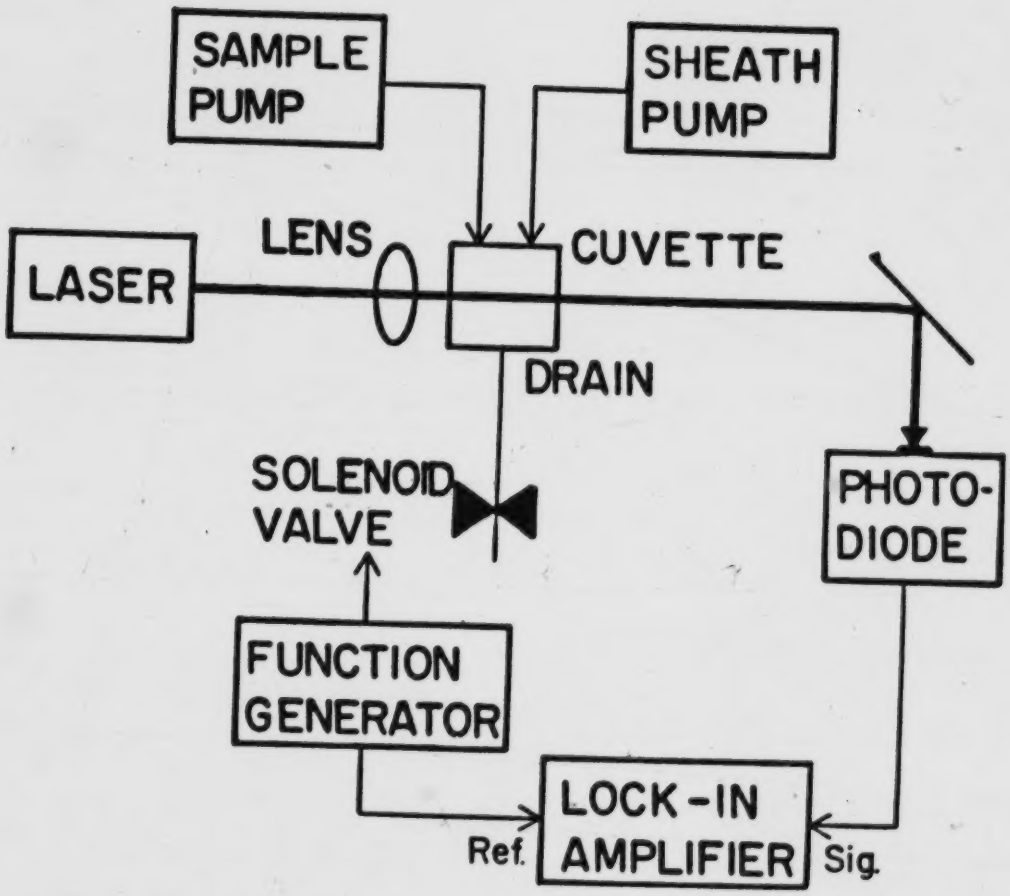

Figure 2-6. Experimental diagram for the refractive index determination using flow-modulation of the sheath-flow cuvette.

The sheath fluid is deionized water. Dilute solutions of methanol in deionized water are used as samples.

3. RESULTS AND DISCUSSION

3.1. Without flow-modulation

All commercial RI detectors are differential in operation and provide an output signal that is proportional to the difference in refractive indices of the liquid in the sample and reference cell. They are also temperature thermostated to minimize any temperature fluctuation causing a refractive index change.

In a sense, the RI detector based upon the sheath-flow cuvette is a differential system. The change in voltage observed by the detector is proportional to the difference in refractive index between the sample and sheath streams. Presumably, temperature fluctuations and other environmental factors will influence both streams by a similar amount, producing no change in signal. In fact, we did an experiment in which the local sheath stream temperature was changed suddenly from room temperature to about 0^0C. This temperature change was accomplished by placing the Teflon tube carrying the sheath stream into a vessel and then pouring ice water into the vessel in order to decrease the temperature in the tube abruptly. Normally an abrupt temperature change of this nature would result in a large refractive index change, which, in turn, would result in a large signal change from the DMM. However, in this experiment only a negligible change in voltage was

observed, suggesting immunity to temperature fluctuations. Furthermore, it may be possible to utilize the sheath-flow cuvette for refractive index detection in a gradient elution chromatographic system. If the sheath flow is derived by splitting a portion of the chromatographic mobile phase, then the sample and sheath will have similar compositions, minimizing the difference in refractive index between the two.

The RI detection using the sheath-flow cuvette produces a linear calibration curve, $r > 0.998$, with a detection limit, 2s, of $\Delta RI = 3 * 10^{-6}$. Changes in refractive index were estimated from the volume fraction of methanol in water, assuming a linear change in refractive index with volume fraction. At changes in refractive index greater than about 10^{-4}, the calibration curve deviated from linearity, demonstrating negative curvature. The detection limit appears to be a result of low frequency instability in the probe laser intensity. In fact, the detection limits correspond to a 3 parts in 10^4 stability in our laser intensity and in our electronics. Higher stability light sources are not common.

3.2. With flow-modulation

One potential improvement in the system occurs when the experiment is modulated, as shown in section 2.2. The data of the calibration curve from flow-modulation within a sheath-flow cuvette are obtained at a modulation frequency of 18 Hz. At slightly higher modulation frequencies, the modulated component of the signal rapidly dropped to zero. Presumably, at the particular flow rates employed in this experiment, the hydrodynamics of the cuvette are not able to reestablish the flow profile at modulation frequencies greater

than about 20 Hz. Occasionally, modulated signals would be observed at higher frequencies, near 100 Hz. These signals were not reproducible and appeared to be associated with acoustic resonances in the flow system.

The sensitivity of the instrument is investigated for other sample stream flow rates. The sensitivity of the instrument is observed to increase monotonically with sample stream flow rate from 0.10 to 2.5 ml/hr, at a constant sheath flow rate of 64 ml/hr. Since the sample stream radius also increases monotonically with sample stream flow rate, we observe an increase in sensitivity with an increase in sample flow rate, figure 2-7.

A linear calibration curve, $r > 0.9995$, is constructed from the detection limits (2s), $\Delta RI = 7 * 10^{-8}$, to the highest concentration sample employed, $\Delta RI = 1 * 10^{-4}$, at a sample stream flow rate of 2.5 ml/hr and a sheath stream flow rate of 64 ml/hr. Using the same instrument without modulation, detection limits are a factor of 50 poorer. Clearly, modulation of the sample stream provides significant improvement in precision of the refractive index determination.

It is interesting to compare the results of the flow-modulated sheath-flow cuvette with other techniques for refractive index measurements. High sensitivity refractive index measurements utilize an interferometer to measure refractive index changes over a relatively long optical path. For example, a laser-based refractive index detection limits of $4 * 10^{-9}$ Δ RI within a 200 μm probe volume for the Fabry-Perot interferometer(11). Although the interferometer instrument produces excellent detection limits, the sensitivity of the instrument is proportional

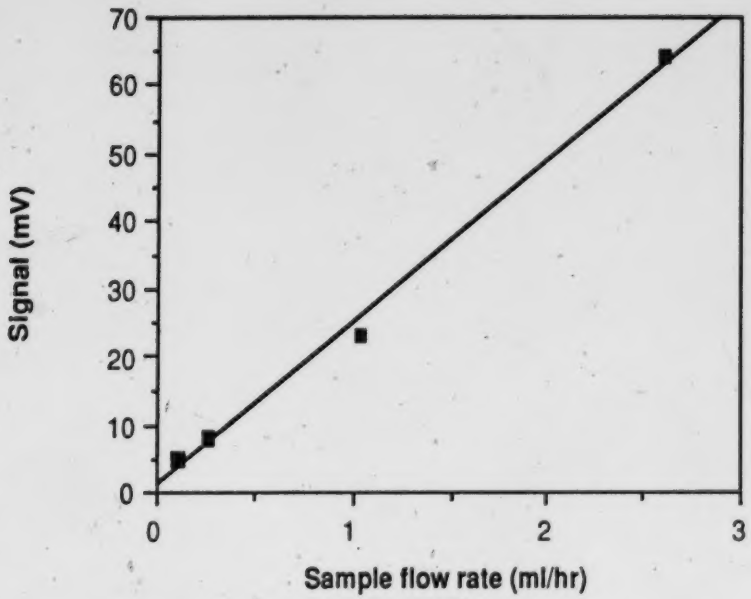

Figure 2-7. Sensitivity vs sample flow rate for flow-modulation system, at a constant sheath flow rate of 64 ml/hr.

to the path length. It is not possible to miniaturize the interferometer refractive index detector without a concomitant loss in sensitivity.

Several miniaturized refractive index detectors have been reported. A small volume Fresnel refractive index detector has been employed to produce detection limits of $2 * 10^{-7}$ ΔRI within a 1 μm flow cell (12). The interaction of a laser beam and a capillary tube has led to the development of a simple refractive index detector which produces detection limits of $6 * 10^{-7}$ ΔRI within a nanoliter cuvette (13-16).

A probe volume of about 400 pl is estimated for this experiment using the sample stream radius and the laser beam spot-size. The probe volume of the sheath-flow cuvette is better than those produced by any other refractive index measurements. Furthermore, the flow-modulated sheath-flow cuvette produces refractive index detection limits which are superior to all but the best long path length interferometric instruments. The probe volume of the sheath-flow cuvette is six orders of magnitude smaller than that of the interferometer. In terms of mass based detection limits, the sheath-flow cuvette is more than four orders of magnitude better than the Fabry-Perot interferometer.

REFERENCES

1. Presby, H. M.; Marcuse, D.; French, W. G. *Appl. Opt.* 1970, 18, 4006.
2. Bristow, P. A. "Liquid Chromatography in Practice", hetp, 1976, 134.
3. Bryne S. H. "Modern Practices of Liquid Chromatography", J. J. Kirkland, ed.; Wiley-Interscience: New York, 1971, 17.
4. Maggs, R. J. "Practical High Performance Liquid Chromatography", C. F. Simpson, ed.; Heyden: London, 1978, 276.
5. Scott, R. P. W. "Liquid Chromatography Detectors", Eslevier: Amsterdam and New York, 1977, 59.
6. Synder, L. R.; Kirkland, J. J. "Introduction to Modern Liquid Chromatography", 2nd ed.; Wiley-Interscience: New York, 1979, 140.
7. Cheng, Y. F.; Dovichi, N. J. *Mikrochimica Acta*, 1986, *III*, 351.
8. Cheng, Y. F.; Dovichi, N. J. submitted.
9. Cannon, B.; Gardner, T. S.; Cohen, D. K. *Appl. Opt.* 1986, 25, 2981.
10. Zarrin, F.; Dovichi, N. J. *Anal. Chem.* 1985, 57, 2690.
11. Woodruff, S. D.; Yeung, E. S. *Anal. Chem.* 1982, 54, 1174.
12. Wilson, S. A.; Yeung, E. S. *Anal. Chem.* 1985, 57, 2611.
13. Bornhop, D. J.; Dovichi, N. J. *Anal. Chem.* 1986, 58, 504.
14. Bornhop, D. J.; Nolan, T. G.; Dovichi, N. J. *J. Chromatogr.* 1987, 384, 181.
15. Bornhop, D. J.; Dovichi, N. J. *LC/GC,* 1986, 5, 427.
16. Bornhop, D. J.; Dovichi, N. J. *Anal. Chem.* 1987, 59, 1632.

CHAPTER THREE

ABSORBANCE MEASUREMENT

(Thermo-Optical Absorbance Determination Within The Sheath-Flow Cuvette)

1. INTRODUCTION

Refractive index detection using the sheath-flow cuvette is based upon the diffraction effect which occurs when a laser beam passes through the sample stream (1,2). If the refractive index of the sample is different from that of the sheath fluid, the sample acts as a weak scatterer to diffract light from the center of the beam profile. The change in the laser beam center intensity is linearly related to the refractive index of the sample stream for about two orders of magnitude, as discussed in chapter two.

The refractive index detector may be converted to an absorbance detector by use of the thermo-optical effect. In this absorbance detector, the sample stream is illuminated by a modulated pump laser beam. Absorbance of the pump laser beam produces a periodic temperature rise within the sample stream. Since the refractive index of most solvents changes with temperature, a second probe laser beam will periodically be diffracted by the heated sample in a manner analogous to that employed in the refractive index detector (3).

When a quantum of light impinges on absorbing matter, the photon is absorbed by the material, figure 3-1. Beer's law states the relationship between the absorbance, transmittance, and concentration as follows:

$$A = -\log T = \log P_0 / P = a\,b\,c \qquad (3.1)$$

where A is the absorbance of a solution, T is the transmission of light through the sample, P_0 is the incident light power, P is the transmitted light power, a is the molar absorptivity, b is the path length, and c is the concentration of the analyte. For very weakly absorbing material, Beer's law is approximately equal to:

$$(P_0 - P) / P_0 = 1 - 10^{-A} \approx 2.303\,A \qquad (3.2)$$

The absorbance of the sample, A, is proportional to the relative intensity change of light. Clearly, an increase in the input light power will not improve the sensitivity for transmission measurement. Fluoresence determination produces much better detection limits because the signal is proportional to the input power and not the relative intensity change. Single molecule determination has been achieved by using laser induced fluorescence (4).

To improve the detection limits for absorbance measurement, it is necessary to use an indirect measurement which is associated with the external process which occurs after absorbance of light. Figure 3-2

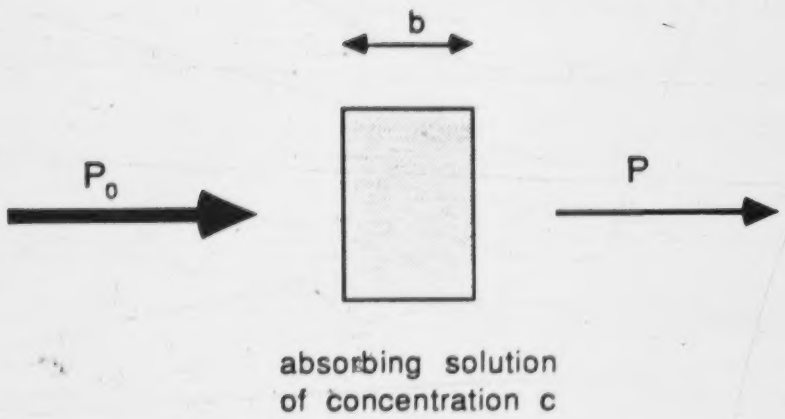

Figure 3-1. Attenuation of a quantum of light by absorbing matter.

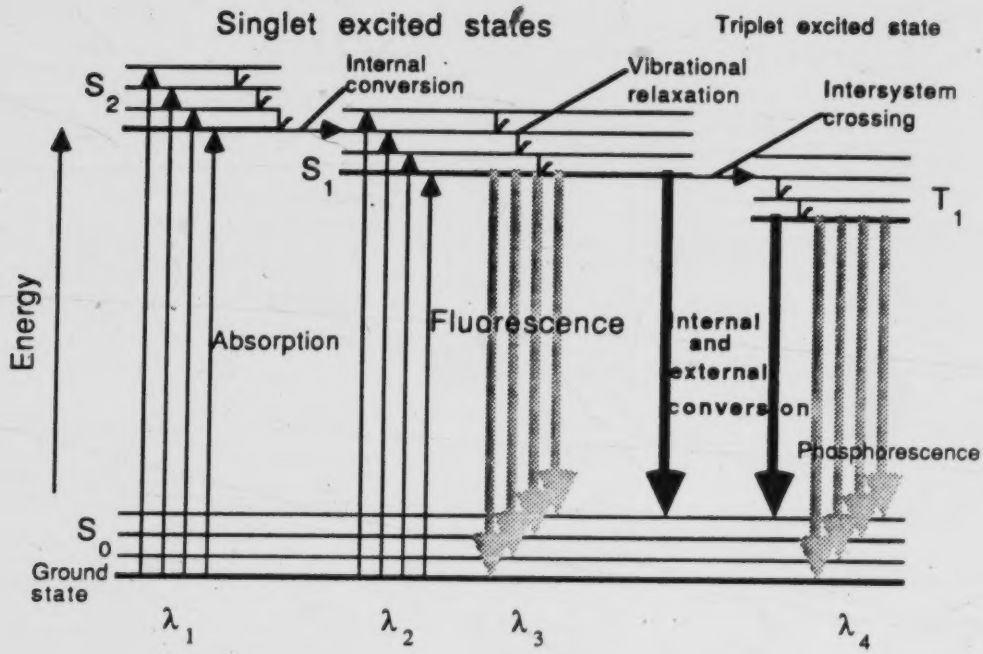

Figure 3-2. Schematic energy-level diagram associated with thermo-optical detection.

shows the schematic energy-level diagram associated with thermo-optical detection. When a quantum of light impinges on a molecule, it is absorbed in about 10^{-15} sec, and a transition to a higher electronic state takes place. This absorption of radiation is highly specific, and radiation of a particular energy is absorbed only by a characteristic structure. For organic molecules, the electron is raised to an upper excited singlet state, S_1, S_2, etc. The absorption transitions usually originate in the lowest vibrational level of the ground electronic state, as shown in figure 3-2.

An excited molecule can return to its ground state by a combination of several steps. As shown by the shaded vertical arrows in figure 3-2, two of them, fluorescence and phosphorescence, involve the release of a photon of radiation. The other deactivation steps, indicated by solid vertical arrows, are radiationless processes.

Internal conversion through overlapping vibrational levels is usually more probable than the loss of energy by fluorescence from a higher excited state. In solution, the excess vibrational energy is immediately lost as heat through collisions between the molecules of the excited species and the molecules of the solvent. This relaxation process is so efficient that the average lifetime of a vibrationally excited molecule is 10^{-12} second or less. As a consequence, fluorescence from solution almost always involves a transition from the lowest vibrational level of an excited state to the ground state. Under these conditions, the fluorescence would be of wavelength λ_3 only, regardless of whether the

excited wavelength is λ_1 or λ_2. Since the electron can return to any one of the vibrational levels of the ground state, several closely spaced peaks are produced. The fluorescence is of longer wavelength than the excitation wavelength. Typically, the lifetime of fluorescence is 10^{-7} to 10^{-9} second.

The phenomenon of phosphorescence involves an intersystem crossing, in which the spin of an excited electron is reversed and a change in multiplicity of the molecule results. Intersystem crossings are common in molecules that contain heavy atoms, for instance iodine or bromine. The presence of paramagnetic species such as oxygen in solution also enhances intersystem crossing and decreases fluorescence. Decay times of 10^{-4} to several seconds are observed in phosphorescence.

Radiationless transitions to the ground state from the lowest excited singlet and triplet states, figure 3-2, involve internal conversion and external conversion, in which deactivation of an excited electronic state involves interaction and energy transfer between the excited molecules and other solutes or the solvent. This process is responsible for the thermo-optical phenomenon.

Two common methods have been applied to improve detection limits for absorbance measurements. One is photoacoustic spectroscopy, which is a technique used to measure the sample density change produced by the temperature rise after absorbance; the other one, applied for the present work, is the thermo-optical method, which is a technique used to

measure the refractive index change produced by the temperature rise associated with absorbance (5-11).

Figure 3-3 represents one of the typical thermo-optical techniques, the cross-beam thermal lens. A pump laser beam, modulated by a mechanical chopper, intersects a coplanar probe laser beam at right angles (3). The sample absorbs energy from the pump laser beam and is heated up when the pump beam is on. The heated sample produces a refractive index change, which, in turn, acts as a diverging lens to defocus the probe beam. The center intensity of the probe beam changes periodically according to the state of the pump beam and is measured at the far field detector.

The temperature rise, ΔT, produced within a flowing sample illuminated at right angles by a short pulse of light, is given by:

$$\Delta T = \frac{2.303\ E\ a\ C}{2\pi\ k\ t_c\ (1 + 2\ t / t_c)} \exp\left\{\frac{-2\ (x^2 + [y + vt]^2)/\ \omega^2}{1 + 2\ t / t_c}\right\} \qquad (3.3)$$

where E is the laser energy, a is the analyte molar absorptivity, C is the analyte concentration, k is thermal conductivity of the solvent, x is the direction perpendicular to both the pump laser axis and flow direction, y is the direction of flow, ω is the pump laser beam spot size, and t is

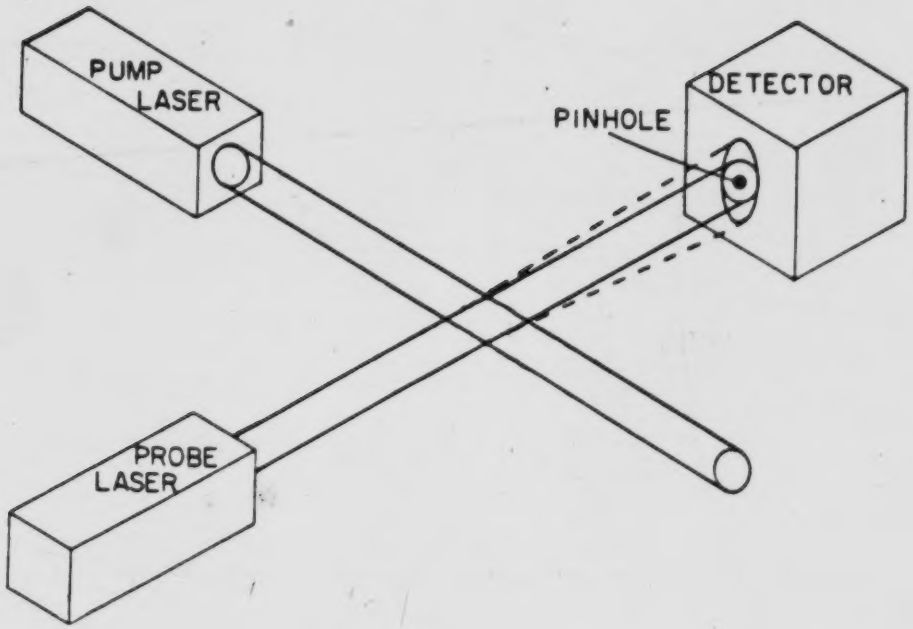

Figure 3-3. Cross-beam thermal-optical technique.

time. The thermal time constant, t_c, is given by:

$$t_c = \frac{\omega^2 \rho C_p}{4k} = \frac{\omega^2}{4D} \qquad (3.4)$$

where ρ is the sample density and C_p is specific heat (3). Equation 3.3 shows that the temperature rise is proportional to both the sample absorbance per unit length and the pump laser power. Weakly absorbing, low concentration samples may be studied by use of a high energy pump laser beam.

For a small temperature rise, the refractive index change induced by the sample absorbance is given by:

$$\Delta n = \frac{\partial n}{\partial T} \Delta T \qquad (3.5)$$

where $\partial n / \partial T$ is the change in refractive index with respect to temperature. Unfortunately, water has only a modest change in refractive index with respect to temperature; organic solvents are much more useful in thermo-optical detection. The refractive index change is localized within the sample stream and may be detected with the refractive index detector developed in chapter two.

2. EXPERIMENTAL

A block diagram of the sheath-flow thermo-optical absorbance detection is presented in figure 3-4. The experiment is constructed on a 4 X 8 foot optical table, NRC Model KST-48. A helium-cadmium laser, operating at 442 nm, provides a linearly polarized 2-mW pump beam. This beam is modulated, typically at 100 Hz, in a symmetric square wave with a mechanical chopper. A microscope cover slip is used to direct about 5 % of the pump beam intensity to a reference photodetector, described below. The main beam is then focused with an 18 X, 10-mm focal length microscope objective into the sheath-flow cuvette, Ortho Model 300-051100. The linearly polarized probe beam is provided by a 2-mW helium-neon laser operating at 632.8 nm. A polarization filter and a 1/4 wave plate are placed in the probe beam path to minimize retroreflections, originating from the sheath-flow cuvette, from returning to the laser cavity. A linear polarization filter is placed in the beam and rotated to maximize the transmitted laser intensity. A 1/4 wave plate is then placed in the beam and rotated until the retroreflection, originating from the cuvette, is extinguished upon passage through the polarizing filter. The probe beam is focused into the sheath-flow cuvette with a 7 X, 18-mm focal length microscope objective. After propagating through the cuvette, the probe beam is reflected from a mirror to a 1-mm^2 photodetector.

The reference and signal detectors are identical Valtec silicon photodiodes. The output of each diode is conditioned with a current-to-voltage converter constructed from a JFET operational

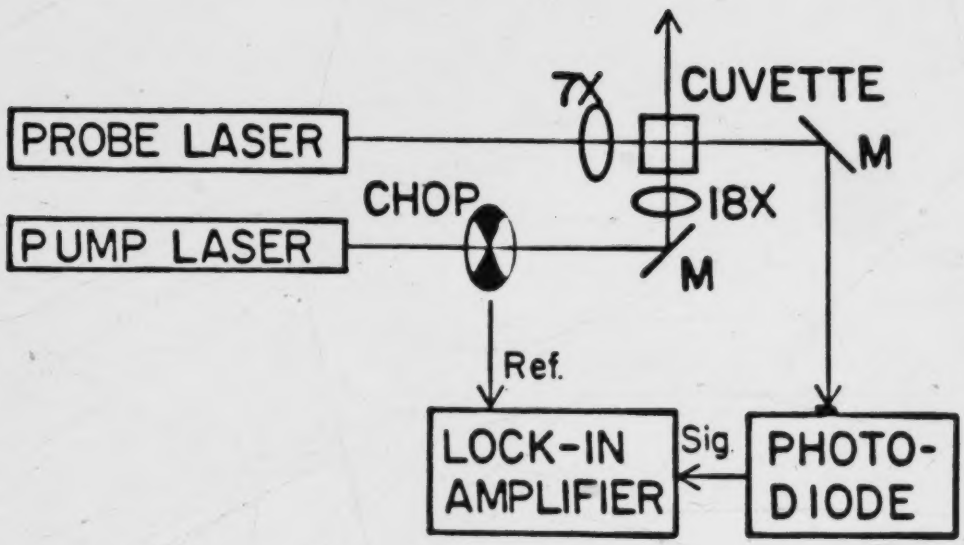

Figure 3-4. Experimental diagram. The pump laser is a 2 mW helium-cadmium laser operating at 442 nm. The probe laser is a 2 mW helium-neon laser operating at 632.8 nm. The laser beams are focused with microscope objectives : a 7X lens is used to focus the probe beam and a 18X lens is used to focus the pump beam. M are mirrors, and CHOP is a mechanical chopper.

amplifier, Linear Devices LF351, wired with a 1-M Ω feedback resistor in parallel with a 47-pF capacitor. The reference photodiode serves as a phase reference for a lock-in amplifier, Ithaco Model 3961, which is used to demodulate the absorbance signal. A one second lock-in time constant is used in all experiments. The mean and standard deviation of the lock-in signal are calculated from a set of 20 data recorded at 5 second intervals.

The sheath flow is provided by a high pressure syringe pump, Isco Model 314, and the sample stream is provided by a low pressure syringe pump, Razel Model A-99. For all of the data presented below, the sheath stream operated at a flow rate of 4.0 ml/hr. The sample stream flow rate varied from 0.2 to 3.0 ml/hr.

All chemicals are reagent grade or better. A stock solution of $2.26 * 10^{-4}$ M amaranth dye is prepared in methanol and a $2.05 * 10^{-4}$ M solution is prepared in water. Dilutions are prepared using both water and methanol. The measured molar absorptivity of amaranth, using a HP 8451A Diode Array Spectrophotometer, is $8 * 10^{3}$ L Mol^{-1} cm^{-1} at 442 nm in water.

All of the optical components used to manipulate the probe beam are fixed in space using well damped, massive fixtures which are firmly attached to the optical table. The pump laser beam focusing lens is mounted on a three axis translation stage to allow complete freedom in the location of the pump beam waist. The sheath-flow cuvette is

mounted on a two axis translation stage to allow precise location at the intersection point of the pump and probe laser beams.

The interaction of the probe beam and the cuvette produces a complicated profile, consisting of a set of light and dark fringes. These fringes are produced because the cuvette is located about a centimeter past the probe beam waist. The probe beam profile is then centered, using the mirror, onto the photodiode. The pump beam is focused into the center of the cuvette, slightly upstream from the probe beam. The position of the pump beam within the cuvette and the position of the probe beam profile with respect to the photodiode are adjusted to maximize the signal recorded by the lock-in amplifier.

3. RESULTS AND DISCUSSION

Although an impulse response model was developed in equation 3.3, the data were recorded using a chopped, cw pump laser beam. Assuming linearity with respect to pump laser energy, the change in probe beam intensity is given by:

$$\Delta I(t) = \int_0^t \Delta I_{impulse}(t - \tau)\, P(\tau)\, d\tau \qquad (3.6)$$

where $\Delta I_{impulse}$ is the time dependent change in the probe beam intensity

produced by a source of unit energy and $P(\tau)$ is the time dependent excitation function used to excite the sample. However, the time dependent thermo-optical absorbance signal is not particularly informative since a lock-in amplifier is used to demodulate the signal. Instead, the frequency dependence of the signal is of more interest since the lock-in response at frequency f may be written as the Fourier transform of the impulse response:

$$\Delta I\,(f) = f\,\{\Delta I\,(t)_{impulse}\} \qquad (3.7)$$

Although the frequency response has been solved for static samples (11-12), the response for flowing samples is more difficult and is not included here.

Thermo-optical measurements in static samples demonstrate a simple dependence upon chopping frequency (13). At low frequency, the signal is constant and at higher frequencies, the signal demonstrates an inverse dependence upon frequency. In essence, the frequency dependence of conventional thermo-optical measurements in static samples is very similar to that of a low pass electronic filter. However, the measurement in flowing samples is more interesting. Figure 3-5 presents the observed dependence of the thermo-optical signal with respect to chopping frequency. For these particular experiments, the sample stream is $2.05 * 10^{-4}$ M amaranth in water at a flow rate of 0.4 ml/hr, and the sheath stream is water at a flow rate of 4 ml/hr. For convenience, the data are presented on a log-log scale. The solid symbols

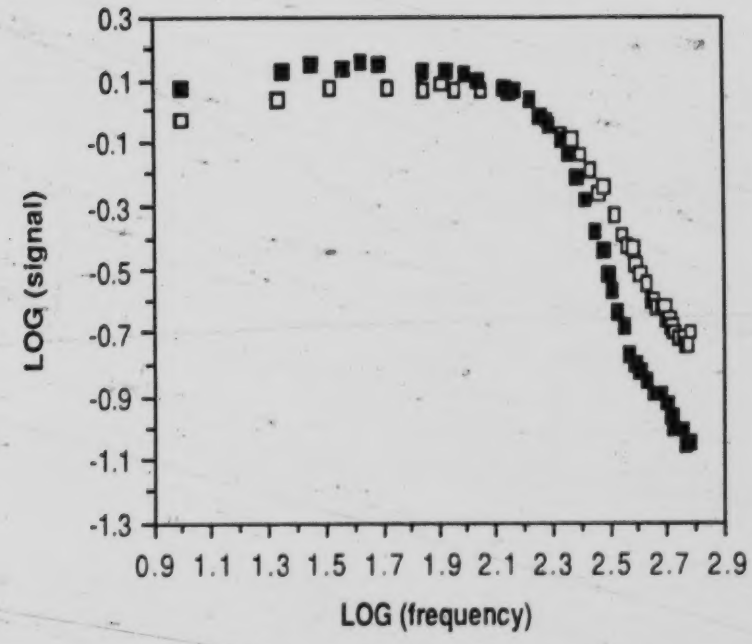

Figure 3-5. Plot of signal versus chopping frequency. Solid symbols indicate the pump and probe beam alignment is optimized at a low chopping frequency. Open symbols indicate the pump and probe beam alignment is optimized at a high chopping frequency.

indicate that the pump beam and probe beam position is optimized at low chopping frequency and then the experiment is carried out from low frequency to high frequency without adjusting the position of the two beams. First, the signal rises slightly from 10 to 50 Hz and then is essentially constant with respect to frequency up to 100 Hz. Above 100 Hz, the signal decreases precipitously. From 220 to 400 Hz, the signal demonstrates an inverse third order dependence upon chopping frequency. Above 400 Hz, the signal appears to be inversely proportional to chopping frequency. Measurements above 600 Hz are very difficult because the signal amplitude has decreased to less than 4 % of the maximum value. The chopping frequency data are influenced strongly by flow.

The open symbols indicate that the pump beam and probe beam position is maximized at high chopping frequency and then the experiment is carried out from high frequency to low frequency without adjusting the position of the two beams. First, the signal rises from 10 to 50 Hz, about 30 %, and then is essentially constant with respect to frequency up to 110 Hz. Above 110 Hz, the signal decreases constantly. In the particular data of figure 3-5, the pump beam is offset slightly upstream from the probe beam; heat flows down stream, generating the refractive index change in the vicinity of the probe beam. The very rapid decrease in signal above a critical value, between 100 Hz and 110 Hz regardless of whether the pump and probe beam alignment is optimized at a low chopping frequency or high chopping frequency, suggests that heat is not being transported efficiently between the pump and probe beams during the time period in which the pump beam illuminates the sample.

Flicker (1/f) noise dominates low frequency measurements. The relatively high frequency roll-off in the thermo-optical signal is propitious in analytical applications. As the chopping frequency approaches 110 Hz, high background noise associated with the line frequency is observed. Not surprisingly, good signal-to-noise ratio is obtained near the high-frequency cut-off of the system, typically 100 Hz, in both experiments.

In measurements of the refractive index using the sheath-flow cuvette, chapter two, the sensitivity of the measurement increased with the radius of the sample stream. Presumably, as the sample stream increased in size, it interacted with a larger fraction of the laser beam, resulting in the increased signal. The sample size is increased by either increasing the sample stream flow rate or decreasing the sheath stream flow rate. A relatively simple formula (14) may be used to estimate the sample stream flow rate based upon the ratio of the sample and sheath flow rates, equation 1.1. Similarly, the thermo-optical signal increases linearly with the sample radius. Data for the thermo-optical signal as a function of sample radius produce linear correlation coefficients ranging from 0.998 to 0.967 over the range of radii from 20 μm to 70 μm. Again, as the sample stream increases in radius, the heated sample interacts with a larger fraction of the probe beam, increasing the signal.

Calibration curves are constructed for amaranth dissolved in both methanol and water for different sample stream radii. Methanol produces better performances than water in thermo-optical measurements. In this system, samples prepared in methanol and analyzed with a pure methanol

solvent result in concentration detection limits which are an order of magnitude superior to detection limits produced for aqueous samples and water sheath stream. Interestingly, one calibration curve was constructed using water as the sheath stream and methanol as the sample stream. The detection limit is very poor for this mixed system, roughly an order of magnitude poorer than the results obtained for the aqueous sample/aqueous sheath system. Presumably, the larger refractive index difference between pure water and pure methanol resulted in increased sensitivity to noise proportional to the probe laser intensity. To obtain high precision absorbance measurements, it is necessary to utilize sample and sheath streams which are very similar in refractive index.

Detection limits obtained for the system consisting of methanol sheath/methanol sample solution are summarized in table 3-1. The calibration curves are linear, $r > 0.999$, over the concentration range studied and the concentration detection limits, 2σ, for amaranth, 1.1 to $1.6 * 10^{-7}$ M, correspond to about 10 parts per billion of analyte. Although the sensitivity and concentration detection limit of the thermo-optical technique increased linearly with sample stream radius, the absorbance detection limit, defined as the product of analyte concentration with molar absorptivity with sample stream diameter, remained constant for the three sets of data. Since the background noise increases proportionately with sample stream diameter, a noise source proportional to the sample stream absorbance must dominate the experiment. One obvious source of background noise is fluctuations in the sample stream radius; variations in sample flow rate would produce

sample[a] flow rate ml/hr	sample radius, μm	concentration[b] detection limit M	absorbance detection limit	linear correlation
1.2	50	1.6×10^{-7}	1.1×10^{-5}	0.999
2.0	61	1.3×10^{-7}	1.1×10^{-5}	1.000
2.9	69	1.1×10^{-7}	1.1×10^{-5}	1.000

a. Sample is amaranth in methanol.
And methanol sheath at a constant flow rate of 4.0 ml/hr.
b. Detection limits are measured at two standard deviations larger than the noise in the background signal.

Table 3-1. Detection limits for the system consisting of methanol sheath/methanol sample solution at three differnet sample radii.

variation in sample stream radius. As noted above, the sensitivity of the measurement is proportional to the sample stream radius. A very high precision pump may be required to drive the sample stream to produce very high precision measurements of sample absorbance.

These absorbance detection limits are very similar to those obtained for other thermo-optical absorbance detectors. For example, thermo-optical absorbance determination in a 50 μm diameter capillary tube produced detection limits which are a factor of two superior to those reported in this manuscript (15). Presumably, the rigid sample capillary tube represents a slightly better sample container than the hydrodynamic flow of the sheath-flow cuvette; also, the sheath stream helps to decrease the temperature rise in the sample stream. On the other hand, the elimination of any contamination of the sheath-flow cuvette windows will be advantageous in a number of analyses dealing with viscous or strongly adsorbing materials.

Lastly, it should be mentioned that very low power lasers were employed in this experiment. The temperature rise induced by absorbance of light is proportional to the pump laser power; use of a higher pump laser will produce a proportional increase in sensitivity (15). It is expected that a pump laser of a few hundred millwatts power will produce absorbance detection limits which are in the order of 10^{-7}. At that detection limit, absorbance by the solvent will generate a significant background signal (15). In conventional thermo-optical techniques, solvent background absorbance will produce a proportional noise source which limits the precision of the measurement; it is not

possible to measure a change in absorbance which is less than a percent of the background absorbance. If the thermo-optical signal is generated by the interface of the sample and sheath streams, then background signals produced by the temperature rise in the solvent should produce an identical refractive index change in both the sample and sheath streams. By measuring the refractive index difference between the sample and sheath streams, sensitivity to refractive index changes which are common to the two streams is eliminated.

REFERENCES

1. Cheng, Y. F.; Dovichi, N. J. *Mikrochimica Acta*, 1986, *III*, 351.
2. Cheng, Y. F.; Dovichi, N. J. submitted.
3. Dovichi, N. J. *Progress in Analytical Spectroscopy*, 1988, 11, 179.
4. Nguyen, D. C.; Keller, R. A.; Jett, J. H.; Martin, J. C. *Anal. Chem.* 1987, 59, 2158.
5. Kreuzer, L. B. *Anal. Chem.* 1974, 46, 235 A.
6. Rosencwaig, A. *Anal. Chem.* 1975, 47, 592 A.
7. Harris, J. M.; Dovichi, N. J. *Anal. Chem.* 1980, 52, 695 A.
8. Whinnery, J. R. *Acc. Chem. Res.* 1974, 7, 225.
9. Jackson, W. B.; Amer, N. M.; Boccara, A. C.; Fournier, D. *Appl. Opt.* 1981, 20, 1333.
10. Dovichi, N. J. *CRC Crit. Rev. Anal. Chem.* 1987, 17, 357.
11. Dovichi, N. J.; Harris, J. M., Los Alamos Conference on Optics '81, D. L. Liebenberg, Ed., *Proc. SPIE*, 1981, 288, 372.
12. Dovichi, N. J.; Nolan, T. G.; Weimer, W. A. *Anal. Chem*, 1984, 56, 1700.
13. Nolan, T. G.; Weimer, W. A.; Dovichi, N. J. *Anal. Chem*, 1984, 56, 1704.
14. Zarrin, F.; Dovichi, N. J. *Anal. Chem*, 1985, 57, 2690.
15. Bornhop, D. J.; Dovichi, N. J. *Anal. Chem*, 1987, 59, 1632.

CHAPTER FOUR

FLUORESCENCE MEASUREMENT (I)[1]

(Laser-Induced Fluorescence Detection Using The Sheath-Flow Cuvette)

1. INTRODUCTION

1.1. Introduction to fluorescence

When a quantum of light impinges on a molecule, it is absorbed in about 10^{-15} sec, and a transition to a higher electronic state takes place. This absorption of radiation is highly specific, and radiation of a particular energy is absorbed only by a characteristic structure. For organic molecules, the electron is raised to an upper excited singlet state, S_1, S_2, etc. The absorption transitions usually originate in the lowest vibrational level of the ground electronic state, as shown in figure 4-1.

An excited molecule can return to its ground state by a combination of several steps. As shown by the straight vertical arrows in figure 4-1, two of them, fluorescence and phosphorescence, involve the release of a photon of radiation. The other deactivation steps, indicated by dotted

1. A version of this chapter has been published. Cheng, Y. F.; Dovichi, N. J. *Fluorescence Detection II*, E. Roland Menzel, Editor, Pro. EPIE 1988, *910*, 112.

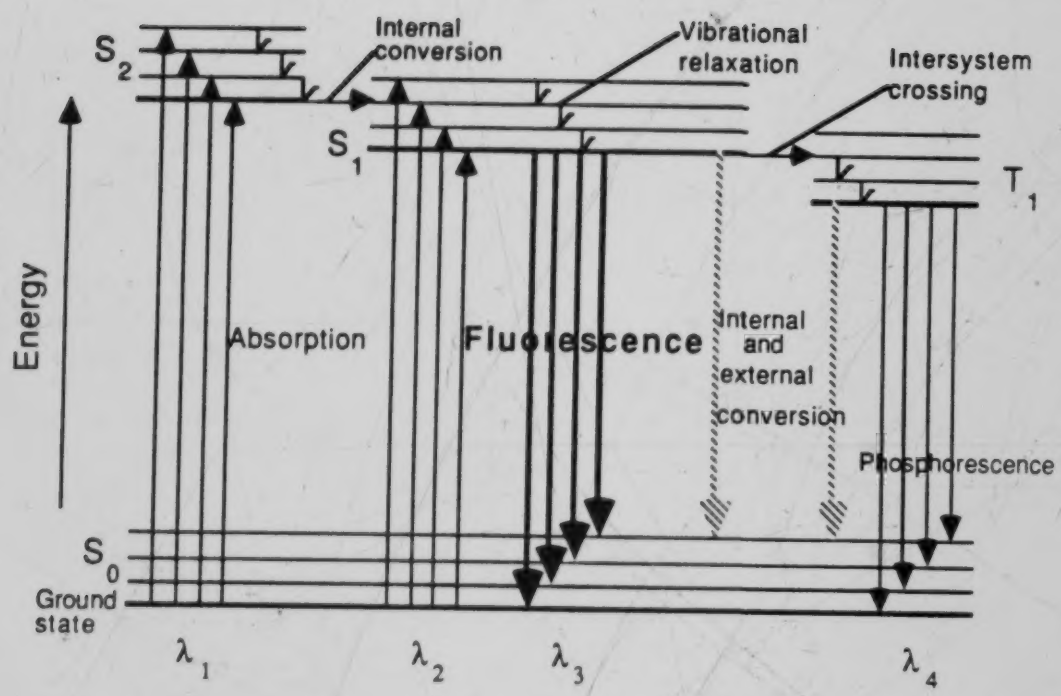

Figure 4-1. Schematic energy-level diagram for a photoluminescent process.

arrows, are radiationless processes, responsible for the thermo-optical measurement of chapter three.

Internal conversion through overlapping vibrational levels is usually more probable than the loss of energy by fluorescence from a higher excited state. In solution, the excess vibrational energy is immediately lost as heat through collisions between the molecules of the excited species and the molecules of the solvent. This relaxation process is so efficient that the average lifetime of a vibrationally excited molecule is 10^{-12} second or less. As a consequence, fluorescence from solution almost always involves a transition from the lowest vibrational level of an excited state to the ground state. Under these conditions, the fluorescence would be of wavelength λ_3 only, regardless of whether the excited wavelength is λ_1 or λ_2. Since the electron can return to any one of the vibrational levels of the ground state, several closely spaced peaks are produced. The fluorescence is of longer wavelength than the excitation wavelength. Typically, the lifetime of fluorescence is 10^{-7} to 10^{-9} second.

The phenomenon of phosphorescence involves an intersystem crossing, in which the spin of an excited electron is reversed and a change in multiplicity of the molecule results. Intersystem crossings are common in molecules that contain heavy atoms, for instance iodine or bromine. The presence of paramagnetic species such as oxygen in solution also enhances intersystem crossing and decreases fluorescence. Decay times of 10^{-4} to several seconds are observed in phosphorescence.

Radiationless transitions to the ground state from the lowest excited singlet and triplet states, figure 4-1, involve internal conversion and external conversion, in which deactivation of an excited electronic state involves interaction and energy transfer between the excited molecules and other solutes or the solvent.

1.2. Fluorescence quantum yield

Every fluorescent molecule possesses a characteristic property that is described by the quantum yield, or quantum efficiency, Φ, which is defined by:

$$\Phi = \frac{\text{number of molecules that fluoresce}}{\text{total number of excited molecules}} \qquad (4.1)$$

The higher the value of Φ, the greater the fluorescence of a compound.

1.3. Fluorescence intensity and concentration

The relation between fluorescence intensity, F, and concentration, c, is given by:

$$F = I_0 \Phi (1 - 10^{-abc}) \qquad (4.2)$$

where Φ is the quantum yield, I_0 is the incident radiation power; a and c are the molar absorptivity and concentration of the molecules, respectively; b is the path length of the cell; and abc is the absorbance A.

This equation indicates that there are three factors other than concentration that affect the fluorescent intensity:

1. The quantum yield, Φ. The greater the value of Φ , the higher will be the fluorescence, as discussed in the previous section.
2. The intensity of incident radiation. A more intense source will yield higher fluorescence as long as neither photodecomposition nor saturation of the sample occur.
3. The molar absorptivity of the fluorescent molecules. In order to emit radiation, a molecule must first absorb radiation. The higher the absorptivity, the greater will be the fluorescent intensity of the compound.

For very dilute solutions, $abc \approx A < 0.05$, equation 4.2 reduces to:

$$F = K I_0 \Phi abc \qquad (4.3)$$

where K is an instrumental constant to handle instrumental artifacts and the fact that fluorescence will emit in all directions but will be viewed

only through a limited aperture. Thus, for very dilute solutions, the fluorescent intensity is proportional to the concentration and pathlength.

1.4. Excitation spectrum and emission spectrum

All fluorescent molecules have two characteristic spectra: the excitation spectrum, which is due to the relative efficiency of different exciting radiation wavelength, and the emission spectrum, which is due to the relative intensity of radiation emitted at various wavelengths.

The shape of the excitation spectrum should be identical with that of the absorption spectrum and independent of the wavelength at which fluorescence is measured. The emission, or fluorescence, spectrum of a compound results from the reemission of radiation absorbed by that molecule. The quantum yield and shape of the emission spectrum are independent of the excitation wavelength. If the exciting radiation is not at the maximun excitation wavelength, less radiation energy will be absorbed and hence less fluorescence will be emitted.

The excitation and emission spectra will be approximate mirror images of each other. Fluorescent peaks other than the mirror image of the excitation spectrum indicate scatter, the presence of impurities, or a significant geometry change from the ground to excited state.

Transmission of radiation in matter can be pictured as a momentary retention of the incident energy, which causes a momentary polarization of the matter. Polarization is then followed by reemission of radiation in

all directions as the matter returns to its original state. This emitted light is called Rayleigh scatter (1) and occurs at all wavelengths. Its intensity varies as the fourth power of the frequency, so its effect can be minimized by choosing longer excitation wavelengths. Another type of scattering emission is Raman scatter (2-4). Raman scatter differs from Rayleigh scatter in that the scattered radiation suffers quantized frequency changes. These changes are due to the vibrational energy level transitions occuring during the polarization process. These bands are due to vibrational energy being subtracted from, or added to, the excitation photon. The Raman scattering intensity is much weaker than Rayleigh scattering, but becomes significant when high intensity sources are used.

The relationship between the fluorescent band and Rayleigh and Raman scattering is shown in figure 4-2 for fluorescein. The excitation wavelength is at 488 nm. The fluorescent signal for fluorescein is shown by a dotted line and Raman scatter for water is shown by a solid line. The Raman scatter is centered at about 580 nm due to symmetric and asymmetric stretching modes of water (5). The Rayeigh scatter occurs at the same wavelength as the excitation wavelength, 488 nm.

1.5. Structure effects

In general, strongly fluorescent molecules are governed by the following factors:

1. Because fluorescence is simply the reverse of absorption, it follows that the more probable the absorption transition, the more

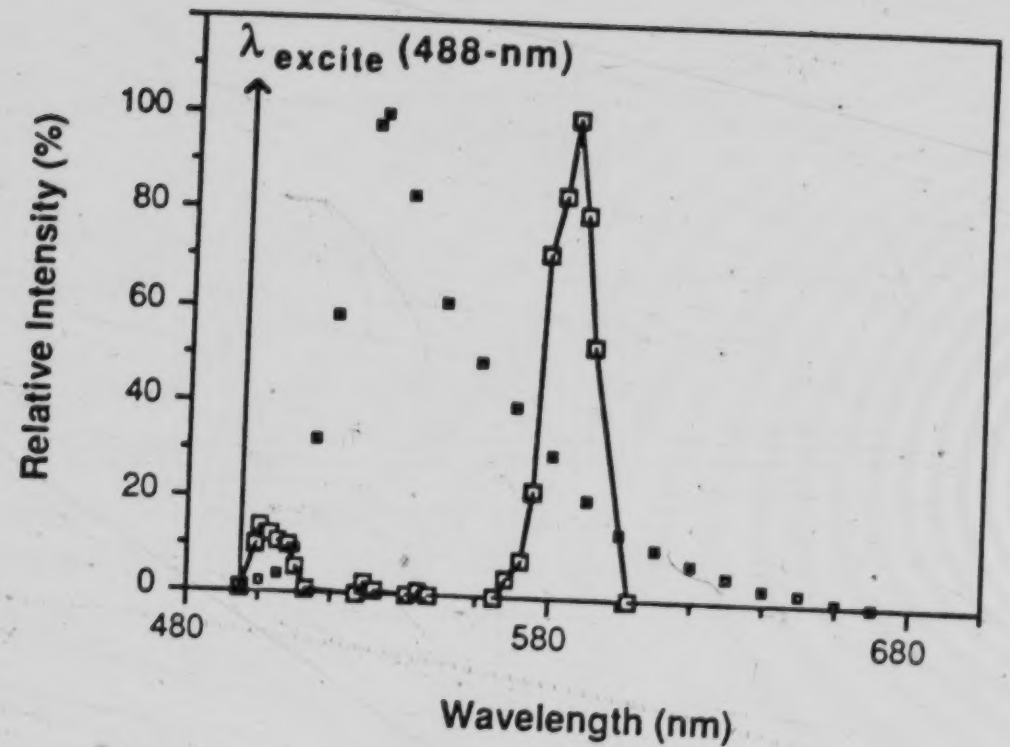

Figure 4-2 Fluorescence spectra of fluorescein shown as a dotted line at λ_{ex} = 488 nm. Rayleigh scatter (not shown) occurs at the same wavelength as the excitation wavelength, 488 nm. Raman scatter from water is shown as a solid line. The band centered at about 580 nm is due to symmetric and asymmetric stretching modes of water molecules.

(Modified from Walrafen, G. E. *J. Chem. Phys.* 1964, 40, 3294)

probable will be the fluorescence transition.

2. The power of the incident radiation should be reasonably high, as long as no photo-dissociation occurs.

3. The electron that is promoted to a higher level in the absorption transition should be located in an orbital not strongly involved in bonding. Otherwise, bond dissociation may occur.

4. The molecule should not contain structural features or functional groups which increase the possibility of radiationless transitions.

In saturated hydrocarbons there are no π-bonding or nonbonding electrons; thus all electronic transitions involve σ-bonding electrons. These transitions involving σ electrons occur at very high energies and significantly disrupt bonding in the molecule. In many aromatic molecules, excitation of the first (π, π^*) singlet is strongly allowed (molar absorptivity, a, > 10^4), whereas population of the (n, π^*) singlet is forbidden (a is only about 10^2). Also, energy differences between the first excited singlet and the lowest triplet are frequently much larger for (π, π^*) than for (n, π^*) transitions. This energy difference increases the intersystem crossing and decreases the fluorescent intensity.

In summary, aromatic hydrocarbons are often very intensely fluorescence.

1.6. Environmental effects

Environmental factors can strongly influence the fluorescent intensity. The effects of some of these variables are considered briefly in this section.

a. Temperature and solvent effects

The quantum yield of fluorescence by most molecules decreases with increasing temperature because the increased frequency of collisions at elevated temperatures improves the probability for deactivation by external conversion. A decrease in solvent viscosity also increases the external conversion and leads to the same result.

In most polar molecules the excited state is more polar than the ground state. Hence an increase in polarity of the solvent produces a greater stabilization of the excited state than of the ground state. Consequently, a shift in both absorbance and fluorescence spectra to longer wavelength (red shift), or lower energy, is usually observed as the dielectric constant of the solvent increases.

Heavy atom solvents usually induce a significant decrease in fluorescence quantum yields and a concomitant increase in the $S_1^* \rightarrow T_1^*$ intersystem crossing (6-7) due to orbital spin interactions, resulting in an increase in the rate of triplet formation.

b. pH efects

The fluorescent spectra of most aromatic compounds containing acidic or basic functional groups are sensitive to the pH of the solvent. Both the wavelength and the emission intensity are likely to be different for the ionized and nonionized forms of the compound. For instance, the pKa of 2-naphthol is about 9.5 at the ground state. In the pH range in which neutral 2-naphthol (HFl) is the predominant form, Guilbault (8) represented the overall excitation reaction sequence as follows :

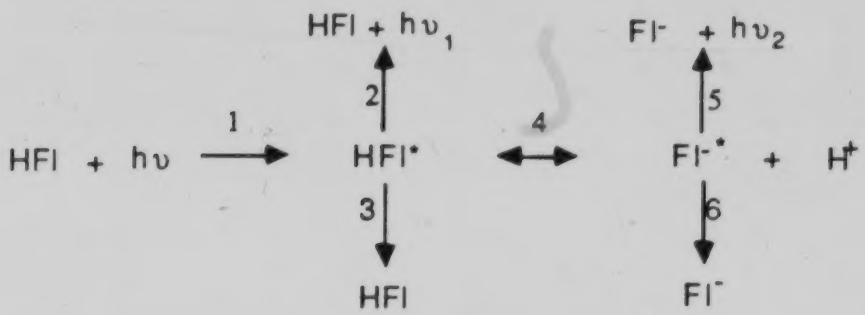

The steps in this reaction sequence were explained as follows :

1. Absorption of radiant energy to produce the excited molecule. In this case, the neutral molecule form, HFl, predominates at pH < 9.5.
2. Deactivation of the excited molecule molecule, HFl*, by molecular fluorescence at 359 nm.
3. Radiationless deactivation of the excited neutral molecule.
4. Dissociation of the excited molecule, producing a proton, H^+, and an excited anion, Fl^{-*}.

5. Deactivation of the excited anion, FI^{-*}, by fluorescence at 429 nm.
6. Radiationless deactivation of the excited anion.

Thus, knowledge of the equlibrium constants for excited state protolysis, coupled with knowledge of the relative fluorescence efficiencies of the two protic forms, can be great value in enhancing the fluorescent sensitivity (9).

c. Quenching effects

An excited fluorescent molecule may lose part or all of its excitation energy, without emission radiation, in a collision with another molecule. This process is called quenching. Fluorescence quenching, by a dissolved O_2 molecule for instance, can be a serious problem.

Mechanisms which have been proposed for the quenching of excited-singlet states by O_2 are the following (10):

1. Chemical oxidation of excited singlet:

$$^1A^* + O_2 \rightarrow A^+ + O_2^-$$

2. Energy transfer from $^1A^*$ to O_2:

$$^1A^* + {}^3O_2 \rightarrow {}^3A^* + {}^1O_2^*$$

$$^1A^* + {}^3O_2 \rightarrow {}^1A + {}^1O_2^*$$

3. Enhanced intersystem crossing in $^1A^*$:

$$^1A^* + {}^3O_2 \rightarrow {}^3A^* + {}^3O_2$$

4. Enhanced internal conversion in $^1A^*$: $^1A^* + {}^3O_2 \rightarrow {}^1A + {}^3O_2$

5. Formation of a complex between O_2 and the ground state ^1A.

The promoted intersystem crossing and conversion of the excited molecule to the triplet state in the presence of oxygen is the only plausible general oxygen-quenching process (11).

1.7. Background signal in laser induced fluorescence

Laser induced fluorescence (LIF) is known for the production of superior detection limits in chemical analysis; the capabilities of LIF extend to the ultimate quantitative limit of single molecule detection (12-13). The excellent detection limits for fluorescence arises because the signal is observed on a very small background so that high excitation intensity may be employed without a significant increase in background signal and noise.

However, nature conspires never to produce a zero background signal. Sources of background signal in fluorescence measurement have been listed by Parker: solvent (and solvent impurity) fluorescence, solvent Raman and Raleigh scatter, window fluorescence, and window Raman and Rayleigh scatter (14) .

Solvent fluorescence is minimized by an appropriate choice of excitation wavelength. For example, no common solvent produces fluorescence upon excitation in the visible portion of the spectrum since

common solvents generate no electronic absorbance in this portion of the spectrum. Solvent impurity fluorescence is eliminated by use of solvents with the highest purity (15).

Solvent Raman and Rayleigh scatter may be minimized by two approaches, one simple and one complex. Rayleigh scatter is generated at the excitation wavelength and may be reduced by over 5 orders of magnitude by appropriate colored glass (or low fluorescence plastic) filters. Similarly, Raman scatter is minimized by appropriate band pass filters, usually constructed from combinations of colored glass and long-wavelength cut-off interference filters. Ideally, analyte fluorescence undergoes a larger Stoke's shift than the highest energy Raman band of the solvent; a simple colored filter is sufficient to reject the scattered light while passing the fluorescence. More generally, Raman scatter overlaps to some extent with fluorescence; a compromise must be made between passing fluorescence and rejecting solvent scatter.

Time gated detection is a more complicated technique for the reduction of Raman and Rayleigh scatter (16). In time gating, light from a pulsed excitation source, usually a mode-locked laser, is used to excite the sample. A fast discriminator rejects photons that are produced coincidentally with the laser pulse, but passes photons produced after the laser pulse. Raman and Rayleigh scatter are instantaneous processes and fluorescence has a finite lifetime as mentioned in section 4.1; time gating decreases the background signal by several orders of magnitude.

Light scatter and fluorescence from the cuvette window may be minimized entirely by use of a windowless cuvette (17). Here, a drop of analyte is formed between the exit of a flow tube and a rod placed a small distance from the tube. Without windows, neither fluorescence nor Raman scatter are generated in the cuvette. Unfortunately, the flowing droplet design suffers two disadvantages. First, the shape of the drop changes with variations in both surface tension and viscosity of the solvent. Because the fluorescence is imaged through the curved surface of the drop, changes in the drop shape produce a corresponding defocusing of the detector system. A second and more important limitation of the flowing drop design is also associated with the curved air to droplet interface. The surface acts to scatter excitation light in a fan about the plane perpendicular to the surface of the drop. This scattered light is a significant source of background signal and is difficult to eliminate completely with spectral filtering.

The sheath-flow cuvette may be used to eliminate background signals associated with the cuvette window (13, 18-21), figure 1- 1. In this cuvette, a sample stream is injected at low flow rates into the center of a flowing sheath stream in narrow, typically 250 μm square, flow chamber. The sample stream retains its identity as a narrow stream flowing in the center of the chamber, surrounded by flowing sheath fluid. A simple mask may be utilized to restrict the field of view of the detector to the illuminated sample stream, reducing the background signal associated with the windows. Furthermore, since the sample and sheath streams have virtually identical refractive indexes, no light

scatter signal is associated with the intersection surface of the two streams.

2. EXPERIMENTAL

2.1. Instrumental

The experimental configuration of laser-induced fluorescence using the sheath-flow cuvette for neat sample solutions is shown in figure 4-3. An argon ion laser usually produces a one watt beam in the light regulated mode at 488 nm. This beam is focused with a 18 mm focal length lens (7x) into the center of the sheath-flow cuvette, Ortho Model 300-051100. The sheath stream is introduced by a high pressure chromatography syringe pump, Isco Model 314, whereas the sample stream is provided by a low pressure syringe pump, Razel Model A-99.

The fluorescent signal is magnified at right angles with a microscope (described in detail later) and then detected by the 1P28 photomultiplier tube (PMT). The output of the PMT is then displayed on a digital multimeter (DMM), Keithly Model 195/1950. The dotted line represents a black box employed to minimize the introduction of any stray light or room light to the PMT. The cuvette, microscope and PMT are mounted on the two or three dimensional micrometer translation stages to allow convenient alignment.

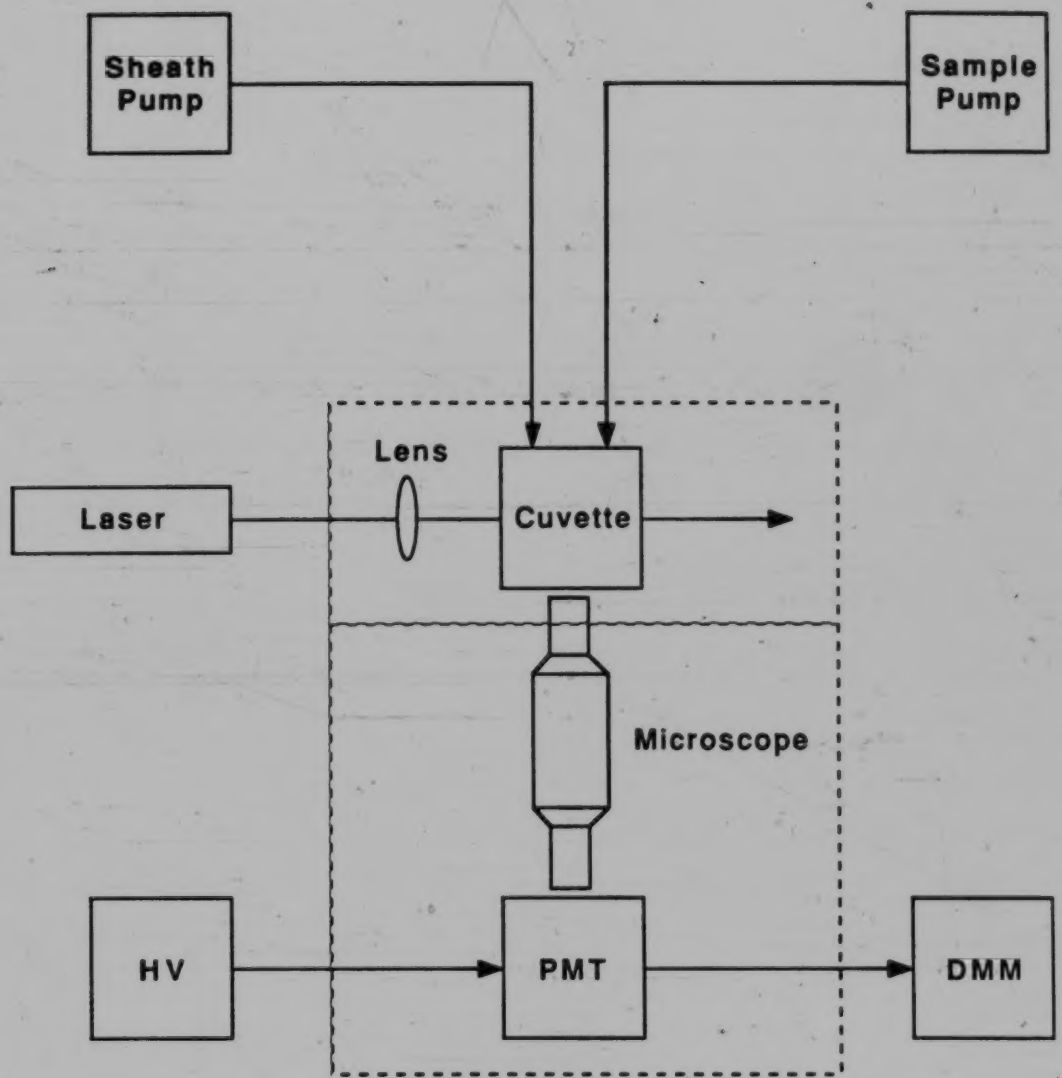

Figure 4-3. Experimental diagram for laser-induced fluorescence detection using the sheath-flow cuvette for neat sample solutions. HV is a high voltage supply, PMT is a photomultiplier tube, and DMM is a digital multimeter.

The configuration of the microscope is shown in detail in figure 4-4. It has a 16 mm focal length microscope objective (18x, 0.45 N.A.), Melles Griot, and a 20x microscope eyepiece. Two filters are placed in the optical train after the objective: a 500 nm long wavelength pass colored glass filter (Schott glass type GG 495) and a 560 nm short wavelength pass interference filter (Ealing 35-5404) to reduce Raman and Rayleigh light scatter from the solvent, discussed in section 1.4 and 1.7. A 200 μm radius pin hole is placed in the reticle position of the eyepiece to block scattered light from the cuvette walls and to maximize the ratio of fluorescence from the molecule to the background signal in the probe volume.

2.2. Chemicals

All chemicals are reagent grade or better. A stock pH 7, 0.02 M phosphate buffer solution is prepared in water which is doubly distilled, deionized, and filtered through a 0.2 μm millipore prior to use. Stock solutions of pH 8.6, 0.2 M carbonate buffer are prepared in the above water. All buffer solutions receive two drops of chloroform to prevent them from growing bacteria. Also, a stock solution of $5.29 * 10^{-7}$ M fluorescein in pH 7.0 phosphate and a stock solution of $4.24 * 10^{-8}$ M FITC-I in pH 8.6 carbonate buffer solution are prepared.

3. RESULTS AND DISCUSSION

To characterize this instrument, neat sample solutions, FITC-I in

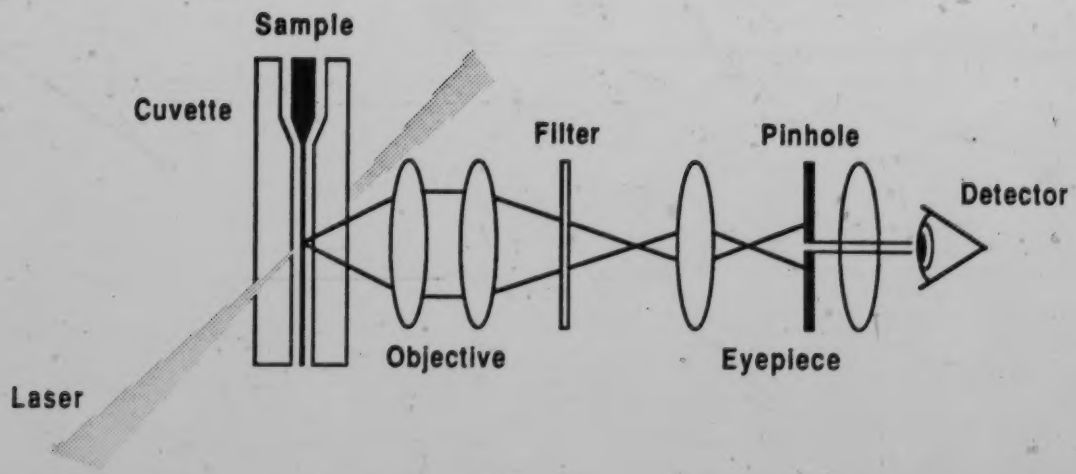

Figure 4-4. Diagram of the microscope for the figure 4-3.

0.2 M pH 8.6 carbonate buffer solution or fluorescein in 0.01 M pH 7.0 phosphate buffer solutions, are introduced into the sheath-flow cuvette by a low pressure pump and a sheath stream is introduced by a high pressure syringe pump.

Figure 4- 5 shows the fluorescent signal at different argon ion laser powers. The sample stream, which is $4.24 * 10^{-10}$ M FITC-I in 0.2 M pH 8.6 carbonate buffer solution, is kept flowing by a low pressure syringe pump at 1.2 ml/hr, with a sheath stream flow rate at 36 ml/hr. The signal is linearly proportional to the laser power from 0.4 watt to 1.2 watt, which is consistent with equation 4-3 and indicates that the fluorescent signal is proportional to the intensity of incident radiation. The abrupt increase in signal when the laser power is beyond 1.2 watts may be due to a change in the beam position, increasing light scatter. For prolonged performance of the laser and to prevent photodecomposition or increased scatter light, all the following experiments are performed at 1 watt. The non-zero intercept is due to PMT dark current.

Figure 4-6 presents the fluorescent signal at different sample radii based upon estimates from simple hydrodynamic theory, equation 1-1. The sample stream is $4.24 * 10^{-9}$ M FITC-I in 0.2 M pH 8.6 carbonate buffer at different flow rates ranging from 0.4 ml/hr to 4.1 ml/hr, and the sheath stream is kept constant at 36 ml/hr. The signal increases linearly from zero radius to about 25 μm radius and then reaches a plateau. That the fluorescent signal increases with the sample radius agrees with equation 4.3, indicating that the fluorescent signal is proportional to pathlength. At sample radii beyond 25 μm, the signal

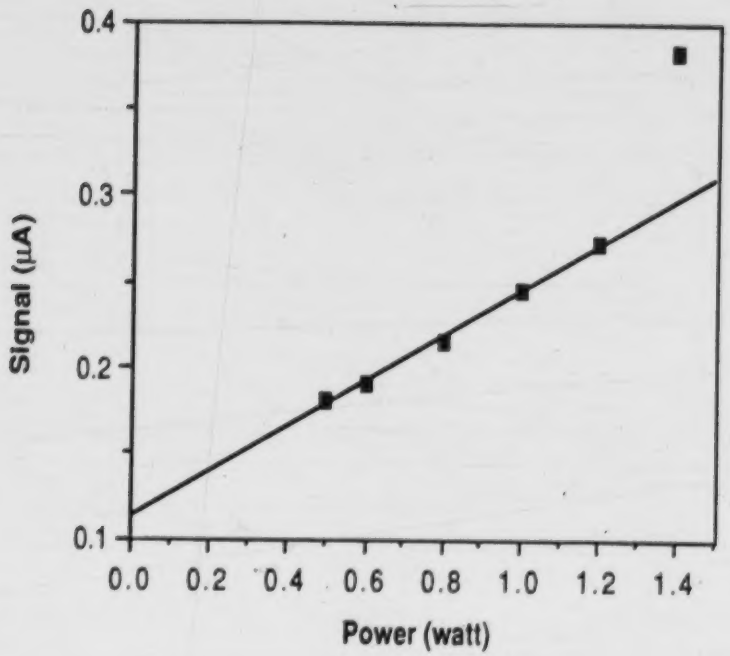

Figure 4-5. Fluorescent signal vs argon ion laser power.

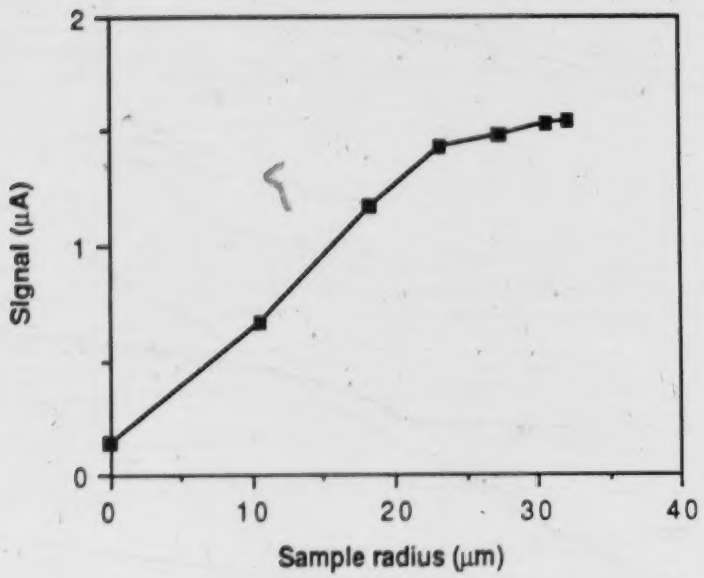

Figure 4-6. Fluorescent signal vs. sample radius.

does not increase due to the pinhole in the optic train blocking the signal. The non-zero intercept is due to light scatter.

Calibration curves (r all greater than 0.999) are constructed from the above experimental conditions at four different sample radii. The sample concentrations for this particular experiment range from $4.24 * 10^{-10}$ M to $4.24 * 10^{-9}$ M. The estimated detection limits (D.L), at 3 times background noise, for the above experiment are shown in figure 4-7. Clearly, better detection limits are obtained at relatively larger sample radii. This is the same concept as explained in the previous experiment.

Neat fluorescein solutions are introduced into the sheath-flow cuvette at a sample flow rate of 0.4 ml/hr and a sheath stream flow rate of 36 ml/hr. The sample stream radius, predicted by simple hydrodynamic theory, is about 10 μm. Under these flowing conditions, the analyte concentration detection limits, at three times backgound noise, are $1.25 * 10^{-12}$ M (100 parts per quadrillion) within a 10 μm radius or a nominal 6 pl probe volume. Within the probe volume, on average only $7.5 * 10^{-24}$ mole or 4.5 analyte molecules are expected at the detection limit. This concentration detection limit is about an order of magnitude poorer than that reported earlier for rhodamine 6G (19). The major limitation of the current instrument is the microscope objective utilized to collect the fluorescence. The 0.45 NA objective collects about 5.3 % of the emitted light wheras the 0.60 NA objective used in the early work is expected to collect 10 % of the emitted light. Improvements in

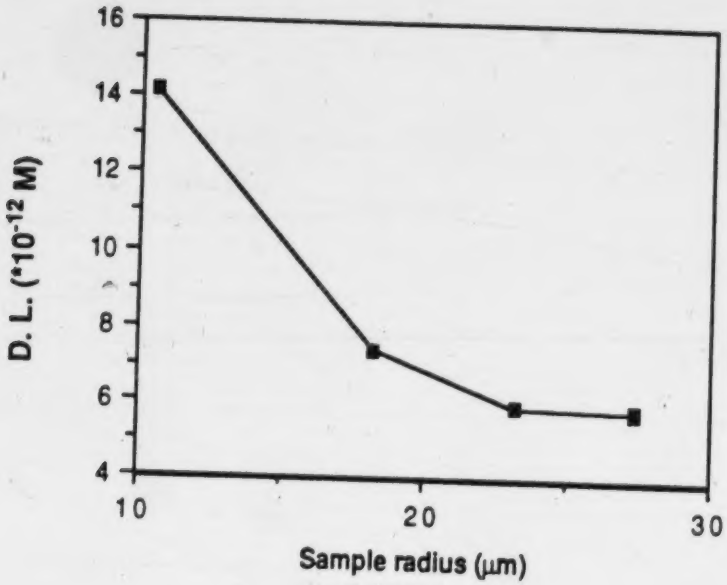

Figure 4-7. Detection limits vs sample radius.

collection effiency, spatial filtering, and photomultiplier quantum yield should generate detection limits near 10^{-13} M fluorescein.

It will be interesting to consider the sheath-flow cuvette for injected plugs of sample in capillary zone electrophoresis. Although the cuvette has been used as a detector cell for both flow injection analysis and liquid chromatography (18,22-23), it has not been applied to capillary zone electrophoresis.

The fluorescein isothiocyanate (FITC) derivatives of amino acids, peptides, and proteins possess absorbance and emission spectra which are similar to that of fluoresccein, figure 4-2. It appears that detection limits approaching or below one attomole are possible for capillary zone electrophoresis using laser induced fluorescence detection in the sheath-flow cuvette. The determination and separation of FITC derivatives of amino acids for this application will be discussed in detail in the next chapter.

REFERENCES

1. Price, J. M.; Kaihara, M.; Howerton, H. K. *Appl. Optics*, 1962, 1, 521.
2. Muller, F.; Veroort, J.; Lee, J. *J. of Raman Spectroscopy*, 1983, 14, 106.
3. Bennette, J. E.; *J. of Raman Spectroscopy*, 1985, 16, 174.
4. Kircheva, P. P.; Simeonov, S. D.; *J. of Raman Spectroscopy*, 1985, 16, 308.
5. Walrafen, G. E. *J. Chem. Phys.* 1964, 40, 3294.
6. Medinger, T.; Wilkinson, F. *Trans. Faraday Soc.* 1965, 61, 620.
7. McGlynn, S. P.; Azumi, T.; Kinoshita M. "Molecular Spectroscopy of the Triple State", Prentice-Hall, Englewood, Cliffs, N. J, 1969, 261.
8. Guilbault, G. G.; "Pratical Fluorescence", Marcell Dekker, Inc., New York, 1973.
9. Schulman, S. G. *Crit. Rev. Anal. Chem.* 1971, 2, 85.
10. Kearns, D. R. *Chem. Rev.* 1971, 71, 395.
11. Parmenter, C. S.; Rau, J. D. *J. Chem. Phys.* 1969, 51, 2242.
12. Hirschfeld, T. *Appl. Opt.* 1976, 15, 2965.
13. Nguyen, D. C.; Keller, R. A.; Jett, J. H.; Martin, J. C. *Anal. Chem.* 1987, 59, 2158.
14. Parker, C. A. "Photoluminescence of Solutions", section 5C, Elsevier, London, 1968.
15. Mattews, T. G.; Lytle, F. E. *Anal. Chem.* 1979, 51, 583.
16. Haugen G. R.; Lytle, F. E. *Anal. Chem.* 1981, 53, 1554.
17. Diebold, G. J.; Zare, R. N. *Science*, 1977, 196, 1439.
18. Hershberger, L. W.; Callis, J. B.; Christian, G. D. *Anal. Chem.* 1979, 51, 1444.

19. Dovichi, N. J.; Martin, J. C.; Jett, J. H.; Keller, R. A. *Science.* 1983, 56, 845.

20. Dovichi, N. J.; Martin, J. C.; Jett, J. H.; Trkula, M.; Keller, R. A. *Anal. Chem.* 1984, 56, 348.

21. Cheng, Y. F.; Dovichi, N. J. *Fluorescence Detection II*, E. Roland Menzel, Editor, Proc. SPIE 1988, 910, 112.

22. Kelly, T. A.; Christian, G. D. Anal. Chem. 1981, 53, 2110.

22. Kelly, T. A.; Christian, G. D. Anal. Chem. 1982, 54, 1444.

CHAPTER FIVE

FLUORESCENCE MEASUREMENT (II)[1]

(Laser-Induced Fluorescence Detection Using The Sheath-Flow Cuvette For Capillary Zone Electrophoresis)

1. INTRODUCTION

1.1. Capillary zone electrophoresis (CZE)

Electrophoresis is a powerful technique for the separation and analysis of charged substances within a fluid medium under the influence of an electric field. The charged components may be proteins, polynucleotides, peptides, amino acids, or other molecules. When suspended in an aqueous solvent, most particles will become either positively or negatively charged. The sign and magnitude of the charge depends upon the nature of the particles and the solvent used. Migration of the ion takes place towards the appropriate electrode when an electric field is applied. Different types of particles are likely to exhibit different migration velocities, depending upon the sign and magnitude of their charges. This method thus permits the separation of different types of particles.

1. A version of this chapter has been submitted for publication. Cheng, Y. F. and Dovichi, N. J. *Science.*

Linus Pauling et. al. (1) used this technique to find that the hemoglobin of patients with sickle cell anemia has a different electrophoretic mobility than that of normal hemoglobin. Since this abnormality is hereditary, electrophoretic studies became of great interest to geneticists. This is one of the most exciting applications of electrophoresis in medical research.

Capillary zone electrophoresis (CZE), first demonstrated by Mikkers et. al. (2) and by Jorgenson and Lukacs (3), is characterized by high resolution, low sample consumption, good mass sensitivity, and a rather simple and effective design. Because of the combined action of electro-osmotic flow with electrophoretic separation, all species travel in one direction, allowing detection of positively, neutral, and negatively charged species in a single run.

In this technique, as shown in figure 5-1, sample is normally introduced as a narrow zone at the positive end of a capillary filled with buffer solution. As the electric field is applied, the whole zone follows the electro-osmotic flow along the capillary tubing toward the negative electrode at the detector end. Each species begins separating according to its own electrophoretic migration. All species travel in one direction, allowing detection in the sequence of positively charged, neutral, and then negatively charged species at the detector, negative end.

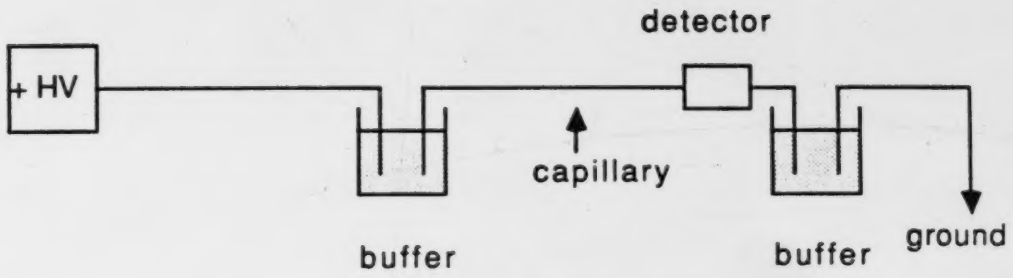

Figure 5-1. Schematic diagram for capillary zone electrophoresis.

1.1.1 Transport mechanism

In CZE, the item of interest is the rate of migration of the analyte. The rate of migration, electrophoresis, is a function of net charge, size and shape of the particles, and retarding factors such as viscosity. A neutral particle should not migrate. However, a liquid flow occurs, induced by the applied electric field, which causes all species to migrate in the same direction. This process is known as electro-osmosis. The following sections will briefly discuss the zeta potential and electric double layer, electrophoretic mobility, and electro-osmotic flow.

1.1.1.1 Zeta potential (ζ) and electric double layer

The electric double layer deals with the structure of the boundary between two phases and is a spatial formation with a non-homogeneous distribution of charges that originates as a result of polar adsorption. The fixed charges of one phase plus the relatively mobile counter ions of the other phase constitute the electric double layer. It is the potential at this layer that governs the electrophoretic mobility of the particle and is called the zeta potential (ζ) (4-5).

1.1.1.2 Electrophoretic mobility (μ_{ep})

If a particle has a net charge of Q, and if E is the electric field strength, the force producing electrophoretic migration is EQ. The

particle will therefore attain a terminal velocity such that the frictional resistance of the medium in which it moves just balances the electrical force. The resisting force is given by Stokes' law : $F = 4 \pi a \eta v_{ep}$ for a spherical particle where a is the particle radius, η is the viscosity of the medium and v_{ep} is the particle velocity. Then electrophoretic mobility (μ_{ep}), which is velocity in unit field, is given by:

$$\mu_{ep} = v_{ep} / E = Q / 4 \pi \eta a \qquad (5.1)$$

Thus the electrophoretic mobility (4,6-7) is governed by the particle size, medium viscosity, and net charge.

Further considering the electrophoretic retardation, it has been shown by Henry (4) that the mobility is related to the zeta potential as:

$$\mu_{ep} = (\zeta_{ion} \varepsilon / 6 \pi \eta) f(ka) \qquad (5.2)$$

where ζ_{ion} is the zeta potential of the particle, ε is the dielectric constant of the solution, and f(ka) varies from 1 to 1.5, depending upon the dimensions of ka. The expression ka is the ratio of particle diameter to double layer thickness.

1.1.1.3 Electro-osmotic flow (μ_{eo})

Electro-osmotic flow (4-5,8) in the capillary is due to the migration of ions from the diffuse layer of the electric double layer at the capillary surface, under the influence of an electrical field imposed tangentially to the surface, toward the oppositely charged electrode. The direction of flow depends upon the charge of the ions in this double layer. Most adsorption effects to the capillary wall are due to anions, which convey a negative character to the wall surface. Cations, being more hydrated than anions, are less likely to be adsorbed. So, the electro-osmotic flow moves toward the cathode end. The electro-osmotic flow (μ_{eo}) is given by:

$$\mu_{eo} = v_{eo} / E = \zeta_{wall}\, \varepsilon / 4\, \pi\, \eta \qquad (5.3)$$

where v_{eo} is the electro-osmotic velocity for unit field, ζ_{wall} is the zeta potential (of the wall), ε is the dielectric constant of the solution, and η is the viscosity. Zeta potentials depend upon the nature of the solid surface and the ionic state of the liquid.

The electro-osmotic flow is different from laminar flow in an important respect. Laminar flow causes a parabolic velocity profile which increases resistance to mass transfer efficiency in a chromatographic system. In electro-osmotic flow, the flow profile is

much flatter, and resistance to mass transfer occurs only near the wall,. that is, in the region given by the double layer thickness (9).

1.1.2 Effect of pH on transport mechanism

The effect of pH on the surface charge of a molecule depends upon the type and number of ionizable groups present. The effect of acidic and basic groups of a protein, for instance, is that the protein will show a net zero charge at the isoelectric point, pI, under a specific pH. Below this pH, the protein will have a net positive charge which will increase with decreasing pH, as will its mobility in electrophoresis. Above the pI, the protein will have a net negative charge and its mobility will increase with increasing pH but this time in the opposite direction. Unfortunately, the correlation between charge and electrophoretic mobility is very complex but the concept of pI values provides a useful guide to electrophoretic behavior (10).

The zeta potential of the wall, which plays an important role for the electro-osmotic flow as shown in equation 5.3, decreases significantly at lower pH, and the electro-osmotic flow will vary correspondingly. Section 1.1.1.3 shows that the zeta potential of the solid surface is influenced by the nature of the solid surface and the ionic state of the buffer solution. Jorgenson and Lukacs have already shown experimentally that the electro-osmotic flow generally decreases

as the solution pH is lowered because hydrogen ions lower the zeta potential by neutralizing anions at the solid surface (11).

1.1.3 Causes of zone broadening in electrophoresis

Several factors causing zone broadening may be identified when considering separation efficiency (N) in zone electrophoresis. Jorgenson and Lukacs (12-13) pointed out that they are:

1. Molecular diffusion: Molecular diffusion will certainly cause zone broadening.

2. Sample concentration: It has been shown (2,14) that migration velocity is a function of solute concentration. A region of high solute concentration changes the local conductivity of an electrophoretic medium, causing a change in the local potential gradient. Distortion of the gradient leads to uneven migration, zone asymmetry, and band broadening. The solution to this problem is to keep the concentration of the sample low compared to the buffer solution. Typically, the sample concentration should be less than 1 % of the buffer concentration to avoid excessive band broadening.

3. Convection currents: Unstable density gradients within the separation medium, caused either by samples with a density different than the buffer or by Joule heating, can lead to disruptive convective flows. These flows are generally minimized through the use of gels, paper, or other stabilizers in the electrophoretic chamber. Unfortunately,

the use of stabilizers may introduce new causes of zone broadening such as both eddy migration, which refers to the fact that not all possible routes of migration through and around the stabilizer will yield the same net migration velocity, and adsorptive interaction between solutes and stabilizers (3).

Joule heat is generated by the passage of electricity through the buffer solution. Since heat is generated uniformly through the medium, but is only removed at the edges of the separation compartment or gel, a temperature gradient arises. The temperature in the center of the system will be higher than at the edges. The center area is hotter and less dense, and therefore results in convection currents. Mikkers et. al. sought to solve these convection problems by performing zone electrophoresis in narrow bore tubes (14). Narrow tubes efficiently transfer heat away from the sample buffer, decreasing the temperature rise in the capillary.

1.1.4 Migration velocity and time, separation efficiency, and resolution

1.1.4.1 Migration velocity (v) and migration time (t)

Consider an electrophoresis system consisting of a tube filled with a buffer medium across which a voltage is applied (15-16). Charged species introduced at positive end of the tube migrate under the

influence of the electric field to the detector, negative end. The migration velocity (v) of a particular species is given by:

$$v = (\mu_{ep} + \mu_{eo}) / E = (\mu_{ep} + \mu_{eo}) V / L \qquad (5.4)$$

where μ_{ep} is the electrophoretic mobility, μ_{eo} is the electro-osmotic flow, E is the electric field gradient, V is the applied voltage, and L is the length of the tube. The time, t, it takes an ion to migrate the entire length of the tube is given by:

$$t = L / v = L^2 / (\mu_{ep} + \mu_{eo}) V \qquad (5.5)$$

This equation shows that the separation time is proportional to the square of the length of the tube and inversely proportional to applied voltage, and also inversely proportional to the net electromigration, $\mu_{ep} + \mu_{eo}$.

1.1.4.2 Separation efficiency (N)

If zone electrophoresis is performed in narrow bore tubes using low sample concentrations relative to carrier electrolyte, Jorgenson and Lukacs (12) assume that molecular diffusion is the only source of solute zone broadening. The spatial variance, σ^2_{long}, of a peak is given by:

$$\sigma^2_{long} = 2 D t \qquad (5.6)$$

where D is the molecular diffusion coefficient of the solute in the zone. Substituting the expression for time from equation 5.5 into 5.6 yields:

$$\sigma^2_{long} = 2 D L^2 / (\mu_{ep} + \mu_{eo}) V \qquad (5.7)$$

The resulting separation efficiency, N, is then given by:

$$N = L^2 / \sigma^2_{long}$$
$$= (\mu_{ep} + \mu_{eo}) V / 2 D \qquad (5.8)$$

Several aspects can be found from this equation :

1. N is directly proportional to the applied voltage, which implies that the use of the higher voltage is desirable for higher separation efficiency.
2. N is independent of the length of the tube and also independent of the analysis time.
3. N is proportional to the ratio of the sum of the electrophoretic mobilty and electro-osmotic flow to the solute diffusion coefficient.

It appears that high voltages applied to short tubes would give the greatest separation efficiency in the shortest analysis time. However, the heat deposit in the tube is inversely proportional to the tube length squared; use of short tubes leads to a large temperature rise.

Normally, in an experiment the separation efficiency, N, is calculated by:

$$N = 5.54 \ (t_r / W_{1/2})^2 \qquad (5.9)$$

where t_r is the retention time (or distance) for the band; $W_{1/2}$ is the width of the band at half-height in time (or in distance).

1.1.4.3 Resolution (Rs)

Jorgenson and Lukacs(12) also showed that the resolution between two peaks is given by the following equation:

$$Rs = 0.177 \ (\mu_1 - \mu_2) \ [V / D \ (\mu_{ave} + \mu_{eo})]^{1/2} \qquad (5.10)$$

where μ_1 and μ_2 are the mobilities of the two zones, and μ_{ave} is their average mobility. This equation shows that the best resolution will be obtained when the electro-osmotic flow just balances the average electrophoretic migration.

The most commonly used equation for calculating resolution, Rs, in an experiment is given by:

$$Rs = \frac{t_{r.j} - t_{r.i}}{1/2\,(W_{t.j} + W_{t.i})} \qquad (5.11)$$

where $t_{r.j}$ is the retention time (or distance) for peak j, $t_{r.i}$ is the retention time (or distance) for peak i, $W_{t.j}$ is the baseline bandwidth in unit of time (or distance) for peak j, $W_{t.i}$ is the baseline bandwidth in unit of time (or distance) for peak i.

1.1.5 Practical limitation —— heat generation

Section 1.1.3. shows that electrical heating and the establishment of a parabolic temperature gradient across the tube provides the principal limitation to the use of high applied voltages and short tubes for electrophoresis.

The heat generated per unit time per unit length of capillary equals the electrical power dissipated per unit length of capillary and is given by (17-18):

$$P / L = K C r^2 V^2 / L^2 \qquad (5.12)$$

where P is power, K is the molar conductance of the buffer, C is the molar concentration of the buffer, r is the capillary radius, and L is the capillary length. Clearly, both decreasing the column radius and increasing the column length should have a significant effect on reducing the thermal loading and zone broadening.

1.1.6 Advantages of small diameter tubes

According to previous discussion, to achieve the highest resolutions of zones, tubes with as small an inner diameter as possible should be used in combination with as high an applied voltage as feasible. To summarize, the possible advantages of performing zone electrophoresis in open tubes of small internal diameter are:

1. A stabilizing medium, which can cause eddy migration and adsorptive interactions with the solutes, is not necessary.
2. The medium is stabilized against convective flow by the wall effect, due to the increased surface to volume ratio; heat transfer inside the tube is then improved.
3. Detrimental effects of remaining temperature gradients are minimized by solute diffusion back and forth across the tube.

1.1.7 Detectors for CZE

The disadvantage of using small diameter capillaries is that detection is made more difficult. Highly sensitive detection without causing any detector dead volume is required for the detection of the eluting species in CZE. On-line detection has been achieved by means of conductivity (19-20), UV absorbance (21-23), mass spectrometry (24), fluorescence (3,25-27), thermo-optics (28), and electrochemistry (29). . Among these, fluorescence and thermo-optical detection are the most sensitive detectors, producing detection limits of about 10^{-7} M for the dansyl and fluorescamine derivatives of amino acids (26) and about 10^{-8} M for the dabsyl amino acids (28). This chapter shows that using the laser induced fluorescence for capillary zone electrophoresis with the sheath-flow cuvette as the detector cell provides selectivity and high sensitivity without degrading separation efficiency.

1.1.8 Estimations of injection volume, concentration at peak maximum, and detection limits

1.1.8.1 Injection volume

There are three methods for introducing sample into the capillary tube for capillary zone electrophoresis: electromigration (3), gravity injection (19,21), and rotary type injection (30). The present work

employs the first technique due to its relative ease and effectiveness. With this method, the samples are electro-osmotically introduced into the capillary by inserting the tubing into the sample vial and applying a constant voltage during a certain time. Thus, sample components are introduced by both electro-osmotic flow, μ_{eo}, and electrophoretic mobility, μ_{ep}. The latter generally depends upon the charge and size of solute, equation 5.1. Hence, the amount of each solute injected is determined by the nature of the solute. The injection volume, V_{inj}, can be estimated by:

$$V_{inj} = V_{col} (t_{inj} / t_r) (HV_{inj} / HV_{ele}) \quad (5.13)$$

and:

$$V_{col} = \pi r^2 L \quad (5.14)$$

where V_{col} is the volume of the capillary, HV_{inj} is the high voltage applied to the injection, HV_{ele} is the high voltage applied to the electrophoresis, t_{inj} is the injection time applied at HV_{inj}, t_r is the retention time of the analyte at HV_{ele}, r is the radius of the capillary, and L is the length of the capillary.

1.1.8.2 Concentration at peak maximum

The injected solutes become diluted during the electrophoresis process. The concentration of the analyte at the peak maximum, C_p, is lower than that of the solution at the point of injection, C_i, and the relation is given by (31):

$$C_i / C_p = (2 \pi / N)^{1/2} V_r / V_{inj} \qquad (5.15)$$

and:

$$V_r = v * t_r \qquad (5.16)$$

where V_r is the retention volume, N is the number of the theoretical plates, v is the volumetric flow rate of the mobile phase, and t_r is the retention time for the analyte.

1.1.8.3 Detection limit

The American Chemical Society's Subcommittee on Environmental Analytical Chemistry defined the detection limits as the analyte concentration that produces a peak having a height equal to three times the standard deviation of the baseline noise (32). According to Knoll (33),

the estimated concentration detection limit, C_{LOD}, for chromatographic peaks is given by:

$$C_{LOD} = K_{LOD}\, h_n\, C_s / h_s \qquad (5.17)$$

where h_n is the largest noise fluctuation observed in the noise measurement interval, h_s/C_s is the analyte peak height per unit amount of analyte, and K_{LOD} is a constant, determined for the measurement interval employed. Values of K_{LOD} , derived and given in reference 33, are listed in table 5-1.

1.2. Fluorescein-isothiocyanate (FITC) derivatives of amino acids

In the present study, fluorescein-isothiocyanate (FITC)-I, figure 5-2 (B), is used to react with eighteen amino acids for the purpose of forming fluorescent chromophores. FITC-I, which has a similar structure, excitation and emission spectra as fluorescein, figure 5-2 (A), has been shown to be a useful reagent for attaching the fluorescein chromophore to the ∝-amino acid group of amino acids, peptides and proteins (34-39). This method has an advantage over the 2,4-dinitrofluorobenzene method (40-41) and the phenyl-isothiocyanate method (42) in that it has higher sensitivity and could also be applied to the sequential analysis of peptides and proteins.

Peak width multiple	K_{LOD}
10	1.9718
20	1.4309
50	0.9194
100	0.6536

Table 5-1. Values of K_{LOD} for calculating C_{LOD}.

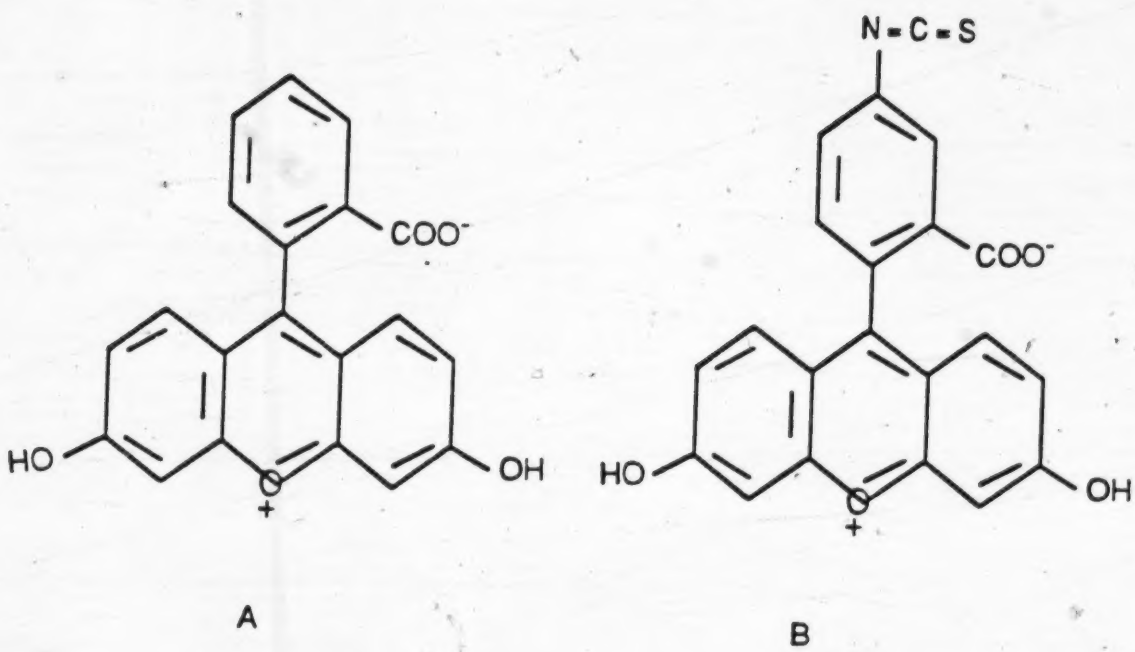

Figure 5-2. A is the chemical structure for fluorescein; B is the structure for the fluorescein-isothiocyanate (FITC)-I. Both of them have similar excitation and emission spectra.

The reaction mechanism for FITC with amino acids is similar to that of Edman's phenyl-isothiocyanate reaction (42), shown below:

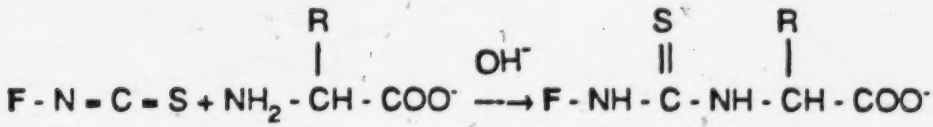

(FITC-I) (Amino acid) (Fluorecein-thiocarbamyl) (FTC-amino acid)

It has been pointed out by Kawauchi et. al. that the thiocarbamylation reaction is affected by both pH and temperature (36). It is best performed in 0.2 M pH 9.0 sodium carbonate-bicarbonate buffer at 20-25^{0}C. At lower pH levels the reaction is slower and at higher pH levels side reactions occur. The main side reaction above pH 10 seemed to be a degradation of FITC to aminofluorescein.

2. THEORY

Consider an electrophoresis system using the sheath-flow cuvette as a detector cell for the capillary which is filled with a buffer medium, and a voltage applied to this system. Charged species introduced at the positive end of the tube migrate under the influence of the electric field to the cuvette's negative end. The main effects of the sheath flow on

separation efficiency can be rationalized in terms of a back pressure during the electromigration. The flow of the sheath stream is pressure based, which is laminar in nature due to frictional forces. The magnitude of the back pressure present in CZE is proportional to the flow rate of the sheath. This back pressure in CZE increases the retention time, decreases the net molecular migration velocity, and distorts the flat electro-osmotic flow profile, therefore increasing band broadening while the zones are still in the separation capillary. The net migration velocity, v_{net}, of a substance is given by:

$$v_{net} = (\mu_{ep} + \mu_{eo}) V/L - v_{sheath} \qquad (5.18)$$

and:

$$v_{sheath} = \alpha Q \qquad (5.19)$$

where μ_{ep} is the electrophoretic mobility, μ_{eo} is electro-osmotic mobility, V is the applied voltage for the electrophoresis, L is the length of the capillary, v_{sheath} is the velocity which is produced by the effect of the sheath stream during the electromigration inside the capillary, α is a proportionality constant, and Q is the volumetric sheath flow rate. These two equations predict that the net migration velocity increases with the applied voltage and decreases with the sheath flow rate.

The time, t, it takes an ion to travel the entire length of the capillary is given by:

$$t = L / v_{net} = \frac{L}{(\mu_{ep} + \mu_{eo})\, V/L - v_{sheath}} \qquad (5.20)$$

$$= \frac{L}{(\mu_{ep} + \mu_{eo})\, V/L - \alpha Q} \qquad (5.21)$$

That is:

$$1/t = (\mu_{ep} + \mu_{eo})V/L^2 - \alpha Q/L \qquad (5.22)$$

Equation 5.22 predicts that the inverse retention time should increase with the applied voltage and decrease with the sheath flow rate.

Back pressure resulting from sheath flow modifies the separation efficiency and resolution. The peak variance produced by radial diffusion for laminar flow in an open tube, σ^2_{sheath}, is given by (43):

$$\sigma^2_{sheath} = 2 \frac{r^2 v^2_{sheath}}{48 D} t \qquad (5.23)$$

where r is the capillary radius, and D is the analyte diffusion constant. Therefore, the overall variance, $\sigma^2_{overall}$, is given by the sum of the variance due to longitudinal diffusion, σ^2_{long}, and that due to sheath flow, σ^2_{sheath}:

$$\sigma^2_{overall} = \sigma^2_{long} + \sigma^2_{sheath} \qquad (5.24)$$

Substituting equation 5.6 for longitudinal diffusion and equation 5.23 for the variance produced by laminar flow into the above equation yields the resulting variance:

$$\sigma^2_{overall} = 2 \left[D + \frac{r^2 v^2_{sheath}}{48 D} \right] t \qquad (5.25)$$

The resulting theoretical plate number, N, is then given by:

$$N = L^2 / \sigma^2_{overall}$$

$$= \frac{L\left[(\mu_{ep} + \mu_{eo})\, V/L - \alpha Q \right]}{2\left[D + (r^2 \alpha^2 Q^2 / 48 D) \right]} \qquad (5.26)$$

This formula predicts that separation efficiency increases with the applied voltage and decreases with the sheath flow rate.

Giddings (44) derived an expression for resolution, Rs, as:

$$Rs = \frac{N^{1/2}}{4} \frac{\Delta\mu}{\bar{\mu}} \qquad (5.27)$$

where N is the number of theoretical plates, $\Delta\mu / \bar{\mu}$ is the relative difference in mobility of the two zones being separated and is equal to:

$$\frac{\Delta\mu}{\bar{\mu}} = \frac{\mu_1 - \mu_2}{\bar{\mu}} \qquad (5.28)$$

where μ_1 and μ_2 are the mobilities of the two zones, and $\bar{\mu}$ is their

average mobility. In the presence of electro-osmosis and sheath flow, the above equation becomes:

$$\frac{\Delta\mu}{\bar{\mu}} = \frac{\mu_1 - \mu_2}{\bar{\mu} + \mu_{eo} - \alpha QL/V} \tag{5.29}$$

Substituting the expression for the relative velocity difference, equation 5.28, into the expression for the resolution, equation 5.27, gives the resolution for the sheath flow system:

$$Rs = \frac{N^{1/2}}{4} \frac{\mu_1 - \mu_2}{\bar{\mu} + \mu_{eo} - \alpha QL/V} \tag{5.30}$$

This equation reveals that the resolution is proportional to the square root of the separation efficiency, $N^{1/2}$, and to the difference between the intrinsic electrophoretic mobilities of the two zones, $\mu_1 - \mu_2$. The best resolution would be obtained when the term for the sheath effect, $\alpha QL/V$, just balances the electromigration, $\bar{\mu} + \mu_{eo}$. However, a large expense in time would be required according to equation 5.21. When the expression for the number of theoretical plates, equation 5.29, is substituted into the above equation, the resulting resolution is:

$$Rs = (1/4)\left\{\frac{L\left[\left(\bar{\mu} + \mu_{eo}\right) V/L - \alpha Q\right]}{2\left[D + \left(r^2 \alpha^2 Q^2 / 48 D\right)\right]}\right\}^{1/2} \left\{\frac{\mu_1 - \mu_2}{\bar{\mu} + \mu_{eo} - \alpha QL/V}\right\}$$

$$= 0.177 \left(\mu_1 - \mu_2\right)\left\{\frac{V}{\left[D + \left(r^2 \alpha^2 Q^2 / 48D\right)\right]\left[\bar{\mu} + \mu_{eo} - \alpha QL/V\right]}\right\}^{1/2} \qquad (5.31)$$

This equation shows that, for the sheath flow system, better resolution would be obtained with (1) a larger difference between the intrinsic electrophoretic mobilities of the two zones, $\mu_1 - \mu_2$; (2) a higher voltage, V, applied to the electrophoretic system; (3) a smaller capillary radius; (4) a relatively longer capillary length; (5) a relatively smaller molecular diffusion coefficient, D. This equation also reveals that the resolution is a function of volumetric sheath flow rate, Q, and is influenced by the correlation between sheath flow rate and analyte properties and experimental conditions.

3. EXPERIMENTAL

3.1 Instrumental

The experimental configuration of laser-induced fluorescence using the sheath-flow cuvette for capillary zone electrophoresis is shown in figure 5-3, which is a combination of that employed previously for CZE (3), figure 5-1, and for laser-induced fluorescence detection using the sheath-flow cuvette, figure 4-3. An argon ion laser, usually producing a one watt beam in the light regulated mode at 488 nm, is used as an excitation source. This beam is focused with a 18 mm focal length lens (7x) into the center of the sheath-flow cuvette, Ortho Model 300-051100. The sheath stream is introduced by a high pressure chromatography syringe pump, Isco Model 314, whereas the sample stream is provided by the electrophoretic technique (described in detail later).

The fluorescence is magnified at right angles with a microscope, shown previously in figure 4-4, and then detected by the 1P28 photomultiplier tube (PMT). The output of the PMT is then directed across a resistor (R), typically 2.9 KΩ , in parallel with a capacitor (C), normally 220μF. The product of R and C determines the response time in seconds. Finally, the voltage output is displayed on a strip chart recorder, Fisher Recordall Series 5000. The dotted line in figure 5-3 represents a black box employed to minimize the introduction of any

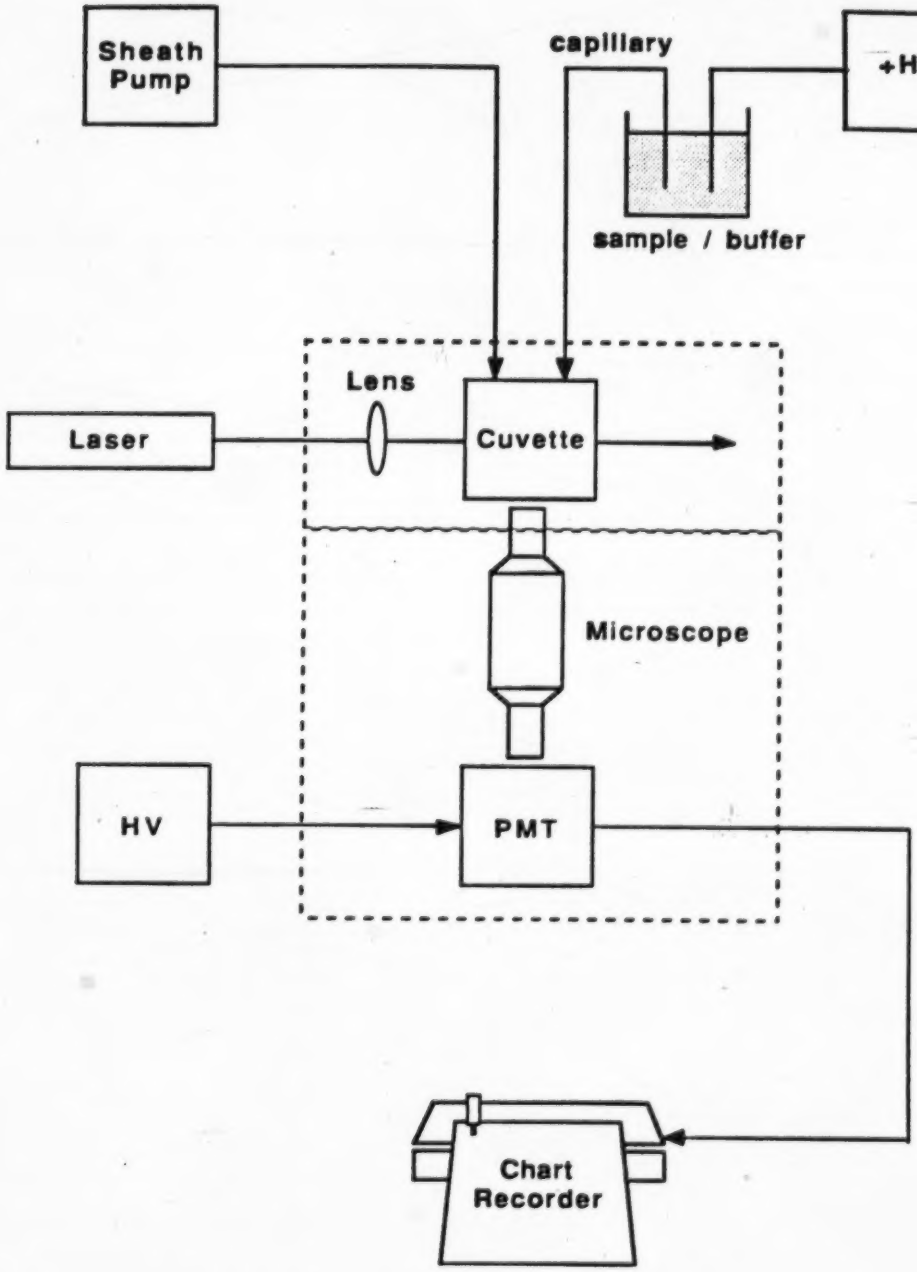

Figure 5-3. Experimental diagram for laser-induced fluorescence detection using the sheath-flow cuvette for CZE.

stray light or room light to the PMT. The cuvette, microscope and PMT are mounted on two or three dimensional micrometer translation stages to allow convenient alignment.

A capillary zone electrophoresis instrument is constructed using a 30 kilovolt DC power supply (Spellman). The positive terminal of this power supply is applied to the sample or buffer vial and then across the fused-silica capillary (Polymicro Technology) which has a 50 μm inner diameter and a length ranging from 80 to 99 cm. The capillary exterior is coated with polyimide to increase its mechanical strength. The ground, negative, terminal of the power supply is also connected to the sheath-flow cuvette body. The positive electrode is contained within a plastic enclosure equipped with an interlock system to protect the operator from accidently contacting the high voltage. A platinum electrode is used to connect the power supply to the sample container.

3.2. Chemicals

All chemicals are reagent grade or better. The 18 amino acids, FITC-I, and fluorescein are from Sigma Chemical Company. A stock pH 7, 0.02 M phosphate buffer solution is prepared in water. The water is doubly distilled, deionized, and filtered through a 0.2 μm millipore filter prior to use. Stock solutions of pH 9 and pH 10, 0.2 M, carbonate buffer are prepared in the above water. All buffer solutions receive two drops

of chloroform to prevent the growth of bacteria. Also, a stock solution of $5.29 * 10^{-7}$ M fluorescein in pH 7.0 phosphate and a stock solution of $4.24 * 10^{-8}$ M FITC-I in pH 9.0 carbonate buffer solution are prepared.

3.3 Preparation of FTC-AA

The procedure for the preparation of FTC-AA is similar to that described by Maeda and Kawauchi in reference 34. Each amino acid is prepared in a 100 ml volumetric flask by dissolving enough amino acid to prepare a 10^{-4} M solution in 0.2 M pH 9.0 carbonate-bicarbonate buffer solution. A solution of $5.46 * 10^{-4}$ M FITC-I is also prepared in a 250 ml volumetric flask in acetone containing a trace amount of pyridine. Two to five ml of each amino acid solution is allowed to react with 20 µl of FITC-I solution in a 10 ml glass vial, containing a magnetic bar, on a magnetic stirrer in the dark for two to four hours at room temperature. No further purification is necessary. The solution is then diluted by taking 10 µl of the reacted solution in 10 ml of 5mM, pH 9.0 carbonate-bicarbonate solution. For the separation of 18 FTC-AAs, each AA is prepared according to the above procedure and 10 µl of each solution is added to 10 ml of 5 mM pH 9.0 or pH 10 carbonate solution. All FTC-AAs are stored in 4^0 C.

3.4 Electrophoresis procedures

Usually, a one hour warm up for this instrumental system is necessary to stabilize the PMT and argon ion laser. To inject the sample, the positive end of the power supply is connected to a non-conducting injection vial filled with the sample solution. The sample is then introduced into the capillary as a narrow zone through electro-osmosis by using the power supply to produce a constant voltage for a certain period of time, typically at 2 KV for 10 seconds. After the injection, the sample vial is replaced with another non-conducting vial filled with the appropriate buffer solution. Again, the electric field is applied at high voltage, typically at 25 KV (for separation purposes and also as the sample stream to the sheath-flow cuvette). Finally, the sheath stream, using the same buffer solution as for the electrophoresis, and the strip chart recorder are turned on and the electropherogram is recorded. A waiting period of about 5 minutes between each run is necessary for dissipating the temperature rise inside the capillary. Continuous operating of this instrument for more than 24 hours is no problem at all.

4. RESULTS AND DISCUSSION

4.1. Preliminary study for capillary zone electrophoresis

To consider the sheath-flow cuvette as a detector for injected

plugs of sample in capillary zone electrophoresis, the following experiments are performed.

Sample stream linear velocity, derived from capillary length divided by retention time, at different voltages applied to the electrophoresis, figure 5-4, is studied first. The sample is $5.29 * 10^{-8}$ M fluorescein in 0.02 M pH 7.0 phosphate buffer injected at 5 KV for 8 second; the sheath stream is 5 mM of pH 7.0 phosphate buffer at 20 ml/hr; and the capillary is a 92 cm tube of 50 μm inner diameter. The linear relationship shows that higher voltage applied to the electrophoresis results in faster net electromigration and larger velocity. This observation agrees with other studies (12-13). Zero velocity occurs at about 4 KV for the electrophoresis system. This result occurs because, during the electromigration, the sheath stream is flowing constantly and produces a force in the capillary toward the injection, positive, end. A drop of solution is formed at the positive end of the capillary when the buffer vial is removed, no potential is applied, and the sheath stream is kept flowing. Electromigration and sheath flow balance at about 4 KV under the above experimental conditions.

At about the same experimental conditions as the previous one and at 22 KV for the electrophoresis, figure 5-5 shows that sample stream linear velocity has a linear relationship with the sheath flow rate. This result arises because the sheath stream pushes electromigration back towards the injection end more forcefully at higher sheath flow rates, in

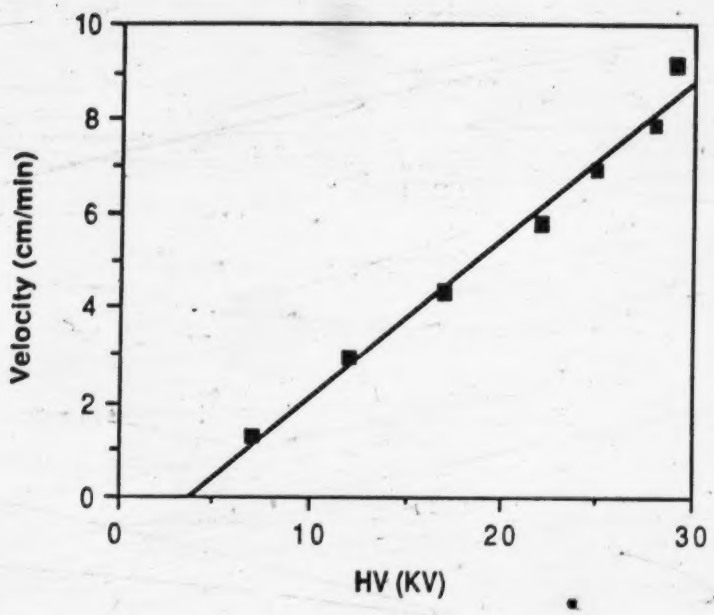

Figure 5-4. Sample stream linear velocity vs. high voltage, HV, applied to the electrophoresis.

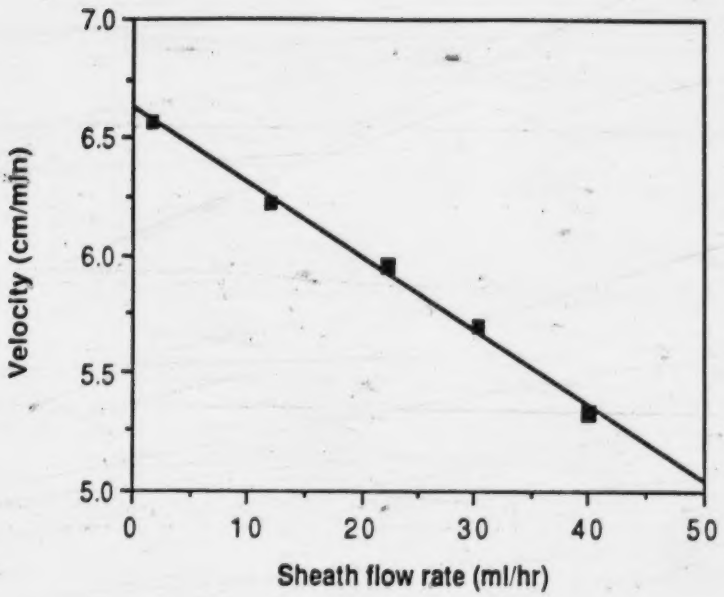

Figure 5-5. Sample linear velocity vs sheath flow rate.

agreement with the prediction given in equation 5.18 under theory in section 2. The slope of figure 5-5 provides - α in equation 5.19.

Figure 5-6 shows a linear relationship between peak height and voltage for the electrophoresis. The higher the voltage applied to the electrophoresis, the faster the net electromigration, which produces a bigger sample radius at a constant sheath flow rate, 20 ml/hr in this experiment. More sample molecules are illuminated at the same time, so a larger fluorescent signal is observed and a higher peak is generated; this is the same phenomena as in the neat sample solutions experiment, chapter 4. Again, the non-zero intercept is due to the sheath stream effect.

An interesting phenomenon is observed for the peak height versus sheath flow rate study, figure 5-7. The sample is $5.29 * 10^{-8}$ M fluorescein in 0.02 M pH 7.0 phosphate buffer solution, injected at 5 KV for 10 seconds. Voltage applied to the column is kept at 28 KV, and the capillary is 92 cm long and 50 μm inner diameter. As expected, at lower sheath flow rates, from 40 ml/hr to 5.6 ml/hr, the sample radius increases and, as well, more sample molecules are illuminated so that, of course, the peak height increases. But, peak height decreases as the sheath flow rate slows to less than 5.6 ml/hr. This decrease is because the sample stream is broadened significantly by diffusion which occurs during the transit from the capillary exit to the detection region.

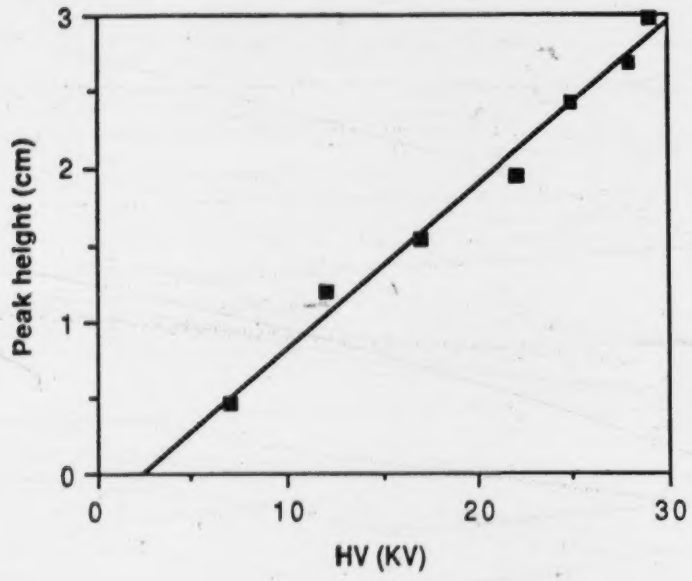

Figure 5-6. Peak height vs. high voltage, HV, applied to the electrophoresis.

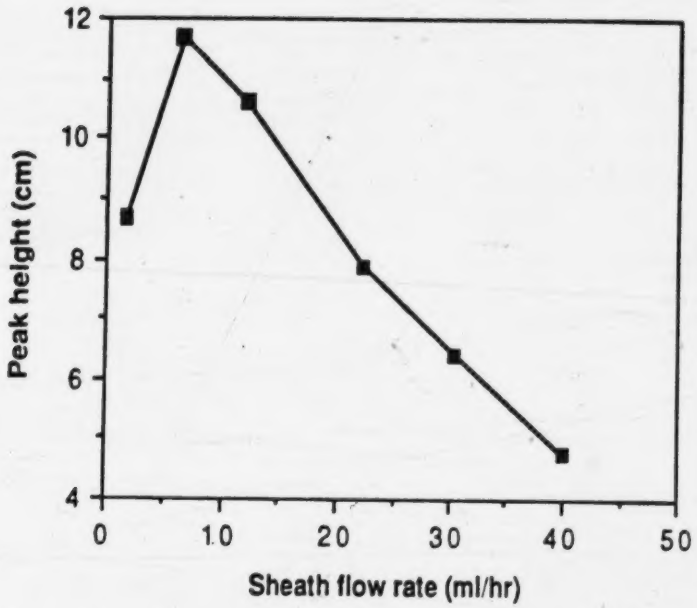

Figure 5-7. Peak height vs. sheath flow rate.

Assuming laminar flow in a square flow chamber, the sample at stream center will travel at a linear velocity, v, given by (45):

$$v = 9U/4B^2$$

where U is the volume flow rate (5.6 ml/hr) and B is the square cell width, 250 μm, yielding a linear velocity of 5.6 cm/sec (for this cuvette, the volumetric flow rate in ml/hr is numerically equal to the linear velocity in cm/sec). Roughly a 5 mm distance separates the inlet point and the detection point. About 80 ms are required for the sample to travel from the capillary tube to the detection region. During this time, the sample stream diffuses into the sheath stream to produce an increase in the sample stream diameter. The average diffusion distance, x, is given by:

$$x = (2Dt)^{1/2}$$

where D is the diffusion constant, $5 * 10^{-6}$ cm^2 s^{-1} for most small analytes. During the 80 ms transit time, the analyte will diffuse an average distance of 9 μm to produce a sample stream diameter of about 10 μm. In the absence of diffusion, the simple hydrodynamic model of equation 1.1 predicts a sample stream radius of 2 μm. Diffusion acts to increase the stream radius to about 10 μm. Since the sample volume is proportional to the area of the sample stream, diffusion produces a factor of 25 dilution in analyte concentration.

Figure 5-8 shows the preliminary electropherogram for the injection of 4.2 nl (3 KV for 15 seconds) of 2.64 * 10^{-9} M fluorescein in 5 mM pH 7.0 phosphate buffer and at sheath flow rate of 5.6 ml/hr. The capillary is 50 µm inner diameter and 92 cm long. The high voltage applied for this experiment is 25 KV. The chart speed is increased 10 times near the peak for more accurate determination of the peak width. The estimated number of theoretical plates is about two hundred thousand, and the detection limit, at three times background noise, is 9.6 * 10^{-11} M, which corresponds to two hundred and forty thousand molecules injected onto the column. Of course, during the process of electrophoresis, dilution occurs within the column to reduce the analyte concentration to 3.9 *10^{-11} M at the detector. The detection limit of 3.9 * 10^{-11} M is more than one order of magnitude poorer than the neat sample solution experiment, chapter four, which is obtained at relatively high volumetric flow rate, 0.4 ml/hr. The difference in performance between the capillary zone electrophoresis detection and the neat sample solution is due to diffusion in the short transit time from the introduction of analyte to the detection of analyte. Also, the sample pathlength is smaller here since the sample radius is smaller. Further improvements will be dissussed in the following section.

4.2. Diffusion study

The transit time for analyte must be decreased to minimize

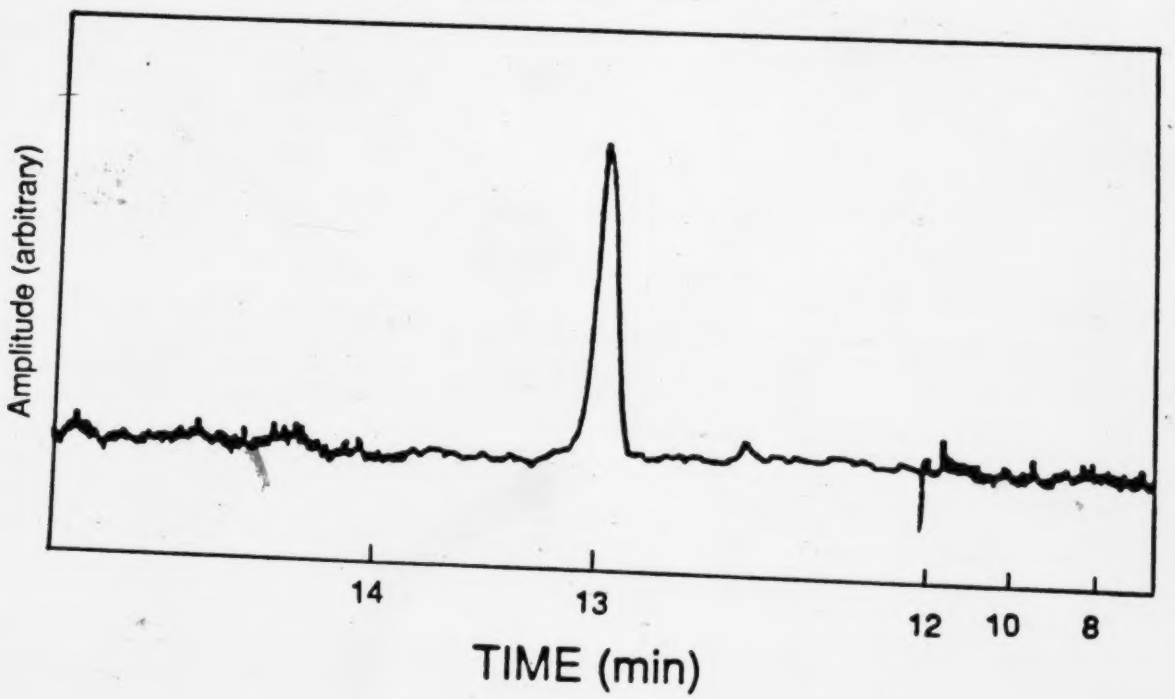

Figure 5-8. Electropherogram of $2.64 * 10^{-9}$ M of fluorescein injected at 3 KV for 15 s, 4.2 nl; capillary, 50 µm ID and 92 cm long; sheath stream, 5.6 ml/hr; voltage for electrophoresis is 25 KV.

diffusion in the cuvette since the radius of the sample stream due to diffusion is proportional to the square root of the transit time. The area of the sample stream is linearly related to the transit time. The transit time may be reduced by increasing the sheath flow rate. Poorer detection limits are obtained, however, because the sample molecules spend less time in the laser beam, and also, as the sample radius decreases, fewer molecules are excited at one time even though the diffusion problem is reduced. Another way to decrease the transit time is to decrease the distance from the introduction of the sample to the probe region. The distance can be reduced by lowering the exit of the capillary tube into the flow chamber of the sheath-flow cuvette. This approach leads to the achievement of better detection limits.

The sample radius is measured at several points after the outlet of the capillary, and at three different sheath flow rates: 1.6, 6.4, and 12 ml/hr. The sample is $5.29 * 10^{-8}$ M of fluorescein in pH 7 phosphate buffer solution. The sheath stream is 5 mM of pH 7 phosphate buffer. The tubing is 50 μm inner diameter and 99 cm long. The voltage for the electrophoresis is 25 KV. The results are shown in figure 5-9, which demonstrates the following three phenomena:

1. Bigger sample radii are observed at lower sheath flow rate. The sheath stream at 1.6 ml/hr is larger than that at 6.4 ml/hr and the sheath stream at 6.4 ml/hr is larger than that at 12.0 ml/hr, due to the fact that transit time is longer for lower sheath flow rates, allowing

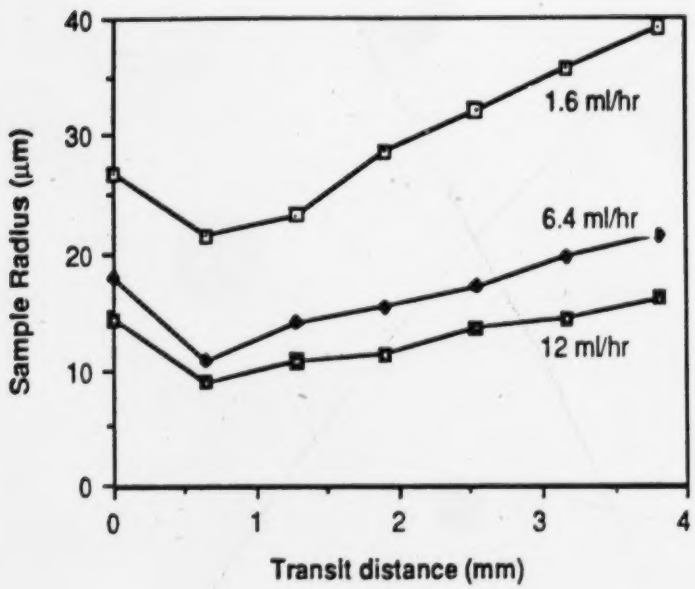

Figure 5-9. Sample radius vs transit distance. 5.29 * 10^{-8} M fluorescein is continuously introduced at 25 KV for electrophoresis as a sample stream; sheath flow rates at 1.6, 6.4 and 12 ml/hr, as indicated in the figure; capillary, 50µm ID and 99 cm long.

more time for diffusion to occur. Also, the hydrodynamic model predicts an increase in radius with decrease in sheath flow rate.

2. As the probe beam is moved closer to the exit of the capillary, a smaller transit distance is allowed, giving less time for diffusion to occur. The sample radius is smaller for each sheath flow rate ranging down from about 3.8 mm to about 0.6 mm for the transit distance.

3. The sample radius increases again when transit distance is less than 0.6 mm, because laminar flow does not occur instantaneously. The sample stream requires approximately 0.6 mm to reach its smallest radius under these experimental conditions. Lucas and Pinkel (46), in their experimental system, observed that sample stream velocity increased steadily after injection and reached a constant value after 6 mm for the transit distance. In the present system it would appear that an increase in sample stream velocity would explain the decrease in sample stream radius which occurs from the outlet of the capillary up to 0.6 mm transit distance.

It would seem that a better detection limit should be obtained at the probe region right after the capillary outlet and at a lower sheath flow rate because diffusion does not have enough time to happen and the sample linear velocity is slow. Sample molecules therefore spend more time in the laser beam, and of course, more fluorescence is generated and a better detection limit is produced.

The proof that a better detection limit is produced under the above argument is shown in figure 5-10. This electropherogram is obtained for injection of 2.1 nl (2 KV for 8 seconds) of $4.23 * 10^{-9}$ M fluorescein in 5 mM phosphate buffer and at a sheath flow rate of 0.56 ml/hr for the 5 mM pH 10 carbonate buffer. The voltage applied to the 50 μm ID, 84 cm long capillary is 25 KV, and the peak occurs at about 8 minutes. The estimated detection limit at three times background noise is $3.09 * 10^{-11}$ M which corresponds to only thirty nine thousand molecules injected onto the capillary. Of course, during the process of electrophoresis, dilution occurs within the column to reduce the analyte concentration to about $4.20 * 10^{-12}$ M at the detection limit. The detection limit of $4.20 * 10^{-12}$ M is quite close to that for the neat sample solutions, $1.25 * 10^{-12}$. Preliminary experimental results indicate that good separation for a minute sample should be achievable using this instrumentation.

4.3. Effect of sheath flow rate on theoretical plate and resolution

The theory part of section 2 predicts that the number of theoretical plates and the resolution are a function of the sheath flow rate. These predictions are tested by using approximately $1.0 * 10^{-7}$ M FITC-I in 5 mM pH 9.0 carbonate buffer solution as the solute, injected at 2 KV for 10 seconds, 5 mM pH 10 carbonate buffer for the

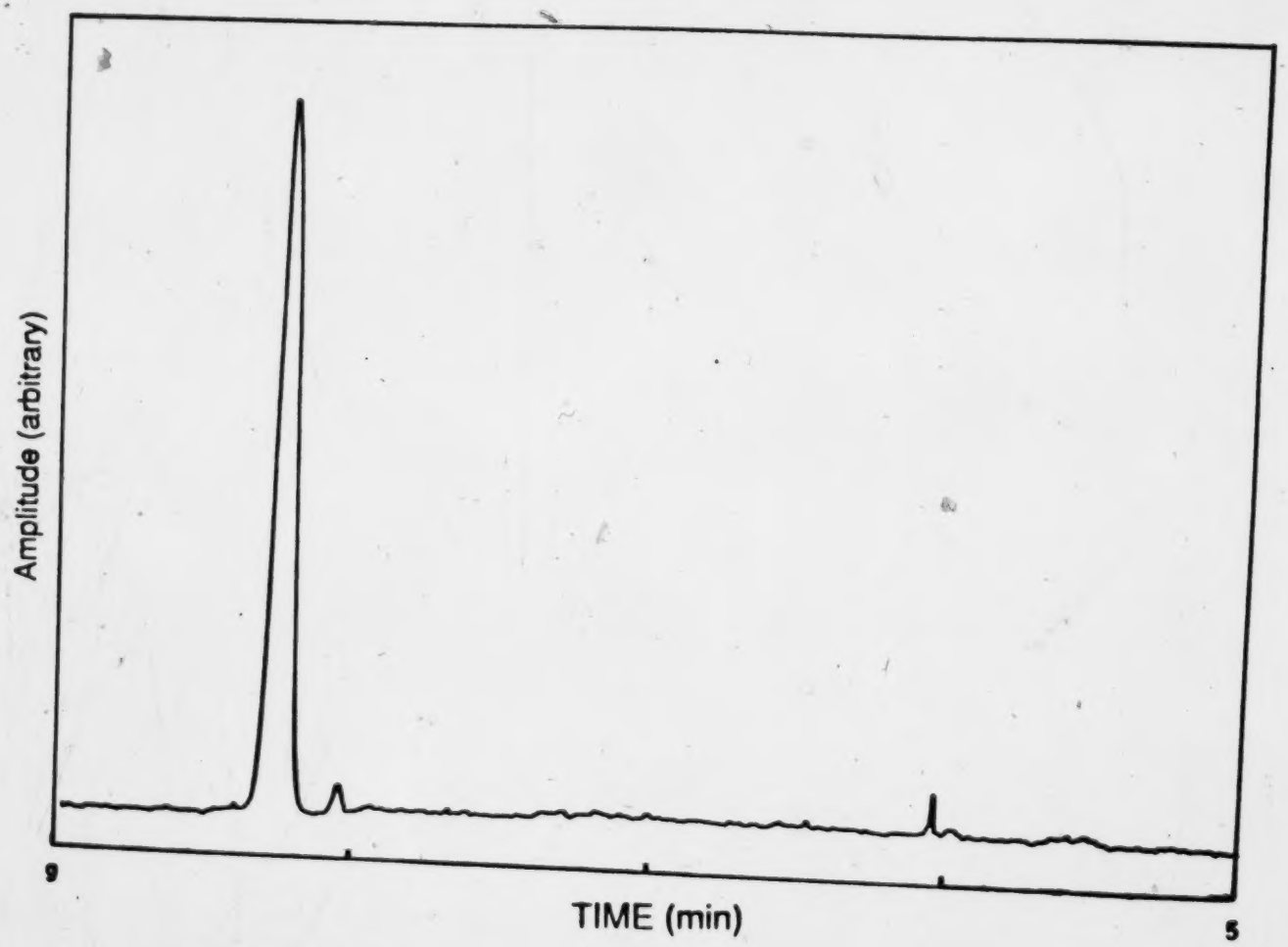

Figure 5-10. Electropherogram of $4.23 * 10^{-9}$ M fluorescein injected at 2 KV for 8 s, 2.2 nl; sheath, 5 mM pH 10 carbonate buffer at 0.56 ml/hr; capillary, 50 μm ID and 84 cm; voltage for electrophoresis, 25 KV.

electrophoresis at 25 KV, capillary 50 μm inner diameter and 97 cm long, and at three different sheath flow rates: 0.56, 5.6, and 14 ml/hr. Also, the capacitor for this experiment is 10 μF, instead of 250 μF, to reduce the time constant of the detector to avoid peak distortion.

For this experiment, N = 870,000 plates when α Q approaches zero at a sheath volumetric flow rate of 0.56 ml/hr, shown by peak 2 in appendix 1-1. The diffusion constant, D, is calculated to be $6.8 * 10^{-6}$ cm^2/sec according to equation 5.26. This value for the diffusion is reasonable for most small molecules. The net migration velocity, v_{net}, is equal to the electromigration velocity, $(\mu_{ep} + \mu_{eo})$ V/L, minus the sheath stream effect on the electromigration inside the capillary, v_{sheath} (or α Q). Retention times are 798, 813, and 832 seconds for sheath flow rates at 0.56, 5.6, and 14 ml/hr respectively. Therefore, v_{sheath} at a sheath volumetric flow of 5.6 ml/hr is calculated to be $2.2 * 10^{-3}$ cm/sec. The same calculation for v_{sheath} at a sheath volumetric flow of 14 ml/hr is $4.9 * 10^{-3}$ cm/sec. The value for α is approximately equal to $3.9 * 10^{-4}$ (cm)(hr)/(ml)(sec) for these particular experiments. The radius of the capillary is $2.5 * 10^{-3}$ cm. The expected number of theoretical plates at several sheath volumetric flow rates are calculated from equation 5.26, and are plotted in figure 5-11 as open symbols. The numbers of theoretical plates according to experimental results, shown as peak 2 in appendices 1-1, 1-2, and 1-3, are also plotted as solid

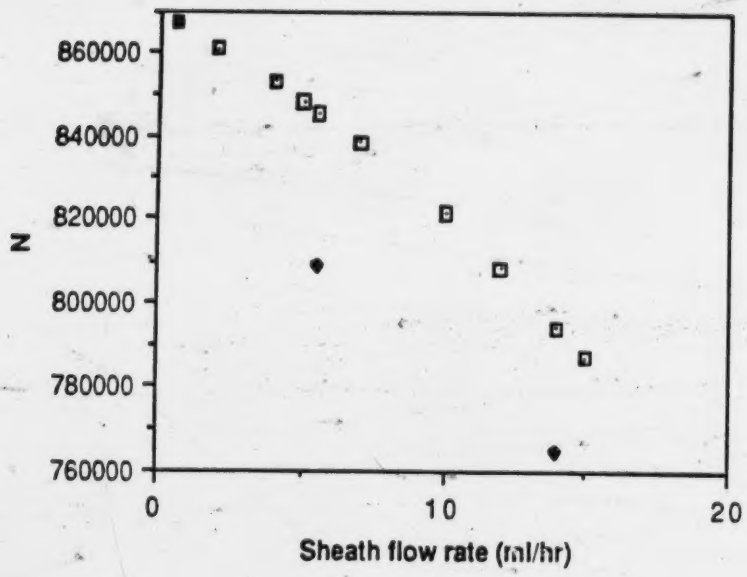

Figure 5-11. Theoretical plate number vs sheath flow rate. Open symbols are theoretical estimates; solid symbols are experimental results.

symbols in the same figure. The differences between theory and experimental result are 3.5 % and 3.8 % at sheath flow rates of 5.6 ml/hr and 14 ml/hr respectively. Poorer separation efficiencies are obtained from experiments than predicted. Presumably, the heat generated inside the capillary causes extra band broadening, discussed previously in section 1.1.3.

The intrinsic difference between the electrophoretic mobilities of the two zones, μ_1- μ_2, represented by the peaks 1 and 2 shown in appendix 1-1, is calculated to be $6.705 * 10^{-3}$ $(cm^2)/(sec)(KV)$ based upon an experiment at a sheath flow rate of 0.56 ml/hr. This value, along with the other parameters derived within this section, is then substituted into equation 5.31 for the resolution, Rs. The predicted Rs values at several sheath flow rates are shown in figure 5-12 as open symbols. The resolution increases slightly from zero to about 5.0 ml/hr and then decreases afterwards for this particular experiment. The estimated resolutions from experimental results, shown in appendices 1-2, and 1-3, are calculated according to equation 5.11 to be 3.077, 3.135, and 2.926 for sheath flow rates at 0.56, 5.6, and 14 ml/hr respectively. The results are also plotted in figure 5.12. Comparing the results from the first experiment at a sheath flow rate of 0.56 ml/hr with the results from the other two, slightly better resolution is obtained at a relatively high sheath flow rate, 5.6 ml/hr; and resolution then decreases at an even higher sheath flow rate for this particular experiment. This observation is consistent with the pheonomena

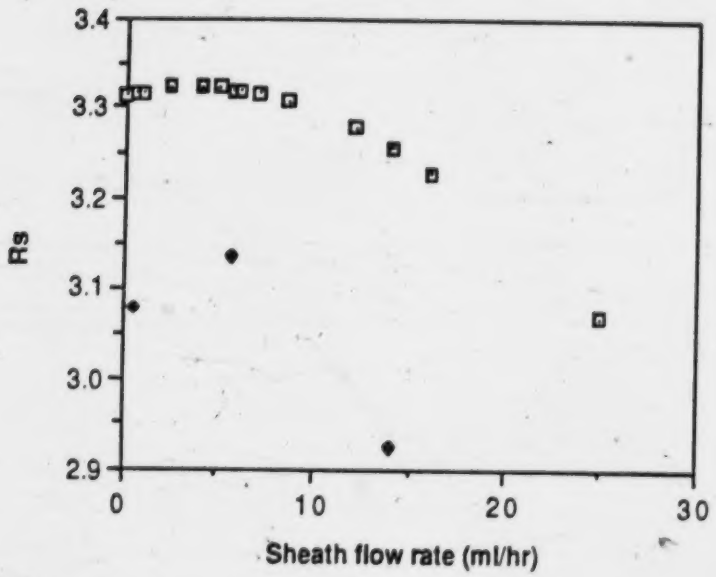

Figure 5-12. Resolution vs sheath flow rate. Open symbols are theoretical estimates; solid symbols are experimental results.

experimental results are 7.2 %, 5.6 %, and 10 % at sheath flow rates of 0.56, 5.6, and 14 ml/hr respectively. Again, the temperature rise inside the capillary for the electrophoresis should be responsible for this difference. Of course, the accuracy of the peak width measurements would contribute to the uncertainty even though the electropherograms are obtained at a relatively fast chart speed, about 2 in/min, and a magnified scale is used to measure the width of the peaks.

4.4. Separation of fluorescein-isothiocyanate derivatives of 18 amino acids

18 FTC- AAs are prepared according to section 3.3. Each sample of amino acid, ranging in volume from 2 ml to 5 ml, receives 20 µl of $5.46 * 10^{-4}$ M FITC solution.The concentration of this limiting reagent in each vial is listed on table 5-2 under C_{rea}, which is in the order of 10^{-6} M. Higher concentrations of this reagent are avoided because the instrumentation is sufficiently sensitive that a strong background signal is produced which effectively masks the derivatives' signal. After two to four hours reaction at room temperature in the dark, the FTC-AA is then further diluted by taking10 µl of each reacted solution and added to 10 ml of 5 mM pH 9.0 carbonate buffer solution for the injection.

The estimated concentration of each FTC-AA, assuming that the limiting reagent is completely bound to the amino acid, is also listed in

FTC-AAs	C_{rea} ($M * 10^{-6}$)	C_{inj} ($M * 10^{-9}$)
Ala	2.175	2.137
Arg	2.175	2.137
Asp	2.175	2.137
Cys	5.406	5.310
Glu	5.406	5.310
Gly	5.406	5.310
His	3.616	3.552
Ile	2.175	2.137
Leu	2.716	2.668
Lys	2.175	2.137
Met	2.175	2.137
Phe	3.616	3.552
Pro	2.175	2.137
Ser	2.175	2.137
Thr	2.175	2.137
Trp	2.175	2.137
Tyr	2.175	2.137
Val	5.406	5.310

Table 5-2. The concentration of FITC-I (limiting reagent), C_{rea}, for the reaction of 18 AAs; and the concentration of each FTC-AA, C_{inj}, being diluted with 5 mM pH 9.0 carbonate buffer for the injection, assuming that the FITC-I is completely bound to each AA.

table 5-2 under C_{inj}. The buffer for the electrophoresis is 5 mM pH 9.0 carbonate solution at 25 KV for the electrophoresis, and the capillary is 99 cm long with a 50 μm inner diameter. The sheath stream is the same buffer as for the electrophoresis and flows at 0.56 ml/hr. The above sample solution is injected at 2 KV for 10 sec.

The blank reaction is also carried out under the same conditions as above. The electropherogram for the blank reaction is shown in figure 5-13. The commercial FITC-I contains some contaminants as can be seen in this figure. Maeda et. al. identifies impurities in FITC-I as isomer II as well as fluorescein, fluorescein-amine (34).

The electropherogram for the separation of 18 FTC-AAs is shown in figure 5-14. The identification of each individual FTC-AA is complicated due to retention time shifting slightly for each run, presumably a result of temperature fluctuations in the capillary. There are two ways to identify each peak. One is to normalize the retention time for individual FTC-AAs as a fraction of the distance between the third and fourth blank peaks, for instance, as the references. The other method, which is applied for the present work, is to run a series of experiments to identify those peaks whose retention times are close to one another. The procedures are as follow: first, electropherograms are obtained from eighteen individual FTC-AAs to determine their relative retention times;

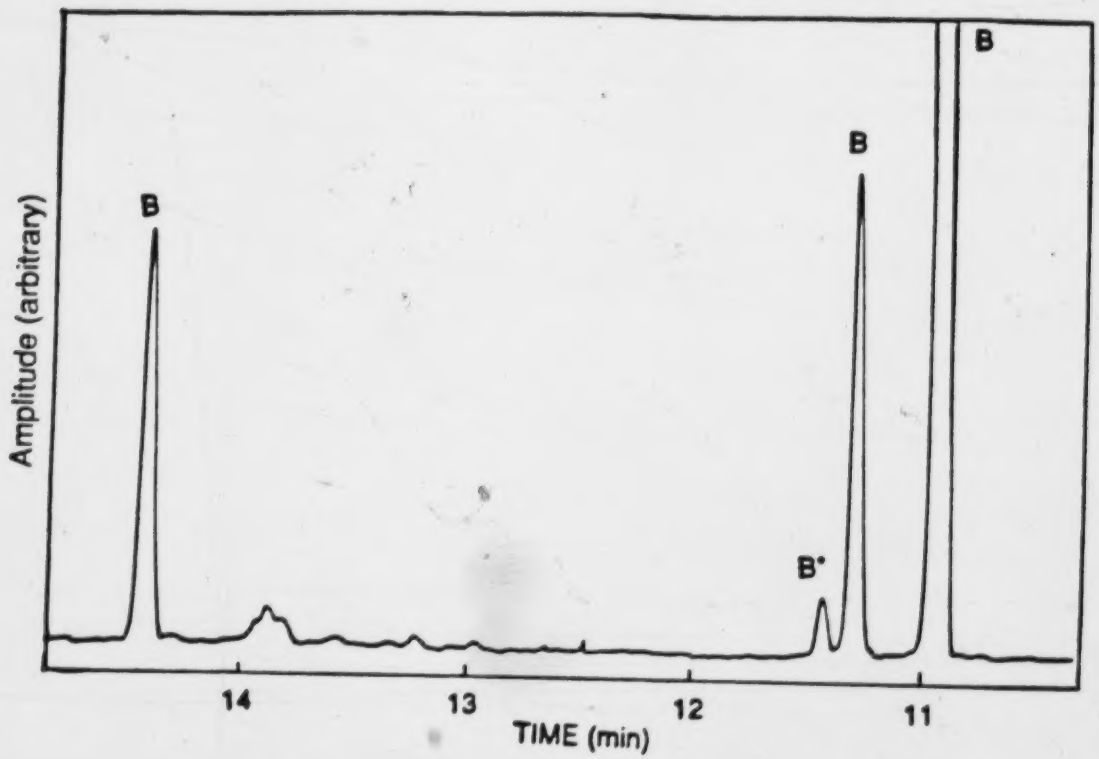

Figure 5-13. Electropherogram of the FITC-I blank reaction. The commercial FITC-I contains some contaminants as can be seen in this figure.

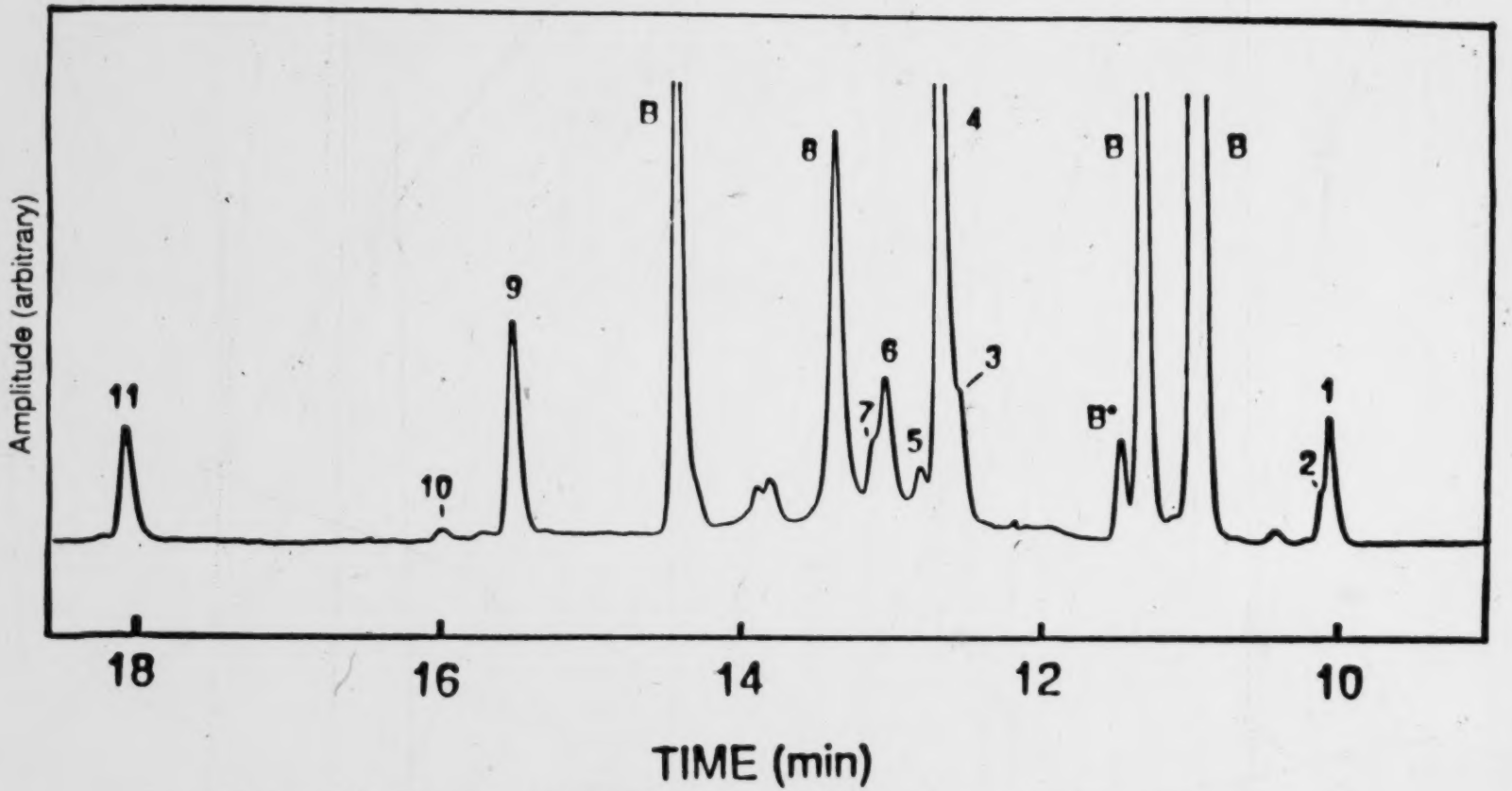

Figure 5-14. Separation of between 3 and 11 attomoles of 18 amino acids. The separation is driven by a 25 KV potential and a pH 9 buffer is used for both the separation and also the sheath stream. Injection was 10 seconds at 2 KV. Peak 1 is Arg, 2 is Lys, B are peaks associated with the reagent blank, 3 is Ile, Trp, and Leu, 4 is Val, His, Phe, Tyr, Pro,and Met, 6 is Ser, 7 is Ala, 8 is Gly, 9 is Glu, 10 is Asp, and 11 is Cys.

second, the electropherogram, figure 5-14, for the mixture of the 18 FTC-AAs is obtained; third, those peaks which are close to one another are identified by conducting several experiments, whose results are shown in appendix. For instance, an electropherogram, appendix 2-1, for a mixture of FTC-Gly, FTC-Tyr, FTC-Pro and FTC-Met is obtained; then an electropherogram, appendix 2-2, for only FTC-Gly is obtained to further confirm its retention time. At this point, it seems apparent that the elution time is the same for FTC-Tyr, FTC-Pro and FTC-Met. Further confirmation is obtained by injecting a mixture of FTC-Tyr and FTC-Pro which appears as a single peak in appendix 2-3. Finally, the electropherogram for FTC-Met alone, appendix 2-4, is obtained and found to overlap the peaks for FTC-Tyr and FTC-Pro. This series of electropherograms confirms the identical elution time for FTC-Tyr, FTC-Pro and FTC-Met.

Table 5-3 lists the relative retention times, t_r, of FTC-AAs with respect to the third blank peak, labeled B* and the estimated volume of each FTC-AA being injected, V_{inj}, based upon equation 5.13. The injection volume is about two nanoliters for each FTC-AA. On the order of a few attomoles of each amino acid is injected. All these data are calculated from figure 5-14 under the assumption that the limiting reagent, FITC-I, is completely reacted. However, some unreacted derivative reagent is always detected. These results are conservative and the true detection limits will be less than those reported here. The number of theoretical plates, N, for this

FTC-AAs	t_r	V_{inj} (nl)	mole $_{inj}$ (atto)	N
Ala	1.144	1.98	4.23	
Arg	0.878	2.58	5.51	120,000
Asp	1.393	1.63	3.48	
Cys	1.578	1.44	7.65	210,000
Glu	1.353	1.68	8.92	180,000
Gly	1.167	1.94	10.3	110,000
His	1.104	2.05	7.28	
Ile	1.085	2.09	4.47	
Leu	1.085	2.09	5.58	
Lys	0.882	2.57	5.49	
Met	1.104	2.05	4.38	
Phe	1.104	2.05	7.28	
Pro	1.104	2.05	4.38	
Ser	1.138	1.99	4.25	
Thr	1.117	2.03	4.33	
Trp	1.085	2.09	4.47	
Tyr	1.104	2.05	4.38	
Val	1.104	2.05	10.9	
Blank(3rd)	1.000			130,000

Table 5-3. Based upon figure 5-14, pH 9.0 for the electrophoresis. Retention time, t_r, of each FTC-AA relative to the third blank peak; estimated sample being injected in volume, V_{inj}; in moles, mole $_{inj}$; and the theoretical plates, N; under the assumption that the FITC-I is completely bound to AA.

experiment is only just above one hundred thousand. The separation efficiency is not good enough to separate these 18 amino acids. About 11 amino acids are separated out of the eighteen. The poor theoretical plate count may be due to an adsorption problem which can be eliminated by the following methods: 1. Dynamically modifying the interfacial double layer between the column wall and the bulk solution with selected ions. 2. Raising the pH of the buffer solution to increase the coulombic repulsion between the analytes and the capillary wall (23).

For the present work, the relatively easy second method is employed to reduce the adsorption problem between the FTC-AAs and the capillary wall. The pH of the buffer solution is adjusted from 9.0 to 10 for the electrophoresis and for the sheath stream. Other conditions remain the same as for the previous experiment. Under these conditions the FTC-AAs should be repelled from the wall and their surface adsorption strongly diminished, thereby increasing the separation efficiency and resolution in the CZE, which can be seen in figure 5-15. Fifteen peaks are observed from the eighteen amino acids injected. The retention time, tr, injected volume, V_{inj}; injected moles, $mole_{inj}$; and the theoretical plate count, N, are listed in table 5-4. Again, all the data are based upon the assumption that the FITC-I is completely bound to amino acid.

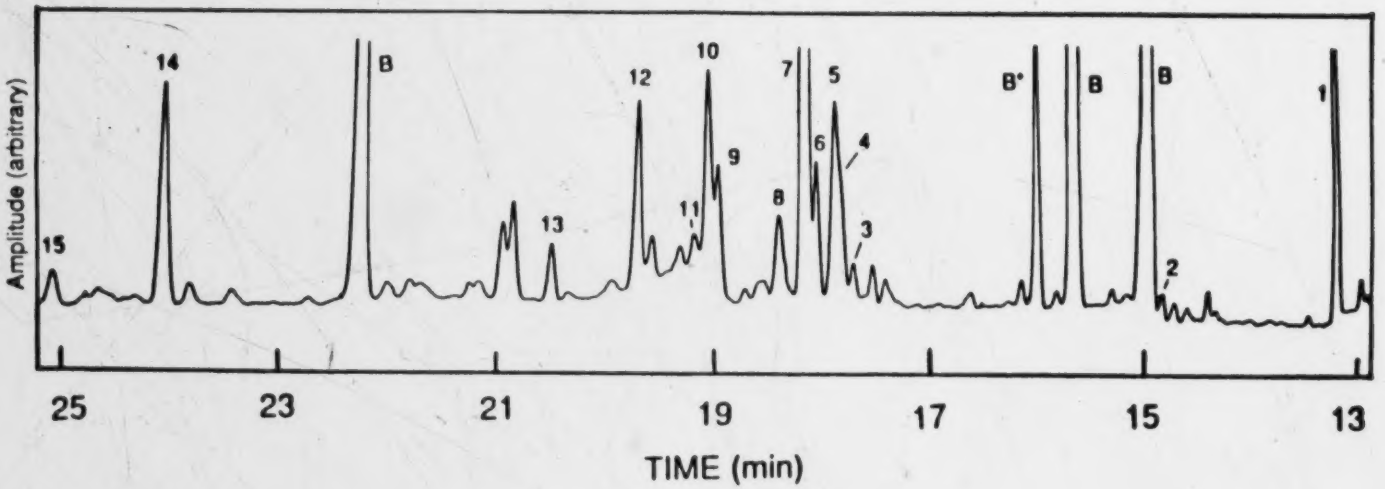

Figure 5-15. Separation of between 2 and 7 attomoles of 18 amino acids. The separation is driven by a 25 KV potential and a pH 10 buffer is used for both the separation and also the sheath stream. Injection was 10 seconds at 2 KV. Peak 1 is Arg, 2 is Lys, B are peaks associated with the reagent blank, 3 is Leu, 4 is Ile, 5 is Trp, 6 is Met, 7 is Phe, Val, His, and Pro, 8 is Thr, 9 is Ser, 10 is Cys, 11 is Ala, 12 is Gly, 13 is Tyr, 14 is Glu, and 15 is Asp.

FTC-AAs	t_r	V_{inj} (nl)	mole $_{inj}$ (atto)	N
Ala	1.196	1.35	2.88	
Arg	0.824	1.96	4.19	
Asp	1.563	1.03	2.20	470,000
Cys	1.188	1.36	7.22	
Glu	1.500	1.08	5.73	460,000
Gly	1.230	1.31	6.96	450,000
His	1.133	1.43	5.08	
Ile	1.112	1.45	3.10	
Leu	1.105	1.46	3.90	
Lys	0.927	1.74	3.72	
Met	1.126	1.43	3.06	
Phe	1.133	1.43	5.08	
Pro	1.133	1.43	3.06	
Ser	1.183	1.37	2.93	
Thr	1.148	1.41	3.01	
Trp	1.116	1.45	3.10	
Tyr	1.278	1.26	2.69	550,000
Val	1.133	1.43	7.59	
Blank(3rd)	1.000			

Table 5-4. Based upon figure 5-15. The retention time, t_r, of each FTC-AA relative to the third blank peak, the estimated sample being injected in volume, V_{inj}; in moles, $mole_{inj}$; and the theoretical plates, N; buffer pH 10 used for the electrophoresis, under the assumption that the FITC-I is completely bound to AA.

Higher fluorescent signals and better separations are obtained for electrophoresis at pH 10 than at pH 9.0. Comparison of these two electropherograms confirms the order of the elution is consistent with the model of section 1.1.1. Molecules with higher negative charges elute later. For instance, glutamic acid and aspartic acid have longer retention times than alanine and glycine. For particles of the same charge, equation 5.1 shows that smaller particles have higher electrophoretic mobility. Particles with higher electrophoretic mobility should move faster towards the positive end because all the FTC-AAs are negatively charged and take longer to reach the negative, detector end. It is observed that the smaller and lighter amino acids, with the same charges under the same experimental conditions come out later than the bigger, heavier ones. For example, aspartic acid elutes later than glutamic acid, and glycine elutes later than alanine. An interesting phenomenon was observed for the FITC-I derivative of cysteine. It eluted last at pH 9 for the electrophoresis but emerged faster at pH 10. Presumbly, the FTC-cysteine at higher pH undergoes structural change, for instance it may undergo a cyclization reaction and change its electrophoretic properties.

The difference in run time for the two electrophoresis buffer solutions, roughly 18 minutes and 25 minutes for pH 9.0 and pH 10 respectively, is expected since both electrophoretic flow and electro-osmotic flow are pH dependent. At higher pH, the amino acids

will have a higher net negative charge. Also an increased electro-osmotic flow is expected, as discussed in section 1.1.2. In these particular experiments, the effect from the former dominates. Presumably the zeta potential of the wall does not alter much from pH 9.0 to pH 10.

Separation and detection of subattomole amounts of amino acids have been demonstrated using this instrumention. Detection limits at three times background noise are listed in tables 5-5 and 5-6 for the present work. Table 5-5 is based upon results from figure 5-14, using a pH 9.0 buffer solution for the electrophoresis and sheath streams. Table 5-6 relates to figure 5-15 using a pH 10 buffer. Within tables 5-5 and 5-6, concentration detection limits are listed under C LOD; mole detection limits under Moles; and molecule detection limits under Molecules. The FTC-Arg peak for figure 5-15 is off scale, therefore, the detection limits for it are listed in table 5-6 as less than the numbers estimated from the highest point shown in the electropherogram. All these data are generated under the assumption that the purchased reagent, FITC-I, is one hundred percent pure and is completely reacted with the amino acids. However, the electropherogram shown would indicate that the FITC-I solution was not one hundred percent pure and had not completely reacted with the amino acid. Detection limits should be better than those listed in tables 5-5 and 5-6.

FTC-AAs	C_{LOD} ($M*10^{-11}$)	Moles ($*10^{-20}$)	Molecules ($*10^{3}$)
Ala	3.6	7.1	43
Arg	2.6	6.6	40
Asp	28	46.	270
Cys	7.3	11.	63
Glu	3.7	6.2	37
Gly	2.0	3.9	24
His	-	-	-
Ile	-	-	-
Leu	-	-	-
Lys	6.0	15.	93
Met	-	-	-
Phe	-	-	-
Pro	-	-	-
Ser	2.2	4.3	26
Thr	9.3	19.	110
Trp	-	-	-
Tyr	-	-	-
Val	-	-	-

Table 5-5. Detection limits, at three times background noise, in terms of concentration, C_{LOD}; of moles, Moles; and of molecules, Molecules injected onto the column. All these data are generated based upon figure 5-14, using pH 9.0 buffer for the electrophoresis and sheath streams under the assumption that the FITC-I is one hundred percent pure and is completely bound to AA.

FTC-AAs	C_{LOD} ($M*10^{-11}$)	Moles ($*10^{-20}$)	Molecules ($*10^{3}$)
Ala	3.4	4.6	27.
Arg	<0.49	<0.95	<5.7
Asp	6.6	6.8	41.
Cys	2.4	3.3	20.
Glu	2.6	2.8	17.
Gly	2.8	3.7	22.
His	-	-	-
Ile	1.7	2.5	15.
Leu	7.0	10.	61.
Lys	8.6	15.	90.
Met	1.6	2.3	14.
Phe	-	-	-
Pro	-	-	-
Ser	1.6	2.3	13.
Thr	2.6	3.7	22.
Trp	1.1	1.7	9.9
Tyr	1.1	1.4	8.4
Val	-	-	-

Table 5-6. Detection limits, at three times background noise, in terms of concentration, C_{LOD}; of moles, Moles; and of molecules, Molecules injected onto the column. All these data are generated based upon figure 5-15, using pH 10 buffer for the electrophoresis and sheath streams under the assumption that the FITC-I is one hundred percent pure and is completely bound to AA.

The concentration detection limits are on the order of 10^{-11} M, which are three orders of magnitude superior to any other amino acid analysis technique. The best previous fluorescence detection is about 10^{-7} M for the dansyl and fluorescamine derivatives of amino acids (26), and thermo-optical detection at about 10^{-8} M for the dabsyl amino acids (28). It is interesting that there is no suitable prefix to describe these state-of-the-art detection limits when converting the detection limits from the concentration into the number of moles injected onto the column, which are in the order of 10^{-20} moles.

In an alternate preparation to that discribed in the opening paragraph of this section and section 3.3, the eighteen AAs are reacted with 2 ml of $5.46 * 10^{-4}$ M FITC-I solution all at once in a 20 ml glass vial. After four hours reaction time in the dark, 200 µl of reacted solution is diluted with 10 ml of 5 mM, pH 9.0 carbonate buffer. The diluted solution is then injected at 2 KV for 8 seconds onto the capillary for the separation. The electropherogram is shown in appendix 3. Many unidentified peaks are observed because side reactions occur among amino acids during the process of attaching fluorescein chromophore to the α-amino acid group of individual amino acids. Further investigation of the reaction mechanism needs to be done.

Of course, other improvements can be considered for this instrumentation, such as better collection efficiency, background subtraction, and optimization of separation efficiency. The major

limitation of the current instrument is the microscope objective utilized to collect the fluorescence. The 0.45 NA objective collects only about 5.3 % of the emitted light. A higher numerical aperture should collect more emitted light, and a higher quantum yield photomultiplier tube should generate a better detection limit. The buffer solution also plays an important role in the separation mode. Further investigations of different buffer systems need to be done.

The lack of an efficient cooling system for the capillary also appears to be an important factor in separation. This system could be improved by surrounding the capillary tube with the sheath stream. The advantage of this is that the sheath stream would help the dissipate the heat which arises inside the capillary.

REFERENCES

1. Pauling, L.; Itano, H. A.; Singer, S. J.; Wells, I. C. *Science*, 1949, 110, 543.
2. Mikkers, F. E. P.; Everaerts, F. M.; Verheggen, P. E. M. *J. Chromatogr.* 1979, 169, 1.
3. Jorgenson, J. W.; Lukacs, K. D. *Anal. Chem.* 1981, 53, 1298.
4. Karger, B. L.; Snyder, L. R; Horvath, L. R. "An Introduction to Separation Science", John Wiley and Sons: Toronto, 1973.
5. Giannovario, J. A.; Griffin, R. N.; Gray, E. L. *J. Chromatogr.* 1978, 153, 329.
6. Lederer, M. "An Introduction to Paper Electrophoresis and Related Methods", Elsevier Publishing Company: New York, 1957.
7. Shaw, D. J. "Electrophoresis", Academic Press: New York, 1969.
8. Nee, T. W. *J. Chromatogr.* 1975, 105, 231.
9. Pretorius, V.; Hopkins, B. J.; Schieke, J. D. *J. Chromatogr.* 1974, 99, 23.
10. Gordon, M. H. "Instrumental Analysis in the Biological Sciences", Blackie: Glasgow, 1987.
11. Lukacs, K. D.; Jorgenson, J. W. *J . High Resol. Chromatogr. and Chromatogr. Communi.* 1985, 407.
12. Wieme, R. J. "Chromatography: A Laboratory Handbook of Chromatographic and Electrophoretic Methods", 3rd ed. Heffmann, E., Reubhold, V. N.: New York, 1975, chapter 10.

13. Vacik, J. "Electrophoresis - A Survey of Techniques and Applications, Part A: Techniques", Elsevier, Amsterdam, 1979, chapter 2.

14. Mikkers, F. E. P.; Everaerts, F. M.; Verheggen, P. E. M. *J. Chromatogr.* 1979, 169, 11.

15. Jorgenson, J. M.; Lukacs, K. D. Science. 1983, 222, 266.

16. Jorgenson, J. W.; Phillips, M. "New Directions in Electrophoretic Methods", ACS Symposium Series 335, Washington, DC, 1987.

17. Hinckley, J. O. N. *J. Chromatogr.* 1975, 109, 209.

18. Brown, J.; Kinckley, J. O. N. *J. Chromatogr.* 1975, 109, 218.

19. Foret, F.; Deml M.; Kahle, V.; Bocek, P. *Electrophoresis*, 1986, 7, 430.

20. Huang, X. H.; Pang, T. K. J.; Gordon, M. J.; Zare, R. N. *Anal. Chem.* 1987, 59, 2747.

21. Fujiwara, S.; Honda, S. *Anal. Chem.* 1987, 59, 487.

22. Terabe, S.; Ichikawa, K.; Otsuka, K.; Tsuchlya, A.; Ando, T. *Anal. Chem.* 1984, 56, 111.

23. Lauer, H. H.; McManigill, D. *Anal. Chem.* 1986, 58, 166.

24. Olivares, J. A.; Nguyen, N. A.; Yonker, C. R.; Smith, R. D. *Anal. Chem.* 1987, 59, 1230.

25. Green, J. S.; Jorgenson, J. W. *J. Chromatogr.* 1986, 352, 337.

26. Gozel. P.; Gassmann, E.; Michelsen, H.; Zare, R. N. *Anal. Chem.* 1987, 59, 44.

27. Gassmann, G.; Huo, J. E.; Zare, R. N. *Science*, 1985, 230, 813.

28. Yu, M.; Dovichi, N. J. *Mikrochimica Acta*. 1988, in press.

29. Wallingford, R. A.; Ewing, A. G. *Anal. Chem.* 1987, 59, 1762.

30. Tsuda, T. *Anal. Chem.* 1987, 59, 799.

31. Meyer, V. R. *J. Chromatogr.* 1985, 334, 197.

32. ACS Committee on Environmental Improvement, Daniel MacDoughal, Chairman. Guidelines for data acquisition and data quality evaluation in environmental chemistry. *Anal. Chem.* 1980, 52, 2242.

33. Knoll, J. E. *J. Chromatogr. Sci.* 1985, 23, 422.

34. Maeda, H.; Kawauchi, H. *Biochem. Biophys. Res. Commun.* 1968, 31, 188.

35. Maeda, H.; Ishida, N.; Kawauchi, H.; Tuzimura, K. *J. Biochem.* 1969, 65, 777.

36. Maeda, H.; Ishida, N.; Kawauchi, H.; Tuzimura, K. *J. Biochem.* 1969, 66, 783.

37. Tuzimura, K.; Kawauchi, H.; *Arg. Biol. Chem.* 1971, 35, 150.

38. Muramoto, K.; Kawauchi, H.; Tuzimura, K. *Arg. Biol. Chem.* 1975, 39, 2241.

39. Muramoto, K.; Kamiya, H.; Kawauchi, H. *Anal. Chem.* 1984, 141, 446.

40. Sanger, F. *J. Biochem.* 1945, 39, 507.

41. Fraenkel-Conrat, H.; Harris, J. I.; Levy, A. L. "Methods of Biochemical Analysis", Glick, D. ed, Interscience Pub. Inc.: New York, Vol. II, 1955.

42. Edman, P. *Acta Chem. Scand.* 1950, 4, 283.

43. Horvai, G.; Pungor, E. CRC. Rev. *Anal. Chem.* 1985, 17, 231.

44. Giddings, J. C. *Sep. Sci.* 1969, 4, 181.

45. Bird, R. B.; Stewart, W. E.; Lightfoot, E. N.; Chapman, T. W. "Lectures in Transport Phenomena", American Institute of Chemical Engineers: New York, 1969.

46. Lukacs, J. N.; Pinkel, D. *Cytometry*, 7, 575.

CHAPTER SIX

CONCLUSION AND FUTURE WORK

It is clear that laser-induced applications using the sheath-flow cuvette as a detector cell produce excellent detection limits for small volume analysis.

High precision laser-based refractive index determinations within picoliter volumes using flow modulation of the sheath-flow cuvette (1), chapter two, produce detection limits of $7 * 10^{-8}$ ΔRI within a $4 * 10^{-10}$ liter probe volume for neat solutions. In this technique, diffraction of the laser beam within the cuvette produces a change in the far-field beam-center intensity which is proportional to the difference in refractive index between the sample and sheath; synchronous demodulation of the laser beam intensity leads to improved refractive index precision. The application of this technique should extend to microbore liquid chromatography, especially for gradient elution since the sheath stream can be produced simultaneously from the same mobile phase reservoir for the separation column. The synchronous change in solvent composition for the sample stream and the sheath stream would eliminate the limitation of the refractive index detector system due to the gradient process.

Thermo-optical absorbance determination within the sheath-flow cuvette (2), chapter three, produces absorbance detection limits of $1.1 * 10^{-5}$ utilizing a 2-mW pump laser beam and a 50 to 70 μm radius sample stream in the cuvette. In this technique, the sample is heated by the modulated pump beam, and a second coplanar probe beam is used to detect the change of the refractive index induced by the pump beam. A lock-in amplifier is used to demodulate the periodic change of refractive index. The change of intensity is proportional to the concentration of the analyte. Although the detection limit for the present work is a factor of two worse than in a 50 μm diameter capillary tube (5-6), the detection limits using a sheath-flow cuvette should be better than those obtained using a straight capillary tube if a much higher power pump beam were used. This improved detection limit should occur because the cuvette cell only detects differences in refractive index between the sample and the sheath streams. The finite solvent background absorbance, which will produce a proportional noise source and limit the precision of the measurement for high power pump lasers, can be eliminated. Another obvious advantage of using a sheath-flow cuvette as a detector cell over others is when dealing with viscous and strongly adsorbing materials which would contaminate the detector windows.

Laser-induced fluorescence detection using the sheath-flow cuvette for neat sample solution, chapter four, produces a detection limit of $1.25 * 10^{-12}$ M within a 20 μm radius sample stream. Subattomole amino acid separation in laser-induced fluorescence

detection using the sheath-flow cuvette for capillary zone electrophoresis (7), chapter five, produces detection limits in the order of 10^{-20} mole for the separation and determination of eighteen amino acids. In the former technique, a one watt argon ion laser operating at 488 nm is used as the excitation source and a microscope set at a right angle to the laser beam is used to collect the fluorescent signal. In the latter technique, a capillary zone electrophoresis system is combined with the laser-induced fluorescence detection used in the first technique. The capillary zone electrophoresis system is constructed by applying a high positive voltage through a 50 μm diameter, 99 cm capillary which is filled with an appropriate buffer. The sheath-flow cuvette is at ground potential. Separation and determination of single molecules should be achievable if further improvements can be done, such as better collection efficiency, background subtraction, and optimization of the separation efficiency, as mentioned in chapters four and five.

Flow modulation is a powerful tool for analytical techniques which produce high background signals. By switching rapidly between the sample and solvent, the instrument is able to measure rapidly and directly the difference between signal and background, as discussed in chapter two for a very high background refractive index measurement. Other examples of background limited measurements include very high sensitivity absorbance and fluorescence techniques. In both cases, the state-of-the-art detection limit is dominated by background signals associated with the solvent. For fluorescence, the background signal is dominated by weak Raman scatter signals from the solvent molecules

(8). For absorbance in the visible portion of the spectrum, the background signal is usually dominated by overtones of vibrational transitions of the solvent (9). It is hoped that further studies using solvent flow modulation within the sheath-flow cuvette will enable more precise measurements of these high background signals.

The application of laser-induced fluorescence detection using the sheath-flow cuvette for capillary zone electrophoresis should be extended to the automatic analysis of protein sequences, with all operations controlled by a computer and the results shown continuously on a terminal or recorder. In the future, using this instrumentation, it should be possible to separate and identify big molecules by modifying the interfacial double layer. DNA (deoxyribonucleic acid) plays an important role in the repository of the hereditary information of the organism. The structure of the nucleic acid molecules determines the structure of protein molecules, which, in turn, control the living process. It is our hope that this technique will provide sequential information of DNA by degradation and identification of fragments automatically.

In the future, the design of the sheath-flow cuvette could be improved by enclosing the capillary carrying the sample stream within the sheath stream to improve dissipation of the heat generated within the capillary during the electromigration process.

In summary, the analytical applications of a sheath-flow cuvette as a detector cell have been demonstrated to provide state-of-the-art

trace analysis, especially when only a minute amount of sample is available. The sheath-flow cuvette should have a promising future in the area of biomedical research.

REFERENCES

1. Cheng, Y. F.; Dovichi, N. J. submitted.
2. Cheng, Y. F.; Dovichi, N. J. submitted.
3. Bornhop, D. J.; Dovichi, N. J. *Anal. Chem.* 1986, 58, 504.
4. Bornhop, D. J.; Nolan, T. G.; Dovichi, N. J. *J. Chromatogr.* 1987, 384, 181.
5. Bornhop, D. J.; Dovichi, N. J. *LC/GC,* 1986, 5, 427.
6. Bornhop, D. J.; Dovichi, N. J. *Anal. Chem.* 1987, 59, 1632.
7. Cheng, Y. F.; Dovichi, N. J. *Fluorescence Detection II*, E. Roland Menzel, Editor, Pro. SPIE 1988, 910, 112.
8. Dovichi, N. J.; Martin, J. C.; Jett, J. H.; Trkula, M.; Keller, R. A. *Anal. Chem.* 1984, 56, 348.
9. Dovichi, N. J. *CRC. Rev. Anal. Chem.* 1987, 17, 357.

APPENDICES

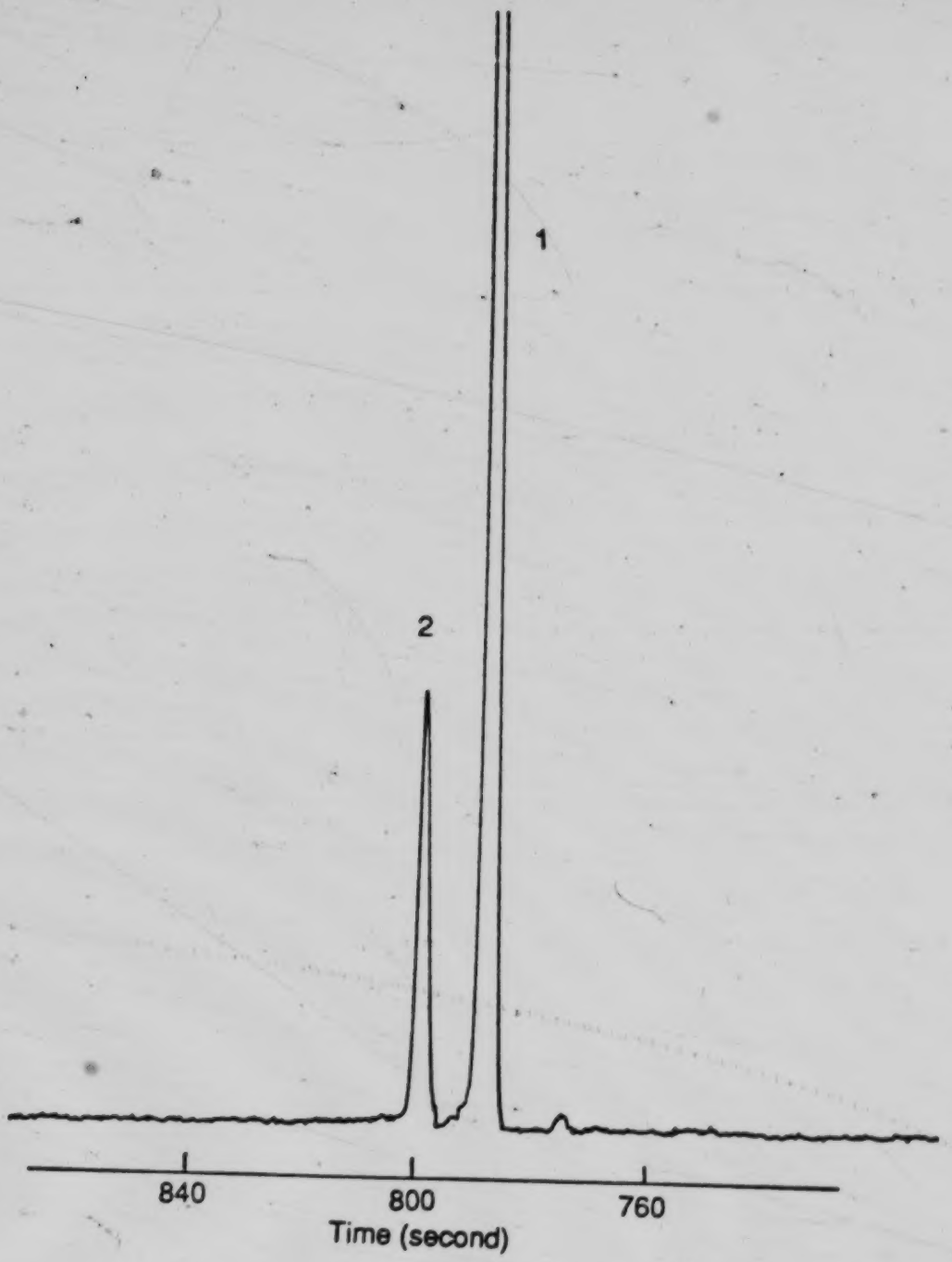

Appendix 1-1. Electropherogram of about $1.0 * 10^{-7}$ M of FITC-I injected at 2 KV for 10 seconds; sheath, 5 mM pH10 carbonate buffer at 0.56 ml/hr; capillary, 50 μm ID and 97 cm long; voltage for electrophoresis, 25 KV.

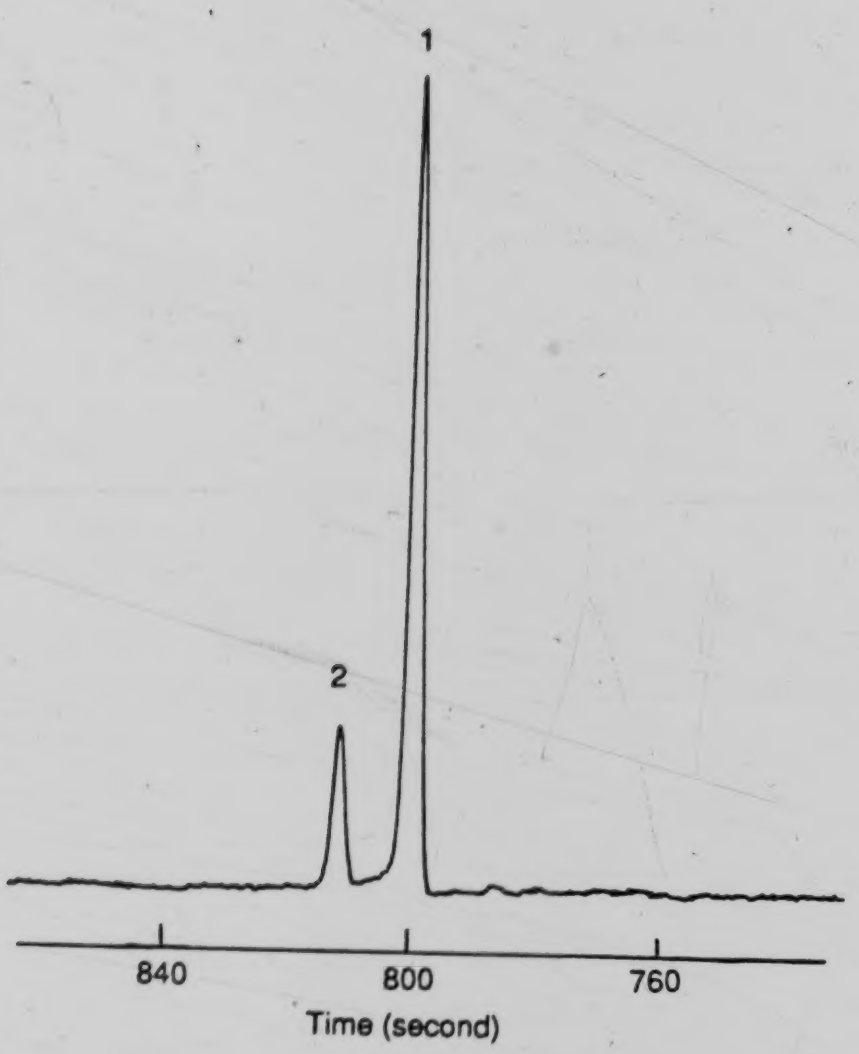

Appendix 1-2. Electropherogram of about $1.0 * 10^{-7}$ M of FITC-I injected at 2 KV for 10 seconds; sheath, 5 mM pH10 carbonate buffer at 5.6 ml/hr; capillary, 50 µm ID and 97 cm long; voltage for electrophoresis, 25 KV.

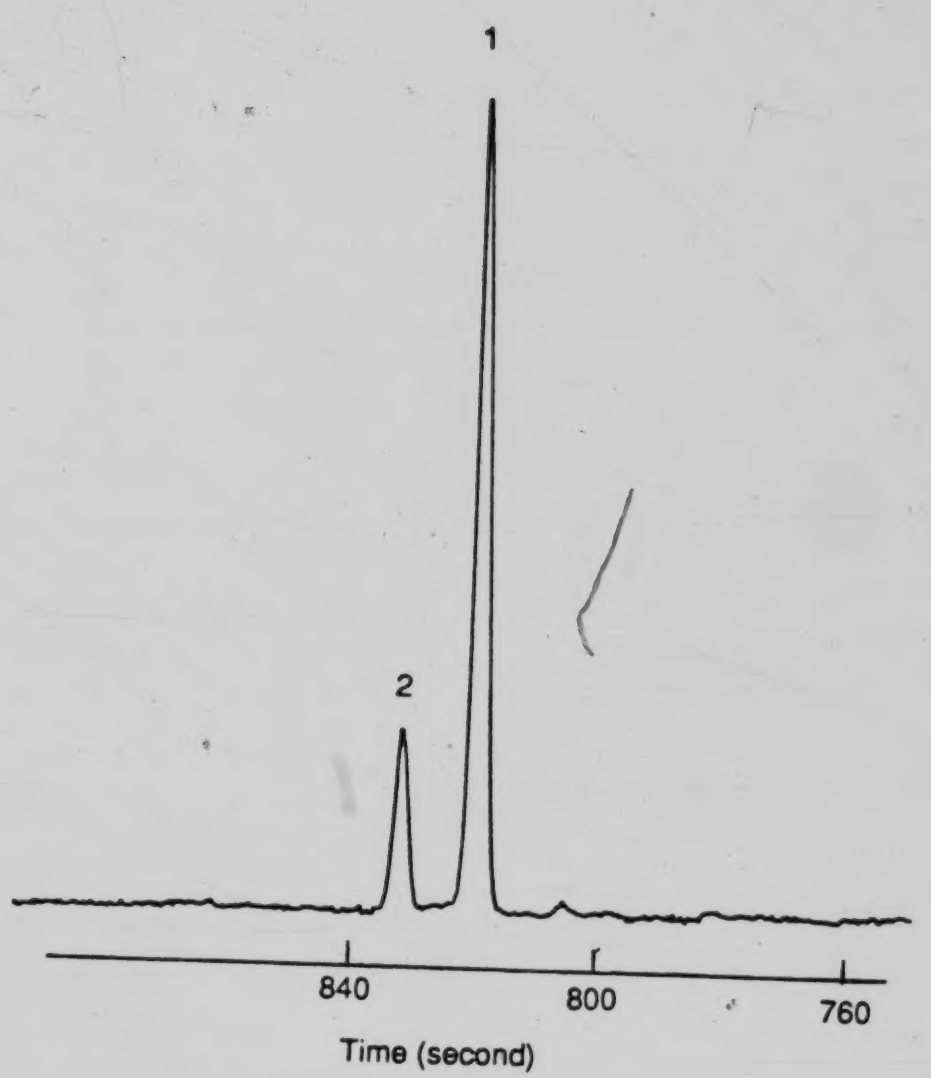

Appendix 1-3. Electropherogram of about $1.0 * 10^{-7}$ M of FITC-I injected at 2 KV for 10 seconds; sheath, 5 mM pH10 carbonate buffer at 14 ml/hr; capillary, 50 µm ID and 97 cm long; voltage for electrophoresis, 25 KV.

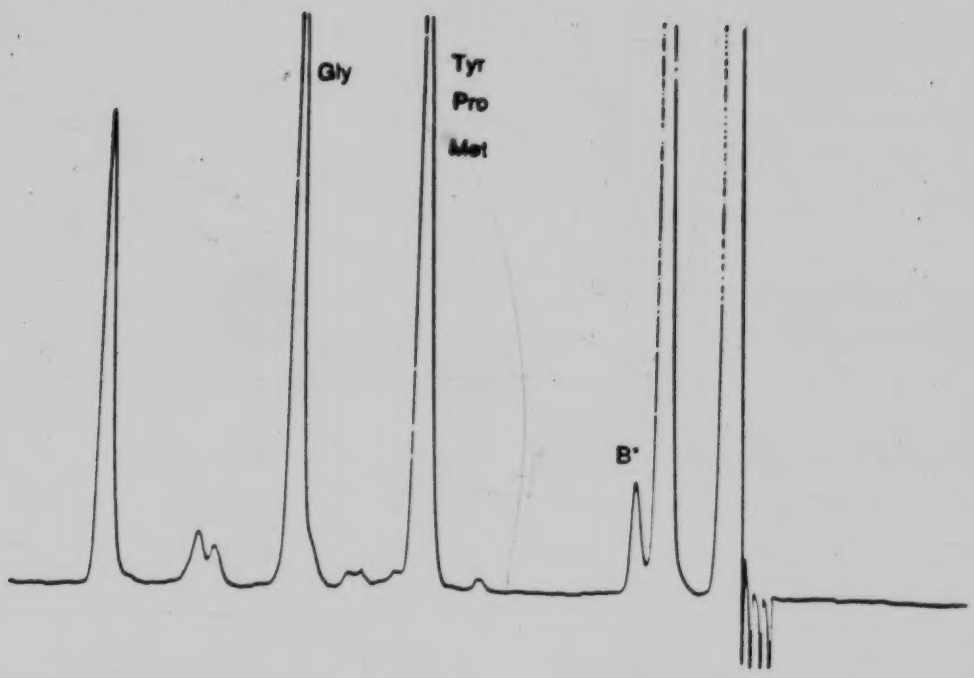

Appendix 2-1. Electropherogram for a mixture of FTC-Gly, FTC-Pro, FTC-Met, and FTC-Tyr. B* is the third blank peak.

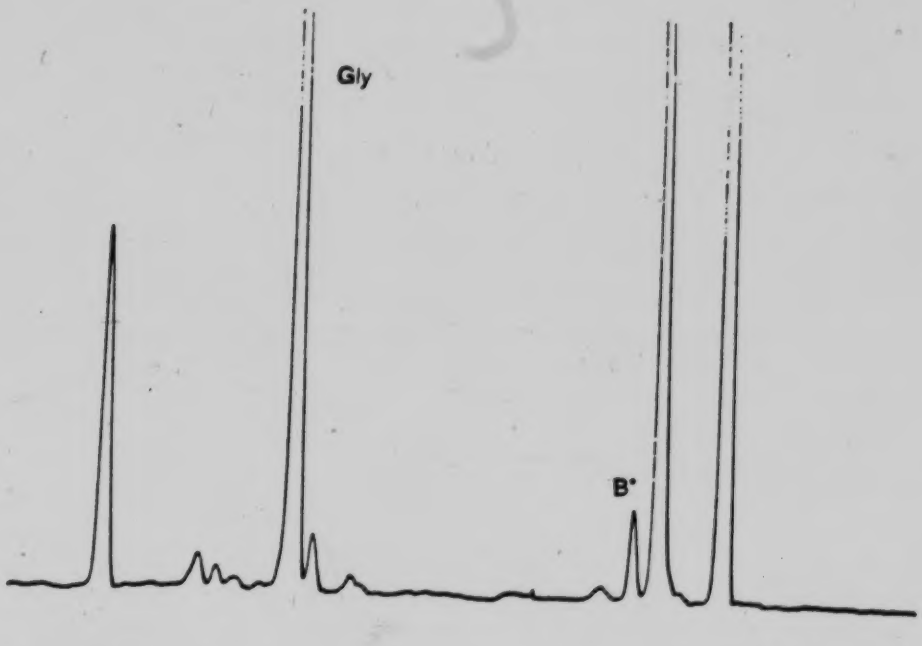

Appendix 2-2. Electropherogram for FTC-Gly. B* is the third blank peak.

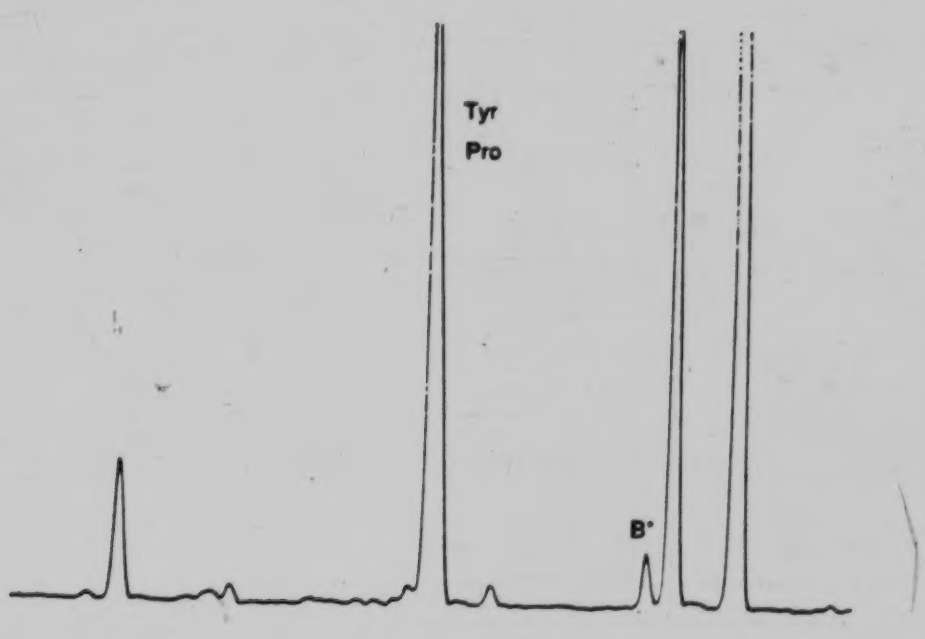

Appendix 2-3. Electropherogram for a mixture of FTC-Tyr and FTC-Pro B* is the third blank peak.

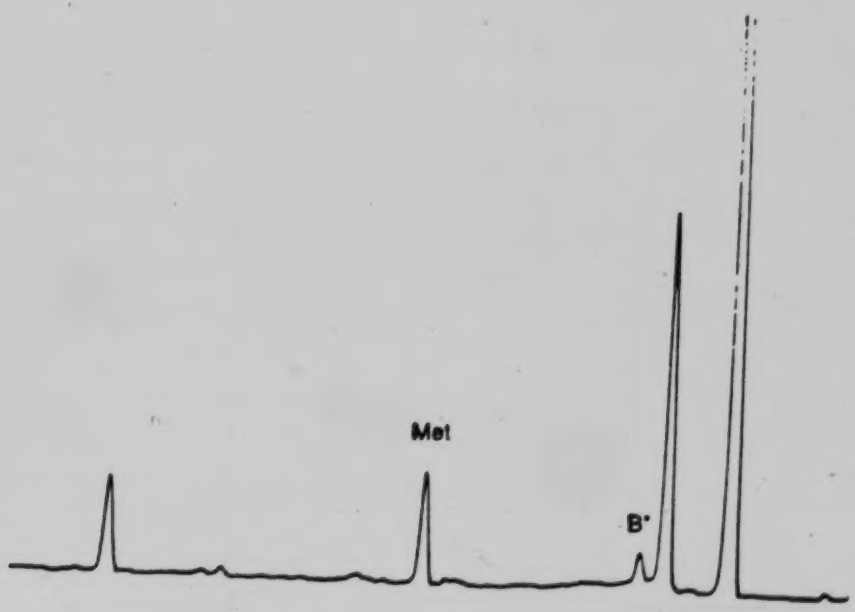

Appendix 2-4. Electropherogram for FTC-Met. B* is the third blank peak.

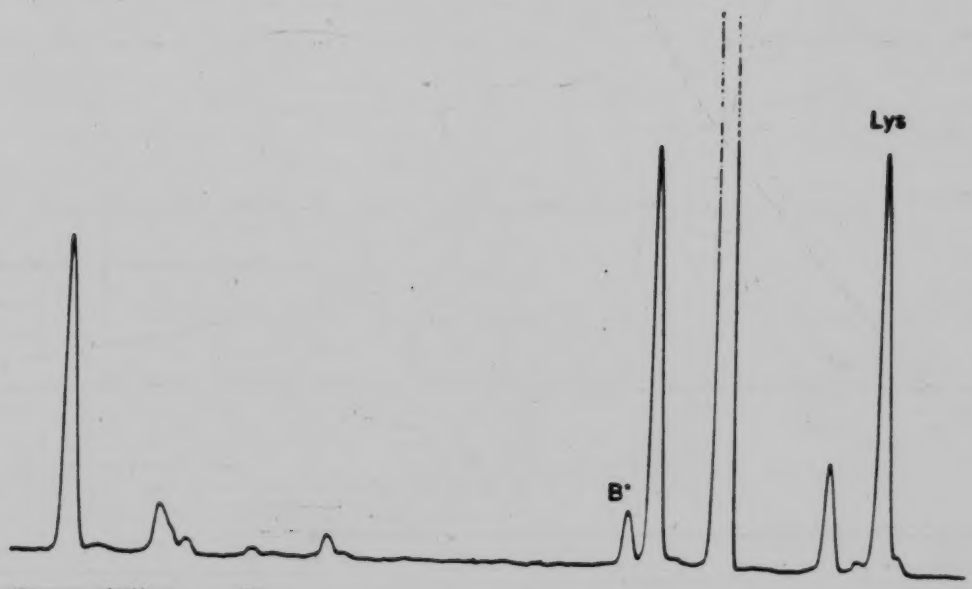

Appendix 2-5. Electropherogram for FTC-Lys. B* is the third blank peak.

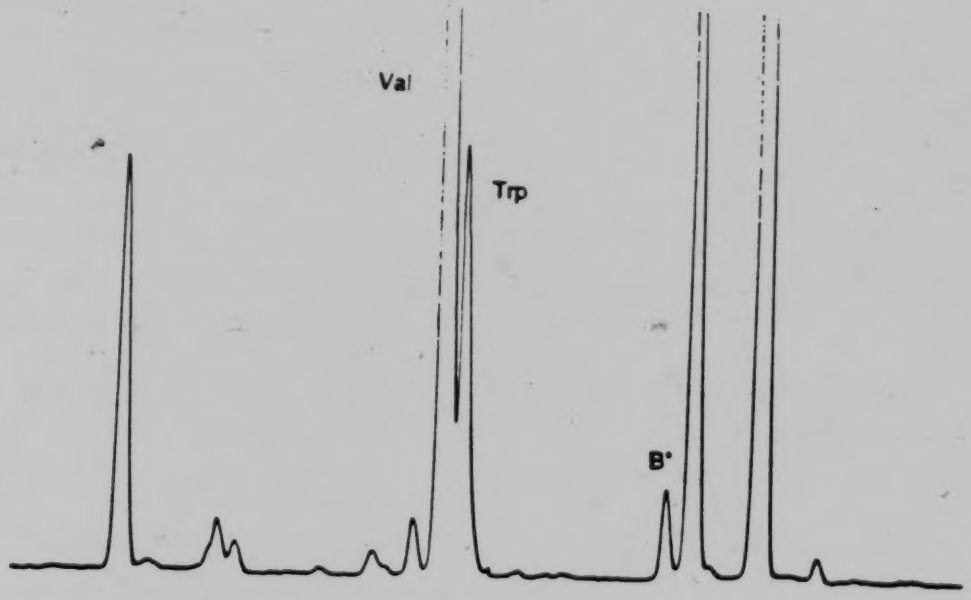

Appendix 2-6. Electropherogram for a mixture of FTC-Trp and FTC-Val. B* is the third blank peak.

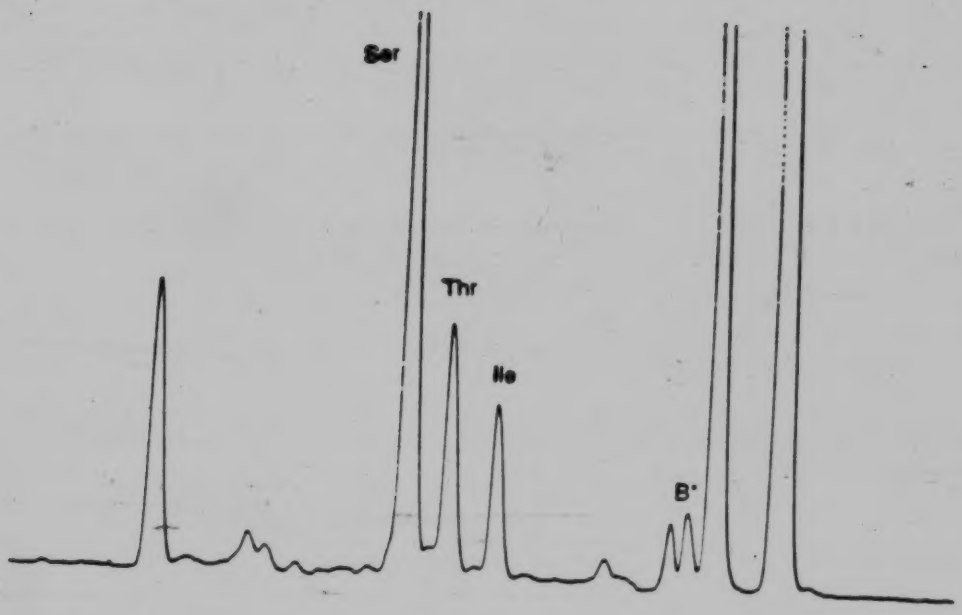

Appendix 2-7. Electropherogram for a mixture of FTC-Ile, FTC-Thr, and FTC-Ser. B* is the third blank peak.

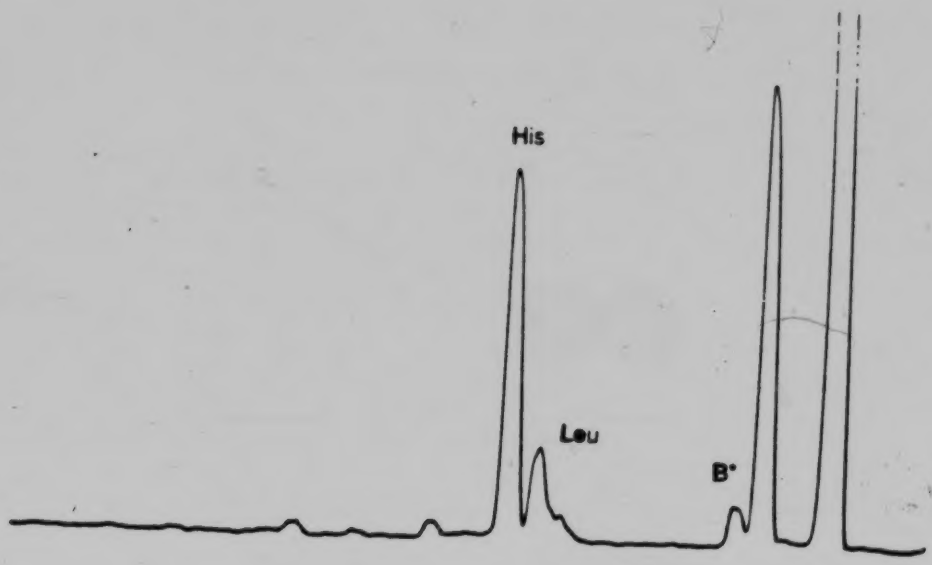

Appendix 2-8. Electropherogram for a mixture of FTC-Leu and FTC-His. B* is the third blank peak.

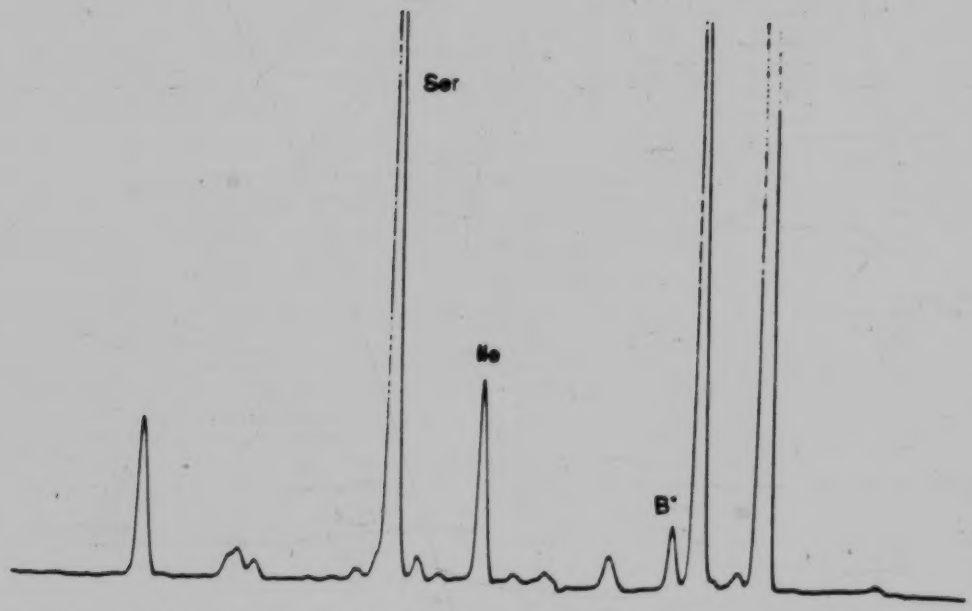

Appendix 2-9. Electropherogram for a mixture of FTC-Ile and FTC-Ser. B* is the third blank peak.

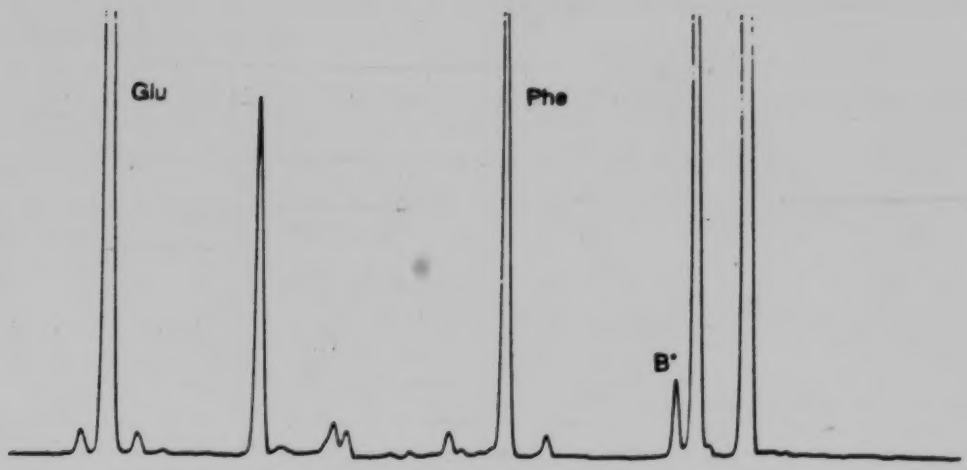

Appendix 2-10. Electropherogram for a mixture of FTC-Phe and FTC-Glu. B* is the third blank peak.

Appendix 2-11. Electropherogram for a mixture of FTC-Arg, FTC-Ala, and FTC-Asp. B* is the third blank peak.

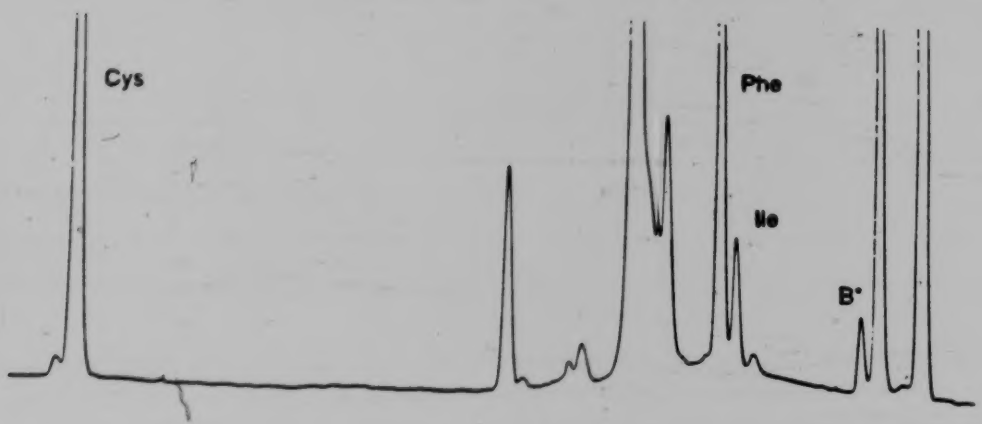

Appendix 2-12. Electropherogram for a mixture of FTC-Ile, FTC-Phe, and FTC-Cys. B* is the third blank peak.

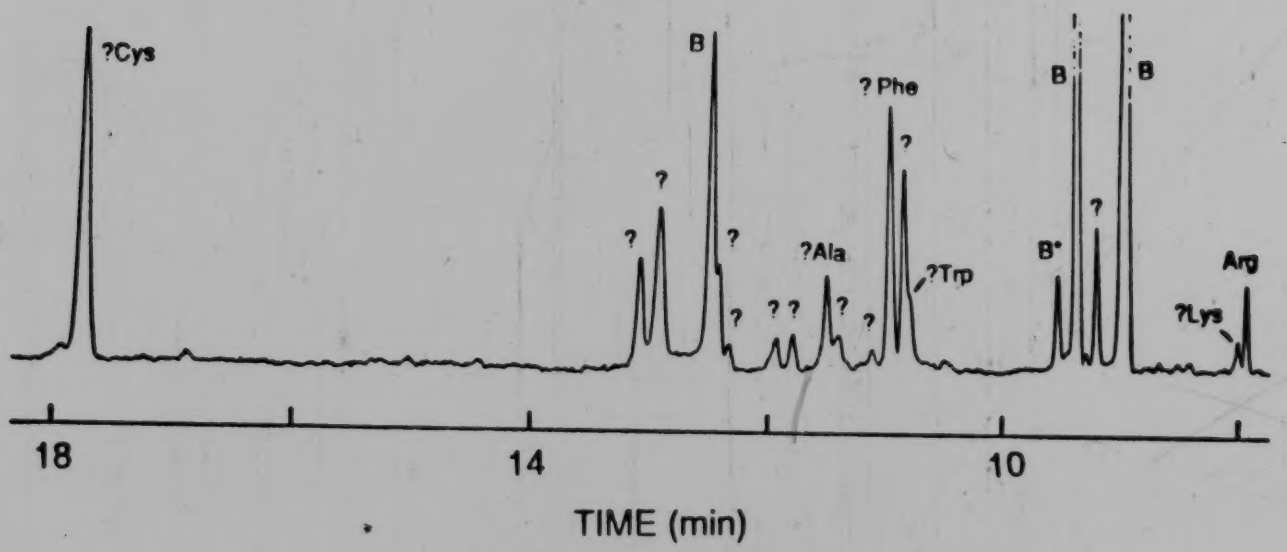

Appendix 3. Electropherogram of eighteen amino acids reacted with FITC solution all at once; injection, 2 KV for 8 sec; sheath, 5 mM pH 9.0 buffer; capillary, 50 µm ID and 97 cm; voltage for electrophoresis, 25 KV. Question marks, ?, represent unidentified peaks. B* is the third blank peak.